On the trajectory design, guidance and control for spacecraft rendezvous and proximity operations

Georgia Deaconu

THÈSE

En vue de l'obtention du

DOCTORAT DE L'UNIVERSITÉ DE TOULOUSE

Délivré par : *l'Université Toulouse 3 Paul Sabatier (UT3 Paul Sabatier)*

Présentée et soutenue le *29/10/2013* **par :**

GEORGIA IULIANA DEACONU

On the trajectory design, guidance and control for spacecraft rendezvous and proximity operations.

JURY

M. ALI ZOLGHADRI	Professeur, Université Bordeaux I	Président du Jury
M. DENIS ARZELIER	Directeur de Recherche, CNRS	Examinateur
M. JEAN-CLAUDE BERGES	Ingénieur, CNES	Membre Invité
M. THOMAS CARTER	Em. Prof., East. Connecticut SU	Examinateur
M. PATRICK DANES	Professeur, UT3	Examinateur
M. ALEXANDRE FALCOZ	Ingénieur, Astrium EADS	Membre Invité
M. CHRISTOPHE LOUEMBET	Maître de conférences, UT3	Examinateur
M. SORIN OLARU	Maître de conférences, SUPELEC	Rapporteur
M. ANDREW SINCLAIR	Associate Prof., Auburn Univ.	Rapporteur
M. ALAIN THERON	Chercheur affilié, LAAS-CNRS	Examinateur

École doctorale et spécialité :
EDSYS : Automatique 4200046

Unité de Recherche :
Laboratoire d'Analyse et d'Architecture des Systèmes du CNRS

Directeur(s) de Thèse :
M. Christophe LOUEMBET et *M. Alain THERON*

Rapporteurs :
M. Sorin OLARU et *M. Andrew SINCLAIR*

Acknowledgements

There are many people that I would like to thank for their direct or indirect contribution to the completion of this thesis. I would like to thank first my advisors, Christophe Louembet and Alain Théron, for their guidance and for the freedom they granted me in choosing the research directions.

This thesis has been supported by the French National Center for Space Studies and by Astrium EADS and I would like to use this occasion to thank Jean-Claude Berges and Alexandre Falcoz for their help and for their participation.

I would like to thank Denis Arzelier, the head of the Methods and Algorithms in Control which hosted me at LAAS-CNRS for the opportunity he offered me a while ago for the internship and for supporting my candidature for this subject. I would also like to thank all the members of the MAC group for making the work environment so enjoyable.

Special thanks to Eric Kerrigan and to Paola Falugi and to the other members of the Control and Power group at the Imperial College of London, for the interesting and challenging discussions and for the good times during my stay in London.

Aş vrea de asemenea sã le mulţumesc pãrinţilor mei, Nicoleta şi Marian, precum şi surorii mele Teodora pentru tot ajutorul oferit pe perioada studiilor.

I would also like to thank Francesco for his care and for his support and my old and new friends that have shared good and bad days with me over the years: Rãzvan, Dinu, Oana, Magda and many others.

Abstract

Recent space missions rely more and more on the cooperation between different spacecraft in order to achieve a desired objective. Among the spacecraft proximity operations, the orbital rendezvous is a classical example that has generated a large amount of studies since the beginning of the space exploration. However, the motivations and objectives for the proximity operations have considerably changed. The need for higher autonomy, better security and lower costs prompts for the development of new guidance and control algorithms. The presence of different types of constraints and physical limitations also contributes to the increased complexity of the problem. In this challenging context, this dissertation represents a contribution to the development of new spacecraft guidance and control algorithms.

The works presented in this dissertation are based on a structural analysis of the spacecraft relative dynamics. Using a simplified model, a new set of parametric expressions is developed for the relative motion. This parametrization is very well suited for the analysis of the geometric properties of periodic relative trajectories and for handling different types of state constraints. A formal connection is evidenced between the set of parameters that define constrained trajectories and the cone of positive semi-definite matrices. This result is exploited in the design of spacecraft relative trajectories for proximity operations, in the impulsive control framework. The resulting guidance algorithms enable the guaranteed continuous constraints satisfaction, while still relying on semi-definite programming tools. The problem of the robustness of the computed maneuvers with respect to navigation uncertainties is also addressed.

Résumé

La réalisation des missions spatiales repose de plus en plus souvent sur la coopération entre différents engins spatiaux. Parmi les opérations de proximité, le rendez-vous orbital est une pratique aussi ancienne que la conquête spatiale, qui continue de générer de nombreux travaux de recherche. Cependant, les motivations et les objectifs des récentes missions de rendez-vous orbital ont largement évolués. En effet, les besoins d'une autonomie accrue, d'une sécurité améliorée, d'une plus grande flexibilité et d'une réduction des coûts, constituent autant d'incitations au développement de nouvelles méthodes de guidage et contrôle. La satisfaction de contraintes très variées, dues à des considérations de sécurité ou à des limitations technologiques incontournables des actionneurs ou des capteurs, contribuent à la richesse du problème posé. Dans ce contexte, le développement de nouveaux algorithmes de commande constitue un vrai défi scientifique que cette thèse tente de relever.

Les travaux de cette thèse sont basées sur l'analyse structurelle des expressions décrivant le mouvement relatif entre deux véhicules en orbite. Sur la base des modèles de transition disponibles dans la littérature, une nouvelle paramétrisation du mouvement relatif est proposée. Celle-ci, particulièrement adaptée à la caractérisation des trajectoires périodiques, offre la possibilité d'une prise en compte de contraintes d'état très variées. Un lien formel est mis en évidence entre les paramètres définissant les trajectoires contraintes et le cône des matrices semi définies positives. Ces résultats sont exploités dans le développement des algorithmes de design de trajectoires pour des opérations de proximité, sous hypothèse de poussée impulsionnelle. Ces algorithmes ont, entre autre, la propriété de permettre la satisfaction des contraintes sur la trajectoire de manière continue dans le temps, tout en utilisant les outils numériques de la programmation convexe. Le problème spécifique de la robustesse des manœuvres aux incertitudes de la chaîne de mesure est aussi abordé dans ce manuscrit. Des approches de type commande prédictive sont mises en place afin de garantir aux opérations une précision souhaitée en présence de perturbations.

Contents

Nomenclature

μ	Earth's gravitational constant
ν	true anomaly
Ω	longitude of the ascending node
ω	argument of perigee
a	semi-major axis
B_0	Earth centered inertial base
B_l	Spacecraft centered local Cartesian base
E	eccentric anomaly
e	eccentricity
i	orbit inclination
M	mean anomaly
n	mean motion
LMI	Linear Matrix Inequality
LP	Linear Program
LTI	Linear Time Invariant
LTV	Linear Time Varying
LVLH	Local Vertical Local Horizontal
MPC	Model Predictive Control
SDP	Semi-Definite Program

Introduction

Résumé: Le succès des missions spatiales repose de plus en plus souvent sur la coopération entre plusieurs véhicules en orbite. L'approvisionnement de la Station Spatiale Internationale par exemple est assuré par des opérations de rendez-vous orbital, tandis que des nombreuses missions scientifiques utilisent des formations de satellites pour relever des mesures. Ce type d'opérations ont des besoins spécifiques en termes d'algorithmes de contrôle, vue la distance réduite entre les véhicules, les contraintes d'autonomie et de sécurité des mission spatiales et les ressources limitées. Les travaux de cette thèse portent sur le développement des algorithmes de guidage pour des opérations de proximité entre les satellites, où la distance réduite permet la navigation relative. L'objectif est de fournir des plans de manœuvres optimisés du point de vue de la consommation de combustible, qui prennent en compte les contraintes opérationnelles de la mission et qui soient robustes à des incertitudes. Le cadre de travail choisi est celui des méthodes dîtes directes, qui permettent la formulation du problème de guidage comme un problème d'optimisation paramétrique.

Background and motivations

Spacecraft rendezvous and docking capabilities are required for a large array of space applications that involve more than one spacecraft. It is a key technology for the in-orbit assembly of large units, such as the space stations (Mir, Skylab, ISS). The space stations further rely on rendezvous and docking missions in order to receive supplies or to exchange the crew. For instance, the unmanned Automated Transfer Vehicle (ATV) from the European Space Agency periodically supplies the International Space Station (ISS) with propellant, water, air, payloads and experiments. Recently, the Dragon spacecraft became the first commercial spacecraft to successfully dock with the ISS.

Space rendezvous has also been used for a variety of other purposes, including the service missions to the Hubble Space Telescope and the EURECA spacecraft retrieval. Other on-orbit servicing missions are under study for existing spacecraft [7, 85]. The increasing number of space debris in the Low Earth Orbit originating from mutual collisions, motivated the study of active debris removal missions [13].

In the recent years, a lot of interest has been shown for space scientific missions that rely on different instruments distributed over a fleet of spacecraft. This configuration can provide several advantages over the traditional monolithic satellite containing the payloads corresponding to several different missions objectives. It can reduce the launch costs by reducing the launch mass and it

can use multiple "mass production" vehicles to assemble the fleet. The robustness of the mission is also increased by this configuration since the payloads are distributed among the spacecraft and can eventually be replaced in case of failure [98]. Formation flying offers more flexibility because the formation can be reconfigured in order to follow new mission requirements. This approach has been considered for scientific missions with very diverse objectives, such as Earth observation (A-train), interferometry for Earth-like planets detection (DARWIN), measurement of gravitational waves from supermassive black hole binaries (LISA) or X-rays space telescope (Simbol-X).

The success of spacecraft rendezvous and formation flying missions depends on the precise control of the spacecraft relative state, often-times in the context of relatively small spacecraft separations. In order to ensure the security of the mission, a high degree of autonomy and robustness is desired for the relative motion control procedure. For missions such as the Mars Sample Return [86], for which the communication delay between the ground station and the spacecraft is very large, an autonomous guidance algorithm which guarantees that no collision will occur between the spacecraft is of vital importance.

The fuel-cost of the spacecraft maneuvers is also a matter of concern. The propulsion system can account for up to 50% of the spacecraft mass at the launch time, reducing the available payload mass and influencing the cost of the launch. The control algorithms must ensure that the computed maneuvers are fuel-optimal, such that the desired lifetime for the mission can be achieved with the smallest amount of propellant.

The spacecraft rendezvous

The orbital rendezvous process consists in executing a series of orbital maneuvers with the purpose of bringing two spacecraft in close vicinity of each other. Usually one of the spacecraft, called the *target*, is considered to be inert, while the second spacecraft, called the *follower* or the *chaser*, executes the maneuvers. When the objective is to physically join the two spacecraft involved in the rendezvous, we speak about docking or berthing.

W. Fehse identified in [29] several phases of a rendezvous mission, each one with its own challenges. For the *launch stage*, the purpose is to bring the two spacecraft in vicinity by placing them in the same orbital plane. The *phasing stage* aims at reducing the phase angle between the target and the follower (see the illustration in Figure 1). During the phasing maneuvers, the follower spacecraft is controlled from the ground station and the navigation is based on absolute measurements with respect to the Earth.

For the *far range rendezvous phase* or the *homing phase*, the follower spacecraft moves towards

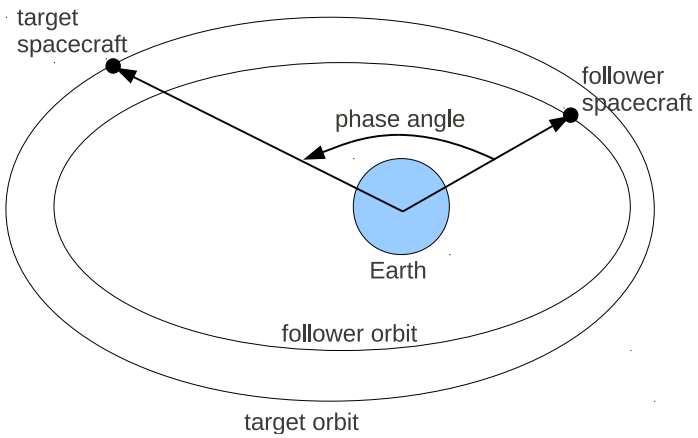

Figure 1: View of the target's orbital plane at the beginning of the phasing stage

a stable position in proximity of the target, using relative navigation measurements. For the ATV rendezvous scenario with the ISS for instance, this stage starts at a range of few tens of kilometres and ends at a range of few kilometres from the target spacecraft. The following *close range rendezvous phase* is usually divided in two stages: the *closing* maneuvers guiding the spacecraft towards the final approach corridor and the *final approach* stage leading to mating conditions.

The different stages of an orbital rendezvous mission are summarized in Figure 2. The works presented in this dissertation are related to the homing and the closing phases, during which the two spacecraft rely on relative navigation measurements in order to achieve the desired final conditions. Some of the presented examples also refer to the final approach phase, leading to the spacecraft docking.

Mission constraints and technical challenges

The spacecraft rendezvous guidance is a complex process due to the different types of conditions and constraints that must be respected during each phase of the mission. For the phases considered in this dissertation, the far range and close range rendezvous stages, the approach trajectory can be required for instance to pass through specified hold points where the follower vehicle must wait for the permission to proceed, either from the ground control station or from the crew of the target spacecraft [29]. Security considerations might impose the choice of approach trajectories that are inherently safe, meaning that they are guaranteed to avoid any collision with target vehicle, even in the case where the thrust capabilities of the chaser spacecraft are compromised. During the final approach maneuvers, the follower spacecraft might also be required to remain inside the

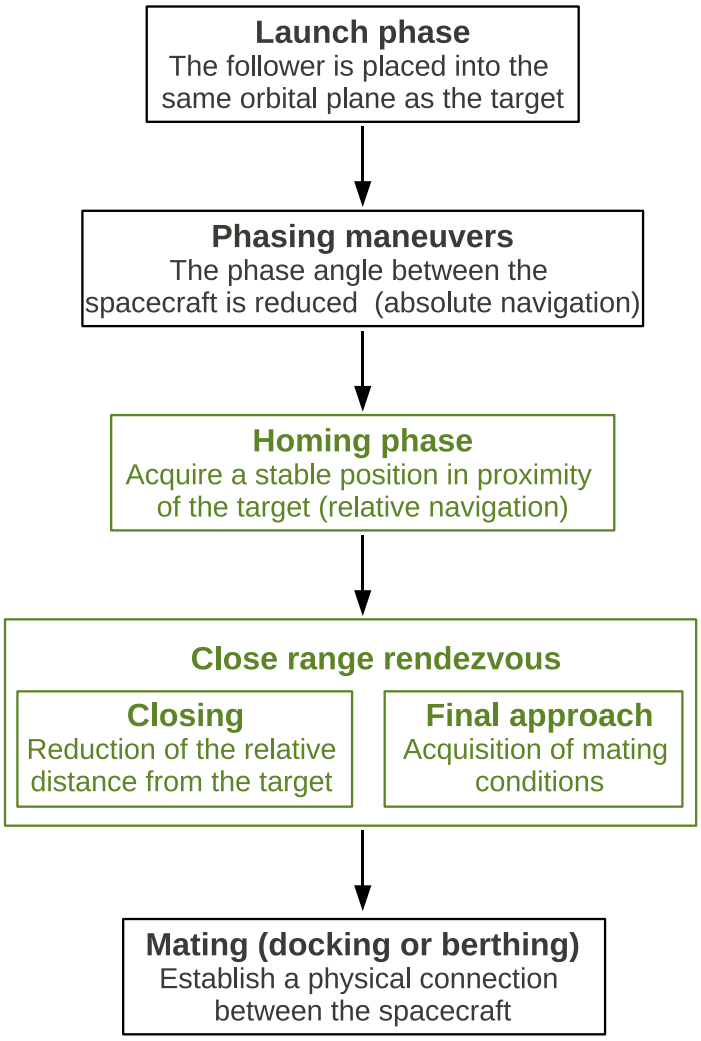

Figure 2: The different phases of a rendezvous mission

visibility cone of the target spacecraft for continuous visual contact. These specifications correspond to constraints that the rendezvous trajectory must respect in order to certify that the mission requirements are met.

Another factor that must be taken into consideration when designing the approach trajectory is the fuel-cost of the maneuvers. Thrust maneuvers can be approximated with impulses, i.e. instantaneous changes of velocity at the time of maneuver. This simplifies the computation and the analysis of a fuel-optimal maneuvers plan for the spacecraft rendezvous [29]. The impulsive approximation is especially well adapted for the liquid propellant engines which are used for a wide span of spacecraft maneuvers, ranging from orbital transfer maneuvers to station keeping and spacecraft attitude control. Any computed maneuvers plan needs to respect the constraints on the available propellant budget for the rendezvous mission.

Orbital disturbances, navigation errors and control execution errors can alter the outcome of the computed maneuvers. The presence and the effects of these disturbances need to be integrated into the rendezvous trajectory design phase. Navigation errors are defined as the difference between the state perceived by the onboard system and the real state of the vehicle. They can be caused by the sensors measurement performance limitations, by errors in the alignment between the sensors and spacecraft axes, by the onboard information processing and filtering, etc. The control execution errors refer to deviations in magnitude, direction or application time from the desired impulsive thrusts. They can be due to mounting errors, to misalignments with the mechanical axes, to the engine performances, etc. The decision autonomy of the spacecraft cannot be increased without providing *a priori* guarantees for its behaviour in perturbed conditions. This must be done while using control algorithms of reduced complexity since the computational resources available on board the spacecraft are limited with respect to those available on ground.

Some of these challenges are addressed in this dissertation. The main objective is to provide algorithms for the computation of robust fuel-optimal maneuvers plans leading to rendezvous trajectories that respect the constraints imposed by the mission's requirements, even in presence of a certain class of uncertainties. A study of the spacecraft constrained naturally periodic trajectories is carried out in relation to the security specifications for the approach trajectory.

The spacecraft trajectory design is a challenging problem due to the presence of trajectory and control constraints, to the robustness considerations and to the large number of design parameters. In the most general case, only the initial time of the mission is fixed and the trajectory design procedure must provide a choice for the final time, the number and the distribution of thrusting instants, the amplitude and the direction of the thrusts. If the design algorithm is intended for use onboard the spacecraft, then restrictions are added on its computational complexity. A brief presentation of the main trajectory design approaches is given in what follows, with a focus on their ability to handle the different mission requirements.

Spacecraft relative trajectory design approaches

The trajectory design for spacecraft rendezvous and proximity operations refers to the computation of a series of maneuvers that steer the spacecraft from some known initial relative conditions to some final desired relative conditions. The design procedure generally consists in solving an open-loop optimal control problem whose solution corresponds to the best approach trajectory that respects the constraints and minimizes a specified criteria. The most common objective is to minimize the total fuel cost of the rendezvous maneuvers. This can guarantee that the mission's fuel budget is

respected and can increase the lifetime of the spacecraft. The techniques for solving this type of constrained open-loop optimal control problems are usually divided into *direct methods* and *indirect methods* [24].

Indirect methods are based on analytical necessary optimality conditions derived using the calculus of variations and the Pontryagin maximum principle. The optimal solution can be found by solving the two-point-boundary-value problem (TPBVP) resulting from these conditions [24]. When using the indirect methods, the optimal spacecraft trajectory for the rendezvous problem is computed *indirectly*, based on the evolution of the adjoint state vector or the so-called *primer vector* [58, 62]. For impulsive trajectories, the primer vector indicates the times and the positions of the thrust impulses that minimize the total fuel cost. However, the resolution of the problem is complicated in the general case, especially when constraints are added to the problem. It also requires a good guess for the initial value of the primer vector. Recent works on the spacecraft rendezvous problem have focused on transforming the necessary conditions for optimality into constructive conditions for the optimal solution [3, 4].

Direct methods rely on the transformation of the optimal control problem into a parameter optimization problem. This is usually achieved through control parametrization and through discretization [45]. The obtained finite-dimensional optimal control problem can be efficiently solved using the existing algorithms [11]. There are different types of direct methods depending on the choice for the decision variables and on the used integration method. Among them, the *direct shooting methods* are used in the cases where the parametrisation concerns only the control variables. The system's dynamics are usually linear and are integrated analytically or numerically [49].

The indirect resolution methods certify the global optimality of a computed solution by checking a set of necessary and sufficient (if available) conditions. However they lead to problems that are hard to solve numerically, especially when constraints are considered. Direct methods are able to deal with state and control constraints more effectively and to integrate robustness elements with respect to different types of disturbances. Even if the obtained solution can only be certified as optimal for the particular parametrization and/or discretization that has been considered, they provide an attractive alternative for the rendezvous guidance problem.

The algorithms developed in this dissertation for the design of spacecraft rendezvous trajectories fall into the category of direct shooting methods. Other than the advantage related to the reduced complexity of the resulting optimization problem, this approach also offers the possibility of including robustness considerations directly in the phase of control synthesis. Several types of uncertainties can be easily handled thanks to robust programming techniques [9]. Our main focus

will be on reducing the effects of relative navigation uncertainties on the final rendezvous precision.

Spacecraft trajectory control: closing the loop

The direct and indirect approaches for spacecraft relative trajectory design provide a series of fuel-optimal maneuvers that need to be executed at the specified instants in order to reach the desired final objective. The maneuvers plan is obtained based on open-loop predictions of the evolution of the spacecraft relative trajectory. As previously discussed, the presence of orbital perturbations, navigation uncertainties or control execution errors might alter the outcome of the computed maneuvers. In order to limit their undesired effects and to reach a specified rendezvous precision, the trajectory control needs to be implemented in a closed-loop manner.

The resolution of a constrained open-loop optimal control problem can be integrated in a closed-loop setting by using the Model Predictive Control (MPC) methodology [84]. Model Predictive Control or Receding Horizon Control is a control technique for which the control action is obtained by solving at each sampling instant a finite-horizon open-loop optimal control problem, using the current state of the system as initial state. The optimization delivers every time a series of *control actions* out of which only the first one is applied to the system. The rest of the plan is discarded because a new solution, based on new measurement information, will be computed at the next sampling time [68].

Model Predictive Control is a popular control technique for spacecraft rendezvous and proximity operations [16,18,26,32,41,43,86]. Its popularity is due to the ability to integrate constraints and uncertainties directly into the trajectory design problem. Different other control approaches have been proposed for spacecraft proximity operations and formation flying, spanning over a large range of techniques. A non exhaustive list includes adaptive control [2,95], non-linear quadratic regulator [6], feedback impulsive control [89], Lyapunov-based nonlinear output feedback control [104], time-delayed feedback control [12] and several others [87,88]. But very few of them consider the presence of constraints or the fuel cost of the maneuvers, and focus only on reaching the specified final conditions.

Instead of determining *off-line* a feedback policy that provides the optimal control for all system states, MPC solves an open-loop optimal control problem *on-line* which takes into consideration the current state of the system. The periodic recomputation of the solution creates an *implicit closed-loop*. The robustness properties of this implicit closed-loop with respect to different types of uncertainties are an important aspect, especially if the objective is to provide the control system on-board the spacecraft with increased decision autonomy.

The presence of uncertainties raises questions related to the changes induced in the control performances. In the case of spacecraft trajectory control, the performances are defined in relation to the fuel consumption and to the precision with respect to the desired final objective of the maneuvers. The Model Predictive Control possesses some inherent robustness properties, defined as the robustness of the closed-loop for the control that has been computed without explicitly considering the uncertainties [36,67]. But for problems that include control and state constraints, the computed control actions must guarantee that no transgressions of the constraints will occur for all the possible realizations of the uncertainties. In this case, the inherent robustness properties are no longer sufficient and the presence of uncertainties needs to be included in the writing of the optimization problem [27,59,69,79]. Another key aspect is the property of recursive feasibility of the control problem in presence of uncertainties. The optimal control is recomputed at each sampling instant and it is important to provide theoretical guarantees that, if the first optimization problem is feasible, then all the subsequent optimization problems will also be feasible. These important properties are investigated for the guidance algorithms proposed in this dissertation.

Objectives and organization of the dissertation

The works presented in this dissertation are oriented following two main axes: the analysis of the spacecraft relative motion and the design and control of the spacecraft relative trajectory. The study of the relative motion concentrates on spacecraft naturally periodic relative trajectories. These periodic trajectories, in the absence of perturbations, require no control in order to be maintained. This property could make them good candidates for parking orbits in between different phases of a rendezvous mission, for autonomous inspection trajectories for on-orbit servicing missions or for fail trajectories in case of system malfunction. Chapter 1 summarizes the most common-used models for representing the spacecraft relative motion. It also provides an overview of the properties of the spacecraft relative trajectories that are of interest for the rendezvous guidance problem, such as periodicity conditions, inter-satellite distance and geometric properties of periodic relative trajectories.

The different periodic motion initialisation techniques presented in the literature do not give any information about the geometric properties of the resulting trajectory. To address this problem, a new parametrization for the spacecraft relative trajectories is developed in Chapter 2. This parametrization provides a good framework for analysing their properties and it is in used in Chapter 3 in order to obtain a formal mathematical description of the spacecraft relative trajectories which respect *continuously in time* some dimensions constraints.

The spacecraft relative trajectory control concentrates around the problem of designing fuel-optimal maneuvers plans leading the spacecraft from an arbitrary initial relative state towards a desired final relative state, following trajectories which respects different mission constraints. Chapter 4 details the writing of the spacecraft rendezvous guidance problem as an impulsive optimal control problem using direct shooting methods. It illustrates the contribution of the results presented in Chapter 3 in obtaining approach trajectories that respect visibility constraints or that are guaranteed to be safe for a large range of system errors. The robustness aspects with respect to navigation uncertainties are treated in Chapter 5. The guidance problem is modified in order to provide a solution which guarantees *a priori* constraints satisfaction for all admissible values for the uncertainties, without modifying the complexity of the control algorithm. Moreover, the proposed control strategy also minimizes the effects of the sensing noise on the precision with which the final objective is achieved.

The presence of perturbations also affects the spacecraft naturally periodic motion. Chapter 6 presents a low-complexity stabilizing control strategy for the spacecraft periodic motion in presence of sensing noise. The developed method is based on the parametrization for the spacecraft relative trajectory presented in Chapter 2.

The key concepts specific to each chapter are summarized in Figure 3.

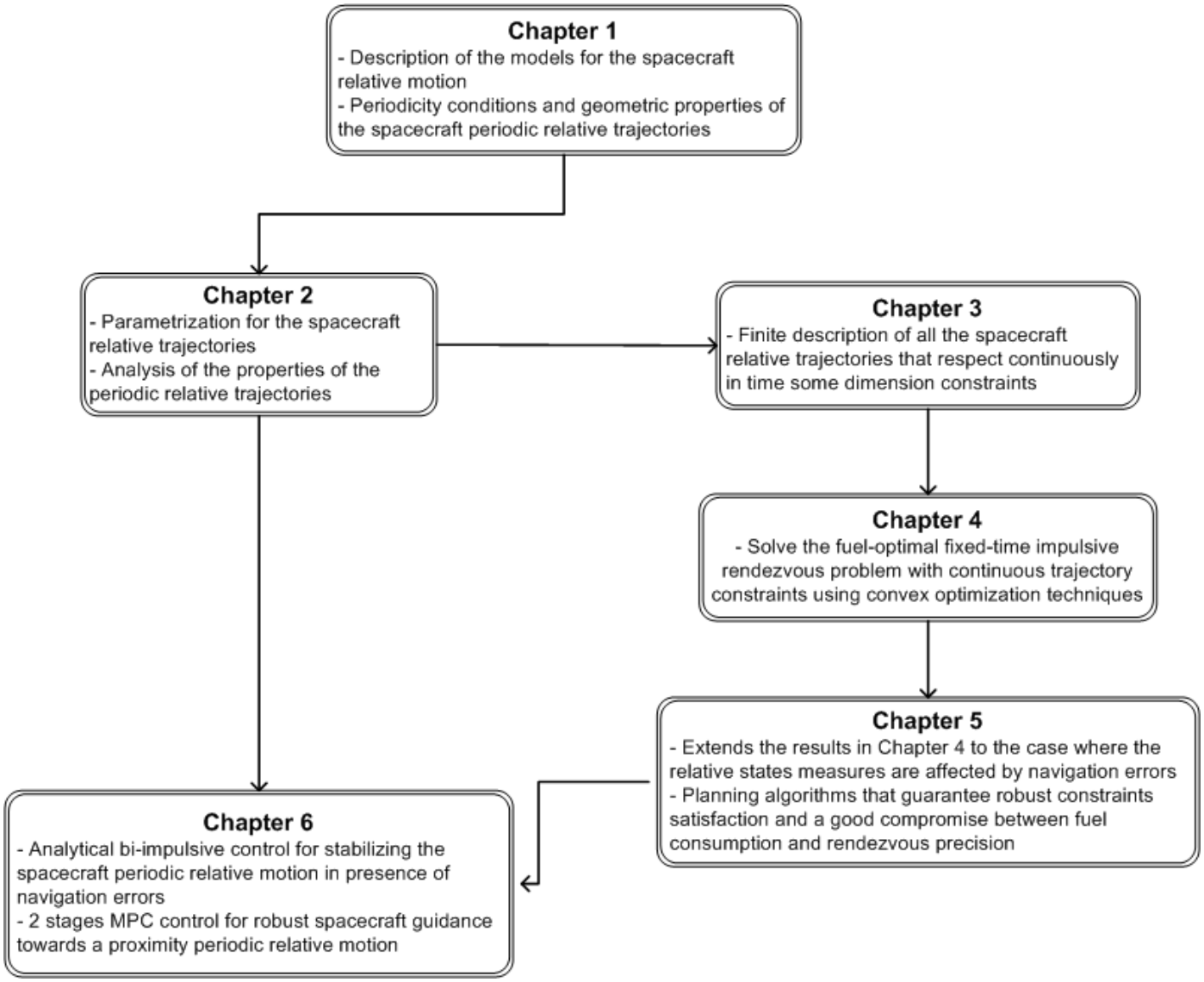

Figure 3: Overview of the key concepts specific to each chapter

Chapter 1

Spacecraft relative motion

Contents

Résumé: L'étude du mouvement relatif des satellites consiste à analyser la dynamique d'un satellite appelé le chasseur par rapport à un autre satellite, appelé la cible. Différentes choix existent pour la représentation de l'état relatif, chacune avec ses avantages. Plusieurs représentations sont passées en revue en ce chapitre, notamment dans le cadre des orbites képlériennes. L'accent est mis sur la description basée sur les positions et les vitesses relatives, exprimées dans un repère cartésien local attaché au satellite cible. Les propriétés des trajectoires relatives sont également étudiées, comme les distances minimale et maximale entre les satellites, l'existence des trajectoires relative périodiques et leur propriétés géométriques.

1.1 Introduction

The spacecraft relative motion refers to the study of the dynamics of a spacecraft, called *the follower*, with respect to the dynamics of another spacecraft, called *the leader* or *the target*. The motion of an individual satellite orbiting the Earth can be expressed using different representations for the satellite's state, each representation providing its own modelling advantages. A similar variety of choices is available for the parameters describing the spacecraft relative state, and some of the

most common descriptions will be presented in this chapter. The final choice is usually driven by the purpose of the study. Historically, models based on orbital elements and orbital elements differences have been used for formation flying applications [16,34,60], while Cartesian models have been preferred for spacecraft rendezvous and collision avoidance problems [17,31,41,57].

Regardless of the representation chosen for the spacecraft relative motion, a distinction can be made between Keplerian models and non Keplerian models. Under Keplerian assumptions, the Earth is represented as an homogeneous sphere and the spacecraft motion is affected only by Newtonian accelerations. The non Keplerian models take into account the Earth's oblateness, usually through the spherical harmonic model for the Earth's potential, the atmospheric drag or the solar radiation pressure, among other orbital disturbances.

The Keplerian framework leads to less accurate but simplified dynamical models for the spacecraft relative motion. These simplified models are well suited for control synthesis purposes, like in the case of maneuvers plans design for spacecraft rendezvous missions for instance. The relatively small distances between the spacecraft when compared to the distance with respect to the center of the Earth and the short time horizons associated with rendezvous missions justify the usage of simplified relative motion models. For this reason we will focus mainly on Keplerian models throughout this dissertation, while referring the interested reader to publications treating some of the other representations.

In what follows, a particular interest will be paid to the periodic solutions of the equations describing the spacecraft relative motion. These solutions enable the satellites to maintain a desired configuration without external intervention and without any fuel expenditure. This property has been extensively used in the formation flight literature [1,5,46,55,92] and has recently gained attention for orbital rendezvous and collision avoidance applications [25,41,43]. Different initialization methods for periodic motion will be presented along with some of the geometrical properties of the resulting trajectories.

1.2 Dynamics of a spacecraft orbiting the Earth

The Keplerian dynamics of a spacecraft with respect to the Earth can be derived from Newton's equations of motion between two mass particles. In this case, the motion of a spacecraft orbiting the Earth is described by the following differential equation [8]:

$$\left(\frac{d^2\vec{R}}{dt^2}\right)_{B_0} = -\frac{\mu}{\|\vec{R}\|^3}\vec{R} \tag{1.1}$$

where $\vec{R}$ represents the vector from the center of the Earth to the spacecraft center of mass and μ is the Earth's gravitational constant. The dynamics are expressed with respect to an Earth centered inertial frame $R_0 = (0, \vec{X}, \vec{Y}, \vec{Z})$ illustrated in Figure 1.1. The fundamental plane for R_0 is the Earth's equatorial plane, the $\vec{Z}$ axis coincides with the rotation axis of the Earth and is oriented towards the North Pole, the $\vec{X}$ axis points the vernal equinox and the $\vec{Y}$ axis is orthogonal to the $\vec{X}\vec{Z}$ plane.

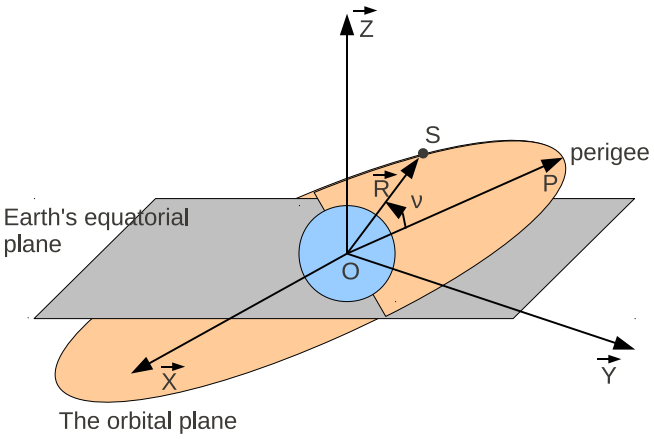

Figure 1.1: The Earth Centered Inertial frame and the satellite trajectory

Even though the differential equation (1.1) governing the relative motion of two bodies is non-linear, the equation admits a general analytical solution [8]. The constants of integration associated to the solution are called the *orbital elements* of the satellite motion and they play an important role in the study of the properties of the spacecraft trajectory.

Let the orbital plane be the plane which contains the trajectory of the orbiting spacecraft (see Figure 1.1). The equation of the spacecraft trajectory expressed using polar coordinates with respect to this plane is given by [8]:

$$R = \|\vec{R}\| = \frac{a(1-e^2)}{1+e\cos\nu} \tag{1.2}$$

where a is called the semi-major axis of the spacecraft orbit, e is called the eccentricity and ν is called the true anomaly. The satellite's orbit is bounded if $e < 1$ and unbounded if $e \geq 1$. For $e = 0$ the spacecraft trajectory is a circle of radius a and for $0 < e < 1$ the trajectory is an ellipse. The true anomaly ν represents the angle between the spacecraft's current position and the direction of the perigee (Figure 1.1).

The parameters a and e define the dimension and the shape of the satellite's orbit, while ν gives the instantaneous location of the satellite on its orbit. Three other quantities defining the spatial

orientation of the orbital plane are required in order to completely characterize the spacecraft trajectory. A common choice is represented by the angles i, Ω and ω defined with respect to the Earth's equatorial plane, as indicated in Figure 1.2.

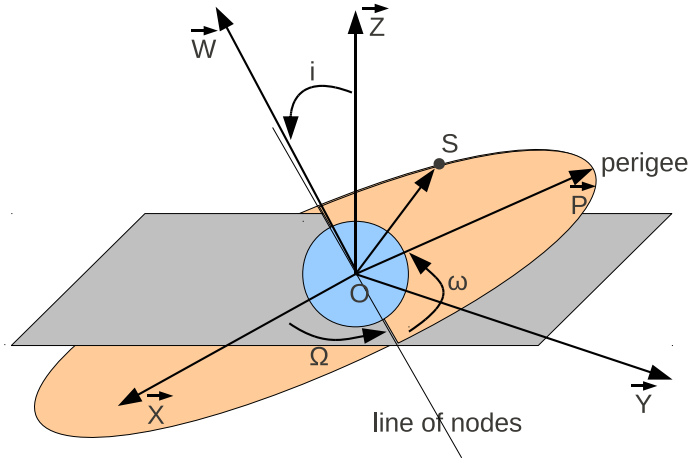

Figure 1.2: The definition of the classical orbital elements

The *line of nodes* denotes the line of intersection between the spacecraft orbital plane and the equatorial plane. The *ascending node* refers to the point where the satellite is crossing the line of nodes in a northbound direction. The *longitude of the ascending node*, Ω, is the angle between the X axis of the R_0 frame and the ascending node, the *argument of perigee*, ω, is the angle between the ascending node and the perigee while the *inclination*, i, is the angle between the orbital plane and the equatorial plane.

The set of orbital elements is defined by:

$$oe = \begin{bmatrix} a & e & i & \Omega & \omega & \nu \end{bmatrix}^T \tag{1.3}$$

and it completely describes the state of a satellite orbiting the Earth. Under Keplerian assumptions, the first five parameters are constant and only the true anomaly changes with time [8]:

$$\dot{\nu} = \sqrt{\frac{\mu}{a^3(1-e^2)^3}}\,(1+e\cos\nu)^2 \tag{1.4}$$

Sometimes, the eccentric anomaly, E, or the mean anomaly, M, are used instead of ν as the varying state. The eccentric anomaly and the true anomaly are related through geometrical transformations (Figure 1.3):

$$\tan\frac{\nu}{2} = \sqrt{\frac{1+e}{1-e}}\tan\frac{E}{2} \tag{1.5}$$

while eccentric anomaly and the mean anomaly are related through Kepler's equation:

$$M = E - e \sin E = M_0 + n(t - t_0) \tag{1.6}$$

As shown in (1.6), the mean anomaly can also be defined as a linear function of time, where $n = \sqrt{\mu/a^3}$ is the mean motion of the satellite, t_0 is the reference time and M_0 is the mean anomaly at t_0.

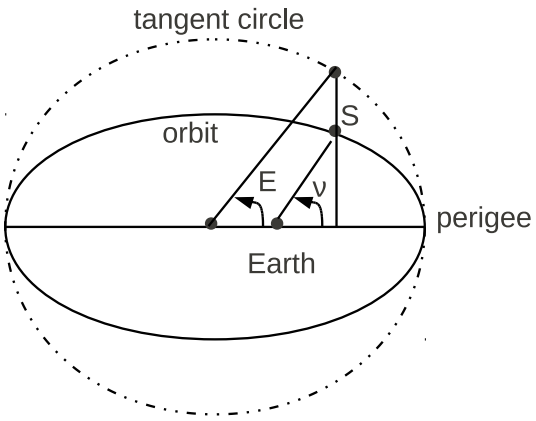

Figure 1.3: The definition of the eccentric anomaly

When the orbit is circular or near circular ($e \approx 0$) or when the orbit is planar or near planar ($i \approx 0$), some of the classical orbital elements oe are not defined. In those cases, the state of the spacecraft can be represented using different functions of the classical orbital elements that avoid this problem. Among the solutions proposed in the literature, we can mention the nonsingular orbital elements, the equinoctial elements or the Delaunay canonical elements, used for studying the satellite motion in a Hamiltonian framework [90].

The choice of using the inertial position and velocity or the various sets of orbital parameters in order to describe the state of a spacecraft orbiting the Earth is made depending on the application. Throughout this dissertation, the classical orbital elements oe are preferred for the representation of the leader's state. This choice is motivated by the fact that, in the Keplerian context considered here, the resulting dynamics have a very simple form (only one state that changes over time). To complete the description of the spacecraft relative motion, the state of the follower satellite must be expressed with respect to the state of the leader and some of the most commonly used representations are introduced next.

1.3 Spacecraft relative motion

The spacecraft relative motion refers to the study of the dynamics of the leader spacecraft combined with the study of the dynamics of the follower spacecraft. As previously stated, there are different possible state definitions which can be used in the description of the motion of a single spacecraft (Cartesian position and velocity, different sets of orbital parameters). In a similar way, different representations can be considered for the spacecraft relative state, each one bearing its own advantages.

1.3.1 Local Cartesian dynamics

The spacecraft relative motion represented using local Cartesian dynamics is defined with respect to a local rotating Cartesian frame centered on the leader satellite. A commonly used frame is the Local Vertical Local Horizontal (LVLH) frame $R_l = (S_l, \vec{x}, \vec{y}, \vec{z})$ illustrated in Figure (1.4). The $\vec{z}$ axis is radially oriented from the leader satellite towards the center of the Earth, the $\vec{y}$ axis is orthogonal to the orbital plane, in the opposite direction with respect to the angular momentum vector, and the $\vec{x}$ axis lays in the leader's orbital plane in the direction of the satellite's velocity.

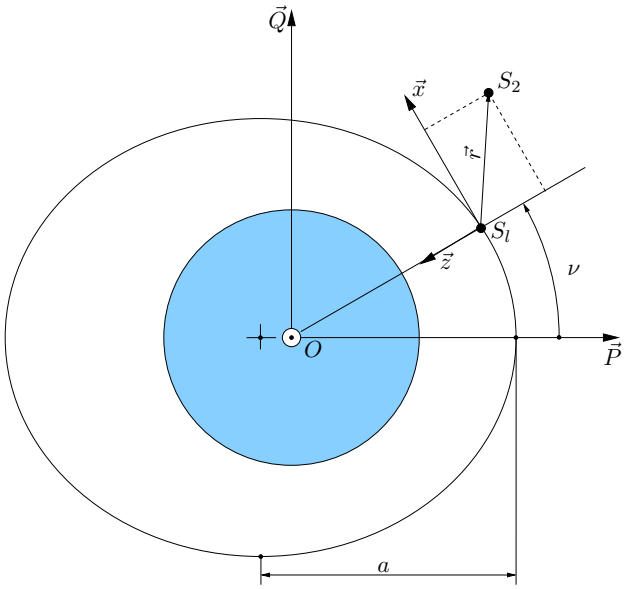

Figure 1.4: The spacecraft relative position and the leader's LVLH frame

The relative position between the leader spacecraft S_l and the follower spacecraft S_f is represented by $\vec{r} = \overrightarrow{S_l S_f}$ in Figure 1.4. Considering that the Keplerian dynamics of each satellite with respect to the Earth can be described using (1.1), the relative inertial acceleration can be written as:

$$\left(\frac{d^2\vec{r}}{dt^2}\right)_{B_0} = -\frac{\mu}{\|\vec{R}+\vec{r}\|^3}(\vec{R}+\vec{r}) + \frac{\mu}{\|\vec{R}\|^3}\vec{R}^3 \tag{1.7}$$

where $\vec{R} = \overrightarrow{OS_f}$ represents the inertial position of the leader spacecraft. The term on the left hand side of (1.7) can be further developed using the derivation rule with respect to a rotating frame:

$$\left(\frac{d^2\vec{r}}{dt^2}\right)_{B_0} = \left(\frac{d^2\vec{r}}{dt^2}\right)_{B_l} + 2\,\vec{\Omega}_{B_l/B_0} \times \left(\frac{d\,\vec{r}}{dt}\right)_{B_l} + \left(\frac{d\,\vec{\Omega}_{B_l/B_0}}{dt}\right)_{B_l} \times \vec{r} + \vec{\Omega}_{B_l/B_0} \times \left(\vec{\Omega}_{B_l/B_0} \times \vec{r}\right) \quad (1.8)$$

The terms in the sum correspond to the spacecraft relative acceleration in the local frame, the Euler acceleration, the Coriolis acceleration and the centrifugal acceleration respectively. The term $\vec{\Omega}_{B_l/B_0}$ represents the rotation velocity of the local basis B_l with respect to the inertial basis B_0.

Assuming that the dynamics of the leader spacecraft are expressed using the orbital elements defined in (1.3) and that the spacecraft relative state is given by the local relative position and velocity $X = \begin{bmatrix} x & y & z & v_x & v_y & v_z \end{bmatrix}^T$, the different terms in (1.8) can be computed individually. In the case of Keplerian motion, we have:

$$\vec{\Omega}_{B_l/B_0} = \begin{bmatrix} 0 \\ -\dot{\nu} \\ 0 \end{bmatrix}_{B_l} \qquad \vec{R} = \begin{bmatrix} 0 \\ 0 \\ R \end{bmatrix}_{B_l} \qquad \vec{r} = \begin{bmatrix} x \\ y \\ z \end{bmatrix}_{B_l} \quad (1.9)$$

After introducing the elements from (1.9), equation (1.8) becomes:

$$\left(\frac{d^2\vec{r}}{dt^2}\right)_{B_0} = \begin{bmatrix} \ddot{x} - 2\,\dot{\nu}\,\dot{z} - \ddot{\nu}\,z - \dot{\nu}^2 x \\ \ddot{y} \\ \ddot{z} + 2\,\dot{\nu}\,\dot{x} + \ddot{\nu}\,x - \dot{\nu}^2 z \end{bmatrix}_{B_l} \quad (1.10)$$

Developing the right hand side of (1.7) leads to the following nonlinear equations for the spacecraft relative dynamics:

$$\begin{aligned} \ddot{x} - 2\,\dot{\nu}\,\dot{z} - \ddot{\nu}\,z - \dot{\nu}^2 x &= -\frac{\mu\,x}{\sqrt{(x^2+y^2+(R-z)^2)^3}} \\ \ddot{y} &= -\frac{\mu\,y}{\sqrt{(x^2+y^2+(R-z)^2)^3}} \\ \ddot{z} + 2\,\dot{\nu}\,\dot{x} + \ddot{\nu}\,x - \dot{\nu}^2 z &= -\frac{\mu(R-z)}{\sqrt{(x^2+y^2+(R-z)^2)^3}} + \frac{\mu}{R^2} \end{aligned} \quad (1.11)$$

In the case where the distance between the two satellites is a lot smaller than the distance from the leader satellite to the center of the Earth ($\|\vec{r}\| \ll \|\vec{R}\|$), the linearized Tschauner-Hempel

equations can be used to describe the spacecraft relative motion [101]:

$$\begin{aligned}\ddot{x} &= 2\,\dot{\nu}\,\dot{z} + \ddot{\nu}\,z + \dot{\nu}^2 x - \frac{\mu}{R^3}x \\ \ddot{y} &= -\frac{\mu}{R^3}y \\ \ddot{z} &= -2\,\dot{\nu}\,\dot{x} - \ddot{\nu}\,x + \dot{\nu}^2 z + 2\frac{\mu}{R^3}z\end{aligned} \tag{1.12}$$

It can be noticed that for the linearized equations, the dynamics on the y axis are decoupled from the dynamics in the xz plane and define a harmonical oscillator.

In the case where the orbit of the leader spacecraft is circular, a simplified form can be obtained for the above equations. If $e = 0$ then $R = a = \text{const}$, $\dot{\nu} = n = \text{const}$ and $\ddot{\nu} = 0$. After introducing these values in (1.12), the well known Hill-Clohessy-Wiltshire equations for the spacecraft relative motion with respect to a circular reference orbit can be deduced [23, 42]:

$$\begin{aligned}\ddot{x} &= 2\,n\,\dot{z} \\ \ddot{y} &= -n^2 y \\ \ddot{z} &= -2\,n\,\dot{x} + 3\,n^2 z\end{aligned} \tag{1.13}$$

It can be noticed that in this case the spacecraft relative dynamics correspond to a Linear Time Invariant system.

The non Keplerian relative dynamics

Long term predictions of the spacecraft relative trajectory are necessary for formation flying missions. In this case, maintaining the assumption that there are no external perturbing forces or nonlinear terms introduces unacceptable prediction errors. Therefore, different models of spacecraft relative motion accounting for some of the effects of orbital disturbances have been developed.

For circular reference orbits, Schweighart and Sedwick presented in [91] a set of constant-coefficient linear differential equations that include the perturbation due to the Earth's oblateness, represented through the J_2 potential. Hamel and de Lafontaine developed in [39] a set of linearized equations of relative motion about a J_2 perturbed elliptical reference orbit. Kechichian gave in [50] the expression of the rotation velocity $\vec{\Omega}_{B_l/B_0}$ for the case where disturbances due to air drag and Earth oblateness are considered. The result is very general but it leads to complex nonlinear expressions for the relative motion that are not easy to use in practice.

Even if the dynamics modelled by the Tschauner-Hempel equations (1.12) do not include the effects of the orbital perturbations, they do have the advantage of being easy to use. They allow the description of the spacecraft relative motion through a Linear Time Varying (LTV) state space

model which is well suited for control synthesis and has been widely used for spacecraft relative trajectory design [6, 41, 47, 86, 93, 99].

1.3.2 Orbital elements differences dynamics

The differential orbital elements are defined as the difference between the orbital elements of the leader spacecraft oe_l and the orbital elements of follower spacecraft oe_f:

$$X_{oe} = oe_l - oe_f = \begin{bmatrix} \delta a & \delta e & \delta i & \delta\Omega & \delta\omega & \delta\nu & (\text{ or } \delta M \text{ or } \delta E) \end{bmatrix}^T \tag{1.14}$$

Under Keplerian assumptions, five of the six orbital elements defining the state of a spacecraft are constant. In this case, the relative dynamics expressed using the differential orbital elements exhibit similar properties. The simplest form for the relative dynamics is obtained when the varying term in the orbital elements is chosen to be the mean anomaly M:

$$\dot{X}_{oe} = \begin{bmatrix} \delta\dot{a} \\ \delta\dot{e} \\ \delta\dot{i} \\ \delta\dot{\Omega} \\ \delta\dot{\omega} \\ \delta\dot{M} \end{bmatrix} = \begin{bmatrix} 0 \\ 0 \\ 0 \\ 0 \\ 0 \\ -\frac{3}{2}\sqrt{\frac{\mu}{a^5}}\delta a \end{bmatrix} \tag{1.15}$$

Variational methods can be used to analyse the effect of perturbing accelerations on the orbital elements describing the spacecraft motion, in the non Keplerian case [90]. The perturbing accelerations can model for instance the effects of the Earth oblateness and/or the effects of the atmospheric drag. The well known Gauss Variational Equations (GVE) represent a specific formulation of the orbital elements variation problem, written for disturbances expressed in the leader's LVLH frame.

The spacecraft relative dynamics represented using the orbital elements differences have been successfully used in formation flight applications, especially for configurations that require a large separation between the spacecraft [1, 16]. In the case of the spacecraft rendezvous, the mission's objectives are usually specified using the relative Cartesian local coordinates, in terms of final relative position and velocity, given some position/velocity constraints. For this reason the description of the relative motion using local Cartesian dynamics is usually preferred in the orbital rendezvous literature [26, 41, 43].

1.4 Linearized Cartesian relative motion

Starting from the Tschauner-Hempel equations (1.12) for the linearized Cartesian relative dynamics, a state space representation of the spacecraft relative dynamics can be obtained. Based on this formulation, closed form solutions for the relative trajectories can be computed. These solutions enable the propagation of the spacecraft relative state without making use of numerical integration, which makes them very valuable for space applications where computational power is limited.

1.4.1 State-space representation

Let the spacecraft relative state vector be defined by the relative position and velocity projected on each axis of the leader's LVLH frame: $X = \begin{bmatrix} x & y & z & v_x & v_y & v_z \end{bmatrix}^T$. If in (1.12) the independent variable time is replaced by the true anomaly of the leader spacecraft, a simplified form can be obtained for the equations describing the relative dynamics between the leader and the follower spacecraft. The derivatives with respect to time are replaced by:

$$\frac{d(\cdot)}{dt} = \frac{d(\cdot)}{d\nu}\frac{d\nu}{dt} = (\cdot)'\dot{\nu} \quad \frac{d^2()}{dt^2} = \frac{d^2()}{d\nu^2}\dot{\nu}^2 + \frac{d()}{d\nu}\ddot{\nu} \tag{1.16}$$

and the following variable change is used:

$$\tilde{X}(\nu) = \begin{bmatrix} (1+e\cos\nu)I_3 & 0_3 \\ -e\sin\nu I_3 & \dfrac{(1+e\cos\nu)}{\dot{\nu}}I_3 \end{bmatrix} X(t) \tag{1.17}$$

where $I_3 \in \mathbb{R}^{3\times3}$ is the identity matrix and $0_3 \in \mathbb{R}^{3\times3}$ is the zero matrix. This operation leads to a periodic state-space model for the spacecraft relative dynamics:

$$\tilde{X}'(\nu) = \tilde{A}(\nu)\tilde{X}(\nu) + \tilde{B}\,\tilde{u} \tag{1.18}$$

where the dynamical matrix $\tilde{A}(\nu)$ is given by:

$$\tilde{A}(\nu) = \begin{bmatrix} 0 & 0 & 0 & 1 & 0 & 0 \\ 0 & 0 & 0 & 0 & 1 & 0 \\ 0 & 0 & 0 & 0 & 0 & 1 \\ 0 & 0 & 0 & 0 & 0 & 2 \\ 0 & -1 & 0 & 0 & 0 & 0 \\ 0 & 0 & \dfrac{3}{1+e\cos\nu} & -2 & 0 & 0 \end{bmatrix} \tag{1.19}$$

the control matrix $\tilde{B}$ is defined by $\tilde{B} = [0_3 \ I_3]^T$ and $\tilde{u} = [\tilde{u}_x \ \tilde{u}_y \ \tilde{u}_z]^T$ represents the acceleration generated by the spacecraft thrusters.

Closed form solutions can be computed for the periodic system (1.18) and the general method for obtaining them is summarized next.

1.4.2 The state transition matrix

The state transition matrix provides a convenient way to represent the solution of the autonomous dynamics of a linear system. For the spacecraft relative motion, computing the state transition matrix would enable the propagation of the relative state starting from any initial conditions, without relying on numerical integration:

$$\tilde{X}(\nu) = \Phi(\nu, \nu_0)\tilde{X}(\nu_0) \tag{1.20}$$

From the dynamics of the system (1.18), it can be deduced that the state transition matrix verifies the following differential equation:

$$\Phi'(\nu, \nu_0) = A(\nu)\Phi(\nu, \nu_0), \qquad \Phi(\nu, \nu) = I \ \forall \nu \tag{1.21}$$

For Linear Time Varying systems such as (1.18), there is no general analytical expression for the state transition matrix. Numerical methods developed for computing Φ are usually based on the resolution of the differential equation (1.21). In the case of the spacecraft relative motion, the special structure of the dynamical matrix $A(\nu)$ enables the computation of an analytical solution.

For the linearized spacecraft relative motion, the dynamics on the y axis are not affected by the motion in the xz plane and are described by the following homogeneous second order differential equation (see (1.18)):

$$\tilde{y}'' = -\tilde{y} \tag{1.22}$$

The solution of (1.22) can be directly expressed as a function of the initial conditions:

$$\tilde{X}_y(\nu) = \Phi_y(\nu, \nu_0)\tilde{X}_y(\nu_0) \tag{1.23}$$

where ν_0 is the initial true anomaly for the uncontrolled motion and:

$$\tilde{X}_y(\nu) = \begin{bmatrix} \tilde{y}(\nu) \\ \tilde{v}_y(\nu) \end{bmatrix} \qquad \Phi_y(\nu, \nu_0) = \begin{bmatrix} \cos(\nu - \nu_0) & \sin(\nu - \nu_0) \\ -\sin(\nu - \nu_0) & \cos(\nu - \nu_0) \end{bmatrix} \tag{1.24}$$

From (1.18), the homogeneous differential equations for the xz plane are given by:

$$\tilde{x}'' = 2\tilde{z}' \tag{1.25}$$

$$\tilde{z}'' = \frac{3}{1+e\cos\nu}\tilde{z} - 2\tilde{x}' \tag{1.26}$$

Integrating (1.25) once leads to:

$$\tilde{x}' = 2\tilde{z} + K \tag{1.27}$$

where K is a constant of integration. After introducing (1.27) in (1.26), a second order differential equation only in $\tilde{z}$ is obtained:

$$\tilde{z}'' + \left(4 - \frac{3}{1+e\cos\nu}\right)\tilde{z} = K \tag{1.28}$$

As recalled by Carter in [20], the method for solving this type of differential equation consists in finding a family of particular solutions φ_1, φ_2 for the homogeneous differential equation such that :

$$\varphi_1\varphi_2' - \varphi_2\varphi_1' = \text{constant} \tag{1.29}$$

and then applying the technique of variation of parameters [80]. The choice of the particular solutions φ_1, φ_2 determines the final form of the transition matrix.

A transition matrix for the periodic system (1.18) has been proposed by Carter in [20]. A slightly different solution has been given by Yamanaka and Ankersen in [103], which presents the advantage of having a simpler form. The Yamanaka-Ankersen transition matrix will be used for some of the developments in this dissertation and it is reproduced here for completeness.

Taking $\tilde{X}_{xz}(\nu) = \begin{bmatrix}\tilde{x}(\nu) & \tilde{z}(\nu) & \tilde{v}_x(\nu) & \tilde{v}_y(\nu)\end{bmatrix}^T$, the propagation of the relative state is given by:

$$\tilde{X}_{xz}(\nu) = \Phi_{xz}(\nu,\nu_0)\tilde{X}_{xz}(\nu_0) \tag{1.30}$$

where the transition matrix $\Phi_{xz}(\nu,\nu_0)$ can be written as:

$$\Phi_{xz}(\nu,\nu_0) = \phi_{xz}(\nu)\phi_{xz}^{-1}(\nu_0) \tag{1.31}$$

The matrix $\phi_{xz}(\nu)$ is defined by [103]:

$$\phi_{xz}(\nu) = \begin{bmatrix} 1 & -\cos\nu(2+e\cos\nu) & \sin\nu(2+e\cos\nu) & 3(1+e\cos\nu)^2 J \\ 0 & \sin\nu(1+e\cos\nu) & \cos\nu(1+e\cos\nu) & 2-3e\sin\nu(1+e\cos\nu)J \\ 0 & 2\sin\nu(1+e\cos\nu) & 2\cos\nu(1+e\cos\nu)-e & 3-6e\sin\nu(1+e\cos\nu)J \\ 0 & \cos\nu+e\cos 2\nu & -\sin\nu-e\sin 2\nu & -3e\left((\cos\nu+e\cos 2\nu)J+\dfrac{\sin\nu}{1+e\cos\nu}\right) \end{bmatrix} \tag{1.32}$$

The term J is related to the choice of the particular solution φ_2 and in the case of the Yamanka-Ankersen transition matrix is given by:

$$J(\nu) = \int_{\nu_0}^{\nu} \frac{d\tau}{(1+e\cos\tau)^2} = \frac{n(t-t_0)}{(1-e^2)^{3/2}} \tag{1.33}$$

From (1.33) it follows that for the initial true anomaly ν_0 we have $J(\nu_0) = 0$. This enables the analytical computation of the inverse of the $\phi_{xz}(\nu)$ matrix at ν_0:

$$\phi_{xz}^{-1}(\nu_0) = \frac{1}{e^2-1} \begin{bmatrix} e^2-1 & -\dfrac{3e\sin\nu_0(2+e\cos\nu_0)}{1+e\cos\nu_0} & e\sin\nu_0(2+e\cos\nu_0) & 2-e\cos\nu_0(1+e\cos\nu_0) \\ 0 & \dfrac{3\sin\nu_0(e\cos\nu_0+1+e^2)}{1+e\cos\nu_0} & -\sin\nu_0(2+e\cos\nu_0) & -(\cos\nu_0+e\cos^2\nu_0-2e) \\ 0 & 3(e+\cos\nu_0) & -(2\cos\nu_0+e\cos^2\nu_0+e) & \sin\nu_0(1+e\cos\nu_0) \\ 0 & -(3e\cos\nu_0+e^2+2) & (1+e\cos\nu_0)^2 & -e\sin\nu_0(1+e\cos\nu_0) \end{bmatrix} \tag{1.34}$$

The complete transition matrix Φ corresponding to the state vector $\tilde{X}(\nu)$ can be obtained by combining the blocks from the Φ_y and Φ_{xz} matrices in the appropriate order.

Overview of closed form solutions

Several works have been dedicated to the computation of the transition matrix for the spacecraft relative motion, in the case where the leader satellite evolves on an arbitrary elliptical orbit. Melton provides in [70] a solution that uses directly the time as the independent variable, obtained using series expansions of the eccentricity. However, this is an approximate solution and it loses accuracy for higher values of the eccentricity. Recently, a transition matrix obtained starting from the Tschauner-Hempel equations that also includes the effects of the J_2 perturbation has been proposed by Yamada and Kimura in [102]. The given solution is cumbersome and not easy to use for control design purposes. Moreover, the obtained transition matrix is shown to be accurate only for short prediction horizons.

Geometric methods for the computation of closed form solution for the J_2 perturbed relative

motion have been presented in [33,39]. They are based on the connection between the local Cartesian relative state and the differential orbital elements and no longer require the resolution of the differential equations of motion. Gim and Alfriend consider in [33] both the short-period and the long-period effects of the J_2 perturbation, leading to a very accurate but complex solution that still requires the knowledge of the evolution of the orbital parameters for the leader satellite. Hamel and de Lafontaine simplify the problem in [39] by neglecting the short-term effects of J_2. They obtain a solution that guarantees a bounded prediction error even for long horizons but that requires the knowledge of the relative secular drift of the mean orbital elements.

Closed form solutions of the spacecraft relative dynamics are sought for the computational advantage obtained from removing the integration process from the trajectory design algorithms. Moreover, they can also provide some insight into the geometrical properties of the resulting trajectories. Some examples of trajectory parametrizations that have been derived from such closed form solutions will be presented in the next section.

1.5 Properties of relative trajectories

The spacecraft ability to maintain a naturally periodic relative motion has been thoroughly investigated, especially in the context of formation flight applications. Some of the initialisation techniques for obtaining periodic solutions to the equations of spacecraft relative motion will be presented next, along with some of the geometrical properties of the resulting trajectories.

The connection between the initial conditions of the periodic motion and the dimensions of the obtained trajectory bears a lot of importance in the mission design process. The estimation of the minimal distance between the spacecraft is essential for collision avoidance purposes while the evaluation of the maximal distance plays an important role in the choice of the sensors for the relative navigation. However, sufficient understanding of this connection has not yet been reached. The next sections summarize some interesting results found in the literature in relation to this topic.

1.5.1 Periodicity conditions

The distance between two spacecraft on Keplerian orbits cannot grow unboundedly [37]. This observation is based on the fact that in the Keplerian case the spacecraft evolve on trajectories that are bounded and do not change over time. However, unless some particular conditions are met, the resulting relative trajectory is not periodic.

The notion of *commensurable motion* was first introduced in [38] and it refers to the relative

motion between spacecraft evolving on orbits that verify the following condition:

$$p\,T_l = q\,T_f,\ p,q \in \mathbb{N} \tag{1.35}$$

where T_l and T_f are the orbital periods of the leader and the follower spacecraft respectively. Since:

$$T = 2\pi\sqrt{\frac{a^3}{\mu}}, \tag{1.36}$$

the condition (1.35) can be easily transformed into a condition on the semi-major axis of the orbits corresponding to the two spacecraft:

$$a_f = \sqrt[3]{\frac{p^2}{q^2}}\,a_l \tag{1.37}$$

or in a condition between the energy of the orbits. The restriction in (1.37) induces a restriction on the relative trajectory. Figure 1.5 illustrates the trajectory obtained by propagating the relative motion over 10 orbital periods for different ratios between the orbital periods of two spacecraft. The relative trajectory appears to lay on a closed surface whose shape and dimensions depend on the ratio chosen between the orbital periods.

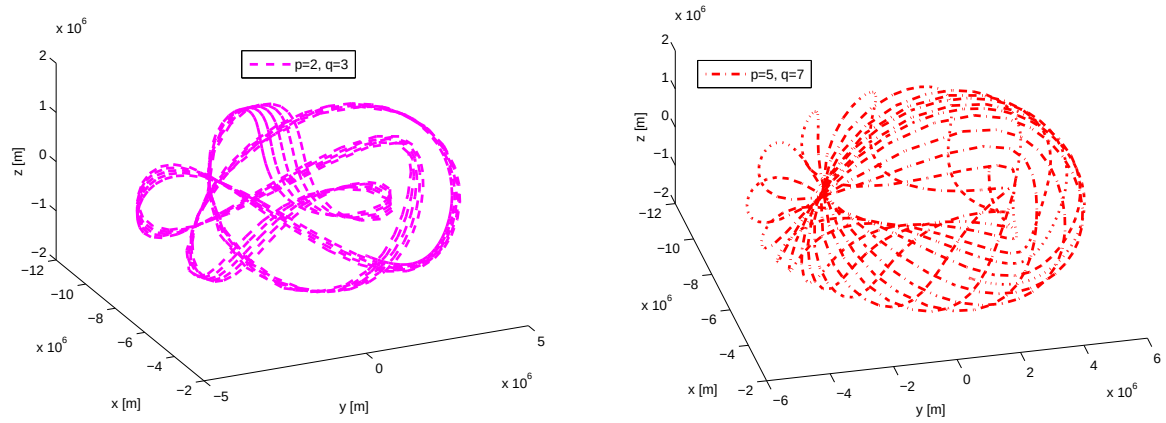

Figure 1.5: Relative trajectories obtained for different ratios between the orbital periods

In the case where $p = q = 1$, constraint (1.37) becomes:

$$a_f = a_l \tag{1.38}$$

In this case, the relative trajectory between the two spacecraft is periodic (see Figure 1.6).

The 1:1 ratio between the orbital periods along with the connection between the semi-major axis and the energy level of the orbit are used by Gurfil in [37] in order to write the *energy matching*

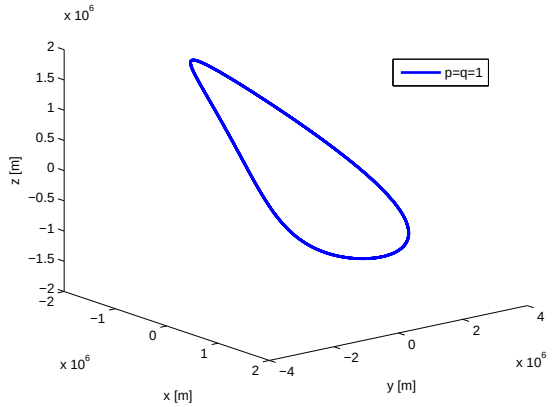

Figure 1.6: Periodic trajectory obtained for $p = q = 1$

condition for periodic motion. Using the nonlinear relative dynamics (1.11), the energy of the orbit of the follower spacecraft is written as a function of the leader's orbital elements and of the relative state. Imposing for the energies of the two orbits to be equal leads to a polynomial periodicity condition:

$$\frac{1}{2}\left((\dot{R} - v_z - \dot{\nu}\, x)^2 + (v_x + \dot{\nu}(R - z))^2 + v_y^2\right) - \frac{\mu}{\sqrt{x^2 + y^2 + (R - z)^2}} = -\frac{\mu}{2a} \tag{1.39}$$

When the spacecraft relative motion is modelled using the linearized dynamics (1.12), the existence of periodic trajectories can be proved by investigating the existence of periodic solutions to the unforced differential equations of motion. For this representation of the relative motion, the dynamics on the y axis are independent from the dynamics in the orbital plane and are naturally periodic. Using Carter's closed form solution for the spacecraft relative motion, Inalhan et al prove in [46] the existence of periodic solutions for the xz motion and also provide an initialisation procedure for obtaining periodic trajectories. The proposed initialisation procedure is valid only at perigee ($\nu_0 = 0$) and is given by:

$$\tilde{v}_x(0) = \frac{e + 2}{e + 1}\,\tilde{z}(0) \tag{1.40}$$

This condition for periodic motion can be extended to arbitrary initial true anomalies, leading to the following generalized expression [92]:

$$\tilde{v}_x(\nu_0) = \frac{2 + 3e\cos\nu_0 + e^2}{(1 + e\cos\nu_0)^2}\,\tilde{z}(\nu_0) + \frac{e\sin\nu_0}{1 + e\cos\nu_0}\,\tilde{v}_z(\nu_0) \tag{1.41}$$

The only assumption made on the relative motion in the development of conditions (1.38) and (1.39) is that of Keplerian motion. Conditions (1.40) and (1.41) are instead obtained using the

linearized model for the relative motion and their application is restricted to the cases where the linearisation hypothesis is valid.

The usage of the presented initialisation techniques is straightforward. They enable the computation of spacecraft relative states starting from which the resulting relative trajectories are periodic. However, the periodicity conditions alone do not provide any information about the geometry of the obtained trajectories such as shape, spatial orientation or minimal and maximal distances between the two spacecraft. To answer these questions a deeper analysis of the obtained trajectories must be carried out.

1.5.2 Inter-satellite distance

The ability to estimate the extremal relative distances between two satellites is a key point in the design of relative trajectories and formations configurations. For two spacecraft on arbitrary elliptic Keplerian orbits, analytical closed-form expressions for metrics quantifying the relative motion have been developed by Gurfil and Kholshevnikov in [38]. The metrics used for the analysis of the motion are the minimum, the maximum and the mean relative distance between the spacecraft. A general expression for the relative distance is given as:

$$\begin{aligned} W(E_l, E_f) = \frac{|\vec{r}|}{2\,a_l\,a_f} = \quad & W_0 + W_1 \cos E_l + W_2 \sin E_l + W_3 \cos E_f + W_4 \sin E_f + \\ & + 2(W_5 \cos E_l \cos E_f + W_6 \cos E_l \sin E_f + W_7 \sin E_l \cos E_f + \\ & + W_8 \sin E_l \sin E_f) + W_9 \cos 2E_l + W_{10} \cos 2E_f \end{aligned} \tag{1.42}$$

where the independent variables E_l and E_f represent the eccentric anomaly of the leader and of the follower spacecraft respectively.

The distance function W is a trigonometric polynomial of second degree in E_l and E_f. Its coefficients W_i depend on the orbital elements of the two spacecraft:

$$\begin{aligned} & 4W_0 = 2(\alpha_l + \alpha_f) + \alpha_l\, e_l^2 + \alpha_f\, e_f^2 - 4\, P_l\, P_f \quad W_1 = e_f\, P_l\, P_f^T - \alpha_l\, e_l \quad W_2 = e_f\, P_f\, S_l^T \\ & W_3 = e_l\, P_l\, P_f^T \quad W_4 = e_l\, P_l\, S_f^T \quad 2W_5 = -P_l\, P_f^T \quad 2W_6 = -P_l\, S_f^T \\ & 2W_7 = -P_f\, S_l^T \quad 2W_8 = -S_l\, S_f^T \quad 4W_9 = \alpha_l\, e_l^2 \quad 4W_{10} = \alpha_f\, e_f^2 \end{aligned} \tag{1.43}$$

where:

$$\alpha_l = a_l/a_f \quad \alpha_F = a_f/a_l \tag{1.44}$$

and:

$$P = \begin{bmatrix} \cos\omega\cos\Omega - \cos i\sin\omega\sin\Omega \\ \cos\omega\sin\Omega + \cos i\sin\omega\cos\Omega \\ \sin i\sin\omega \end{bmatrix} \quad S = \sqrt{1-e^2}\begin{bmatrix} -\sin\omega\cos\Omega - \cos i\cos\omega\sin\Omega \\ -\sin\omega\sin\Omega + \cos i\cos\omega\cos\Omega \\ \sin i\cos\omega \end{bmatrix} \tag{1.45}$$

The eccentric anomalies corresponding to the minimal and maximal distances between the two satellites can be obtained by solving the system of trigonometric equations:

$$\frac{\partial W(E_l, E_f)}{\partial E_l} = 0 \quad \frac{\partial W(E_l, E_f)}{\partial E_f} = 0 \tag{1.46}$$

Reference [52] presents a method based on Gröbner basis for eliminating one of the independent variables, either E_f or E_l. This procedure transforms the system (1.46) into an 8th degree univariate trigonometric polynomial. The roots of this polynomial enable the computation of the eccentric anomalies E_l and E_f for which the extremal distances are obtained. These eccentric anomalies can then be introduced in (1.42) in order to evaluate the corresponding relative distances.

The presented method can be used to evaluate the extremal distances between two spacecraft after that the designer fixed their orbital elements. However, our purpose is to determine a procedure for the computation of the orbital elements of the follower spacecraft that lead to some desired values for the extremal distances between the spacecraft. In this case, a part of the coefficients in the equations (1.46) transform from constant terms into decision variables. This changes the nature of the equations and the resolution method presented in [52] can no longer be used. The method in its current form cannot be easily integrated into a relative trajectory design procedure.

Slightly simpler expressions for the relative distance can be obtained in the case of spacecraft periodic motion. The following section presents analytical expressions for the extremal distances computed for some particular periodic spacecraft formations configurations, along with some geometrical properties of the periodic relative trajectories.

1.5.3 Geometry of the periodic spacecraft relative motion

The study of the geometry of the spacecraft periodic motion usually starts from the computation of parametric expressions for the periodic trajectories. Different parametrizations have been developed in [48,55,92], each one providing insight into different aspects of the periodic motion.

In [55], Lane and Axelrad expressed the relative periodic trajectory as a function of the differential orbital elements $\delta oe = [\delta a\ \delta e\ \delta i\ \delta\Omega\ \delta\omega\ \delta M]$. It is assumed that the difference between the orbital elements of the leader spacecraft and the orbital elements of the follower spacecraft δoe

is small and the periodicity of the relative motion is achieved by imposing $\delta a = 0$. According to (1.38), this is equivalent to imposing a 1:1 ratio between the orbital periods of the two spacecraft. The following parametric expressions are obtained:

$$\begin{aligned} x &= -a\cos\nu\,\delta e + \frac{a\,e\sin\nu}{\sqrt{1-e^2}}\,\delta M \\ y &= \left(a + \frac{R}{1-e^2}\right)\sin\nu\,\delta e + \frac{a^2}{R}\sqrt{1-e^2}\,\delta M + R(\delta\omega + \cos i\,\delta\Omega) \\ z &= R\sin\theta\,\delta i - R\sin i\cos\theta\,\delta\Omega \end{aligned} \tag{1.47}$$

This trajectory parametrization is used to show that when eccentric reference orbits are considered, the periodic relative trajectory is not an ellipse in any plane, except in some degenerate cases. Conditions for obtaining periodic in-track formations, follower formations and in-track/cross-track linear trajectories are extracted from expressions (1.47), along with an analytical evaluation of the minimal and maximal separation between the spacecraft for these particular configurations.

In-track formations can be obtained by imposing the x and z position to be always zero. This is achieved if $\delta e = \delta M = \delta i = \delta\Omega = 0$ and in this case the extremal distances are given by:

$$d_{\min} = a\,\delta\omega(1-e) \quad d_{\max} = a\,\delta\omega(1+e) \tag{1.48}$$

The follower formations are defined by two spacecraft that share the same groundtrack. This configuration is obtained by imposing $\delta\Omega = -(W_e/n)\,\delta M$ and $\delta a = \delta e = \delta i = \delta\omega = 0$, where W_e is the Earth's rotation rate. The parameters $\delta\Omega$ and δM can be chosen in order to achieve a desired spacecraft separation at perigee.

The in-track/cross-track formations require that the position on the x axis be always zero. An initialization technique leading to this configuration with a desired spacecraft separation at perigee is also developed in [55].

Starting form Carter's solution for the relative motion, Jiang et al. provide in [48] rational expressions for the spacecraft periodic relative trajectories projected onto the leader's LVLH frame:

$$\begin{aligned} x &= -c_1 + \frac{2\,(e\,c_2\,w - c_1)}{w^2+1} \\ y &= (1-e)c_2 + c_3 + \frac{2\,(c_1\,w + e\,c_2)}{w^2+1} + \frac{2\,(c_1\,w - e\,c_3)}{(1-e)w^2+1+e} \\ z &= -c_5 + \frac{2\,(c_4\,w + c_5)}{(1-e)w^2+1+e} \end{aligned} \tag{1.49}$$

where $w = \tan(\nu/2)$ and c_i are parameters that depend on the leader's orbital elements and on the differential orbital elements. It is demonstrated that quadratic curves are obtained when the

periodic relative trajectories are projected onto the coordinate planes of the LVLH frame and that none of these curves are ellipses in the general case. It is also concluded that the spacecraft periodic trajectories are usually three-dimensional and lay on quadratic surfaces, most frequently on one-sheet hyperboloids, and in rare cases on elliptic cones or elliptic cylinders. The number of self-intersections of the projections of the relative trajectory is computed and this information is used to identify a possible risk of collision and to design formations with special shapes such as figure-eight shapes in the coordinate planes.

A further parametrization for the spacecraft periodic motion has been proposed by Sengupta and Vadali in [92]:

$$\begin{aligned} x &= \frac{\rho_1}{a(1-e^2)} \sin(\nu+\alpha_0)(1+e\cos\nu) \\ y &= \frac{\rho_1}{a(1-e^2)} \cos(\nu+\alpha_0)(2+e\cos\nu) + \frac{\rho_2}{a(1-e^2)} \\ z &= \frac{\rho_3}{a(1-e^2)} \sin(\nu+\beta_0) \end{aligned} \tag{1.50}$$

where the parameters ρ_1, ρ_2, ρ_3, α_0 and β_0 depend on the leader's orbital elements and on the differential orbital elements. These equations are used to study the effects of the eccentricity of the reference orbit on the relative periodic trajectories. The analysis is done using Fourier series expansions with both the time and the true anomaly as independent variables. The identified effects are the presence of higher harmonics, amplitude scaling (for the same choice of parameters, the orbit tends to shrink in the along track direction and expand in the out-of-plane direction as the eccentricity increases), phase shift and skewness of the relative orbit plane. Correction methods are proposed for reducing some of these effects.

Various sets of parametric expressions are used for the study of periodic trajectories and the previous list is not exhaustive. The cited references help illustrating some of the main characteristics of the spacecraft periodic relative motion and some of the difficulties encountered in its study. It is interesting to remark from the presented parametrizations that the spacecraft periodic relative trajectories can be defined as functions of 5 constant parameters that depend on the value of the initial relative state and on the orbital parameters of the leader. However, in the general case, a clear link between the value of these parameters and the dimension or the shape of the resulting periodic trajectories has not yet been established and the designer needs to treat each case individually.

1.6 Conclusions

This chapter summarizes some of the most common representations of the spacecraft relative motion. It is showed that in general the spacecraft relative state is defined by 12 parameters: 6

parameters that define the state of the leader spacecraft and 6 parameters that describe the state of the follower spacecraft with respect to the leader. The general relative dynamics are however simplified in the Keplerian case, especially if the orbital elements are chosen to represent the dynamics of the leader spacecraft. In this case, out of the six corresponding parameters, only one changes over time. Moreover, in the case of periodic relative motion, the spacecraft relative trajectory can be written as a function of only five constant parameters.

When designing relative trajectories, the dynamics of the leader are considered known and the decision variables are the remaining parameters that define the spacecraft relative state. The challenge is to choose their value such that the resulting trajectory exhibits some desired properties like periodicity, minimal and maximal separation between the spacecraft, a certain shape etc. The following chapters will present a new set of parameters for the spacecraft relative motion. This new description allows for the parameters corresponding to trajectories that respect some dimensions constraints to be defined in a way suitable for integration into an optimization-based trajectory design procedure.

Chapter 2

Parametric expressions for the spacecraft relative trajectory

Contents

Résumé: Une bonne compréhension des propriétés du mouvement relatif des satellites est nécessaire pour pouvoir obtenir des trajectoires relatives qui respectent les différentes contraintes imposées par chaque mission (forme, dimension, etc.). Cependant, les propriétés exposées dans le chapitre précédent n'apportent pas de solution satisfaisante à ce défi. Le présent chapitre introduit un nouveau set d'expressions paramétriques pour le mouvement relatif, basé sur la matrice de transition de Yamanaka-Ankersen. Ces expressions paramétriques offrent un cadre de travail adapté à l'analyse des propriétés géométriques des trajectoires. Elles mettent en évidence le fait que pour les trajectoire périodiques la dynamique des paramètres est constante. Une étude qualitative illustre le lien entre la valeur des paramètres et les dimensions des trajectoires qui en résultent.

The study of the properties of spacecraft relative motion is motivated by the need to design spacecraft trajectories that respect different types of constraints (dimension, shape etc.). Several parametric expressions for the periodic relative motion have been presented in the previous chapter, each representation providing different insights into the geometrical characteristics of the spacecraft relative trajectory. However, no procedure for choosing the parameters in such a way that the relative trajectory exhibits some desired properties has been provided in the general case.

A new set of parametric expressions for the spacecraft relative motion is derived in this chapter. The aim is to provide a framework for the analysis of the spacecraft relative dynamics. The

expressions are obtained starting from the Cartesian model for the relative motion, which is usually preferred for spacecraft rendezvous applications. By working in the space of parameters, some interesting properties of the spacecraft relative motion can be evidenced. Our main focus is on the study of the influence that the values of these parameters have on the dimensions of the resulting spacecraft autonomous trajectory.

In the case of periodic relative motion, it is showed that a constant set of parameters can be used to define the periodic trajectory. The values of these constant parameters are proved to be directly connected to the properties of the resulting trajectory. An important role is also played by the eccentricity of the reference orbit and illustrations are provided for some of its effects.

2.1 Definition of the parameters

Consider the relative motion between two spacecraft on arbitrary elliptical Keplerian orbits. As seen in the previous chapter, the propagation of the autonomous spacecraft relative trajectory, starting from an initial relative state $\tilde{X}(\nu_0)$, can be expressed as:

$$\tilde{X}(\nu) = \Phi(\nu, \nu_0)\tilde{X}(\nu_0),\ \nu \geq \nu_0 \tag{2.1}$$

where $\Phi(\nu, \nu_0)$ denotes the Yamanaka-Ankersen transition matrix [103]. The relative state $\tilde{X}(\nu)$ is defined by the spacecraft relative position and velocity expressed in the LVLH frame attached to the leader: $\tilde{X}(\nu) = \begin{bmatrix}\tilde{x}(\nu) & \tilde{y}(\nu) & \tilde{z}(\nu) & \tilde{v}_x(\nu) & \tilde{v}_y(\nu) & \tilde{v}_z(\nu)\end{bmatrix}^T$.

Parametric expressions for the relative position between the spacecraft can be obtained by expanding the terms in (2.1) and then factoring out some of the terms related to the independent variable ν:

$$\begin{aligned}
\tilde{x}(\nu) &= (2 + e\cos\nu)(d_1\ \sin\nu - d_2\ \cos\nu) + d_3 + 3\,d_0\,J(\nu)(1 + e\cos\nu)^2 \\
\tilde{y}(\nu) &= d_4\ \cos\nu + d_5\ \sin\nu \qquad\qquad ,\nu \geq \nu_0 \\
\tilde{z}(\nu) &= (1 + e\cos\nu)(d_2\ \sin\nu + d_1\ \cos\nu) - 3\,e\,d_0\,J(\nu)\sin\nu(1 + e\cos\nu) + 2\,d_0
\end{aligned} \tag{2.2}$$

The parameters d_i in (2.2) are computed directly from (2.1) and can be written as a function of the initial conditions of the relative trajectory propagation. Let $D(\nu_0) \in \mathbb{R}^6$ be the *vector of parameters* for the spacecraft relative motion evaluated at ν_0, defined as:

$$D(\nu_0) = \begin{bmatrix}d_0(\nu_0) & d_1(\nu_0) & d_2(\nu_0) & d_3(\nu_0) & d_4(\nu_0) & d_5(\nu_0)\end{bmatrix}^T \tag{2.3}$$

The elements of the vector $D(\nu_0)$ depend *linearly* on the initial spacecraft relative state from which the relative trajectory is propagated:

$$D(\nu_0) = C(\nu_0)\tilde{X}(\nu_0) \tag{2.4}$$

The matrix $C(\nu) \in \mathbb{R}^{6\times 6}$ is defined as a function of the eccentricity of the orbit of the leader satellite and the true anomaly for which the vector of parameters needs to be evaluated:

$$C(\nu)=\begin{bmatrix} 0 & 0 & \frac{-(3\,e\cos\nu+e^2+2)}{e^2-1} & \frac{(1+e\cos\nu)^2}{e^2-1} & 0 & \frac{-e\sin\nu(1+e\cos\nu)}{e^2-1} \\ 0 & 0 & \frac{3(e+\cos\nu)}{e^2-1} & \frac{-(2\cos\nu+e\cos^2\nu+e)}{e^2-1} & 0 & \frac{\sin\nu(1+e\cos\nu)}{e^2-1} \\ 0 & 0 & \frac{3\sin\nu(1+e\cos\nu+e^2)}{(e^2-1)(1+e\cos\nu)} & \frac{-\sin\nu(2+e\cos\nu)}{e^2-1} & 0 & \frac{-(\cos\nu+e\cos^2\nu-2e)}{e^2-1} \\ 1 & 0 & \frac{-3\,e\sin\nu(2+e\cos\nu)}{(e^2-1)(1+e\cos\nu)} & \frac{e\sin\nu(2+e\cos\nu)}{e^2-1} & 0 & \frac{e^2\cos^2\nu+e\cos\nu-2}{e^2-1} \\ 0 & \cos\nu & 0 & 0 & -\sin\nu & 0 \\ 0 & \sin\nu & 0 & 0 & \cos\nu & 0 \end{bmatrix} \tag{2.5}$$

2.2 Properties of spacecraft relative trajectories

The advantage of expressing the spacecraft relative position in the form (2.2) is that it enables the direct identification of some of the effects that the values of the parameters have on the spacecraft relative trajectory. Parameters d_1 and d_2 influence the amplitude of the motion in the xz plane while parameters d_4 and d_5 define the amplitude of the periodic motion on the y axis. The value of the parameter d_3 corresponds to an offset term on the position on the x axis and the parameter d_0 defines an offset on the z axis and influences the contribution of the integral term $J(\nu)$.

When propagating the linearized spacecraft autonomous relative motion in the general non-periodic case, it can be noticed that the amplitude of the relative trajectory in the xz plane appears to grow unboundedly (see Figure 2.1). This is not surprising since the term $J(\nu)$ grows linearly in time (1.33), but its effect is modulated by the value of the parameter d_0.

According to (2.4), the values of the parameters D depend on the instant when they are evaluated. Changing the initial time for the propagation will also change the value of the parameters. The definition (2.4) can actually be seen as a state transformation that maps the spacecraft Cartesian relative state $\tilde{X}(\nu)$ to the state space corresponding to the vector of parameters. This suggests that some insight on the properties of the spacecraft relative trajectories could be gained by analysing directly the dynamics of the vector D.

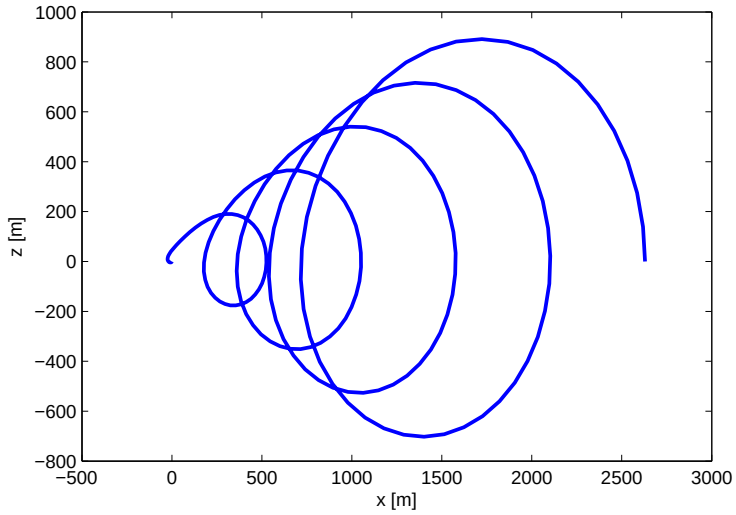

Figure 2.1: Spacecraft autonomous relative trajectory in the xz plane

2.2.1 Dynamics of the vector of parameters

The variable change defined by:

$$D(\nu) = C(\nu)\tilde{X}(\nu) \tag{2.6}$$

represents a valid state transformation since the matrix $C(\nu)$ is always invertible on the domain on which the spacecraft closed trajectories are defined:

$$\det(C(\nu)) = \frac{1}{1-e^2} \neq 0, \ \forall\, 0 \leq e < 1 \tag{2.7}$$

The passage from the space of the D parameters back to the Cartesian relative state is given by the inverse matrix:

$$\tilde{X}(\nu) = C^{-1}(\nu)D(\nu) = F(\nu)D(\nu) \tag{2.8}$$

where $F(\nu) \in \mathbb{R}^{6\times 6}$ is defined as:

$$F(\nu) = \begin{bmatrix} 0 & \sin\nu(2+e\cos\nu) & -\cos\nu(2+e\cos\nu) & 1 & 0 & 0 \\ 0 & 0 & 0 & 0 & \cos\nu & \sin\nu \\ 2 & \cos\nu(1+e\cos\nu) & \sin\nu(1+e\cos\nu) & 0 & 0 & 0 \\ 3 & 2e\cos^2\nu + 2\cos\nu - e & 2\sin\nu(1+e\cos\nu) & 0 & 0 & 0 \\ 0 & 0 & 0 & 0 & -\sin\nu & \cos\nu \\ -\dfrac{3e\sin\nu}{1+e\cos\nu} & -\sin\nu(1+2e\cos\nu) & 2e\cos^2\nu - e + \cos\nu & 0 & 0 & 0 \end{bmatrix} \tag{2.9}$$

The dynamics of the vector of parameters $D(\nu)$ can be deduced from the dynamics defining the

spacecraft relative motion. When the relative state is represented using local Cartesian coordinates, the relative dynamics can be modelled by a linear periodic dynamic equation:

$$\tilde{X}'(\nu) = \tilde{A}(\nu)\tilde{X}(\nu) \tag{2.10}$$

where the matrix $\tilde{A}(\nu)$ is defined as in (1.19). After differentiating (2.6) with respect to the independent variable ν, we obtain:

$$D'(\nu) = C'(\nu)\tilde{X}(\nu) + C(\nu)\tilde{X}'(\nu) \tag{2.11}$$

Introducing (2.8) and (2.10) in the previous equations leads to:

$$D'(\nu) = A_D(\nu)D(\nu) \tag{2.12}$$

with the matrix $A_D(\nu)$ defined by:

$$A_D(\nu) = C'(\nu)C^{-1}(\nu) + C(\nu)\tilde{A}(\nu)C^{-1}(\nu) \tag{2.13}$$

The expression for the dynamic matrix $A_D(\nu)$ can be obtained through direct computation:

$$A_D(\nu) = \begin{bmatrix} 0 & 0 & 0 & 0 & 0 & 0 \\ 0 & 0 & 0 & 0 & 0 & 0 \\ -\dfrac{3e}{(1+e\cos\nu)^2} & 0 & 0 & 0 & 0 & 0 \\ \dfrac{3}{(1+e\cos\nu)^2} & 0 & 0 & 0 & 0 & 0 \\ 0 & 0 & 0 & 0 & 0 & 0 \\ 0 & 0 & 0 & 0 & 0 & 0 \end{bmatrix} \tag{2.14}$$

A state transition matrix can be easily computed for the dynamical system (2.12). Assuming that the spacecraft relative motion is propagated using the Yamanaka-Ankersen transition matrix as in (2.1) and using the transformation (2.8), we obtain:

$$D(\nu) = C(\nu)\Phi(\nu,\nu_0)C^{-1}(\nu_0)D(\nu_0) = \Phi_D(\nu,\nu_0)D(\nu_0) \tag{2.15}$$

where the state transition matrix $\Phi_D(\nu, \nu_0)$ is given by:

$$\Phi_D(\nu,\nu_0) = \begin{bmatrix} 1 & 0 & 0 & 0 & 0 & 0 \\ 0 & 1 & 0 & 0 & 0 & 0 \\ -3eJ(\nu,\nu_0) & 0 & 1 & 0 & 0 & 0 \\ 3J(\nu,\nu_0) & 0 & 0 & 1 & 0 & 0 \\ 0 & 0 & 0 & 0 & 1 & 0 \\ 0 & 0 & 0 & 0 & 0 & 1 \end{bmatrix} \tag{2.16}$$

The term $J(\nu, \nu_0)$ is the same integral term defined in (1.33).

The dynamic matrix A_D and the transition matrix Φ_D highlight some interesting properties of the spacecraft relative motion. It can be seen that the parameters d_4 and d_5 that define the motion on the y axis are always constant in time, implying that the motion on the y axis is always bounded. This is consistent with the fact that the motion on the y axis is known to be periodic. The parameters d_0 and d_1 are also constant while the values of d_2 and d_3 change over time. The evolution of d_2 and d_3 is conditioned by the value of d_0. It can be seen that in the general case their modulus grows linearly with respect to time. The parameters remain constant only when $d_0 = 0$ and the importance of this particular case is discussed in what follows.

2.2.2 Properties of periodic trajectories

Expressions (2.2) show that the integral term $J(\nu)$ is the only non periodic term in the propagation of the spacecraft relative position. In the particular case where:

$$d_0(\nu_0) = 0 \tag{2.17}$$

the resulting relative trajectory is *periodic* because the drifting term $J(\nu)$ is cancelled. This leads to the following simplified parametric expressions for the propagation of spacecraft periodic relative trajectories:

$$\begin{aligned} \tilde{x}(\nu) &= (2 + e\cos\nu)(d_1(\nu_0)\sin\nu - d_2(\nu_0)\cos\nu) + d_3(\nu_0) \\ \tilde{y}(\nu) &= d_4(\nu_0)\cos\nu + d_5(\nu_0)\sin\nu \\ \tilde{z}(\nu) &= (1 + e\cos\nu)(d_2(\nu_0)\sin\nu + d_1(\nu_0)\cos\nu) \end{aligned} \tag{2.18}$$

Expressions (2.18) reveal the fact that the spacecraft relative periodic trajectories are always centered around zero on the y and z axes. An offset can be set on the x axis through the d_3 parameter. The parameters corresponding to the amplitude of the motion on the y axis can be

fixed to zero in order to obtain a planar periodic trajectory:

$$d_4 = 0 \quad d_5 = 0 \tag{2.19}$$

and, as in the general case, the dimensions of the trajectory in the xz plane depend on the value of d_1 and d_2. Moreover, according to the dynamics of the vector D given in (2.12), all the parameters are constant in time in the particular case of periodic motion. This means that:

$$C(\nu_i)\tilde{X}(\nu_i) = C(\nu_j)\tilde{X}(\nu_j) = D(\nu_0),\ \forall \nu_i \neq \nu_j \text{ for } D(\nu_0) \text{ such that } d_0(\nu_0) = 0 \tag{2.20}$$

Once the constant vector of parameters corresponding to a periodic trajectory is known, equation (2.8) can be used to calculate at any time the corresponding local Cartesian relative state. This representation offers more flexibility than the typical methods for specifying periodic trajectories which rely on the usage of simple parametric curves, such as circles or ellipses, in order to be able to easily compute the corresponding spacecraft relative state [40, 65, 105].

Given the definition (2.6), it can be seen that for constraint (2.17) to be verified, the spacecraft relative state must satisfy:

$$M_p(\nu)\tilde{X}(\nu) = 0 \tag{2.21}$$

where $M_p(\nu) \in \mathbb{R}^{1\times 6}$ denotes the first line in the $C(\nu)$ matrix (2.5). This periodicity constraint on the relative state is actually equivalent to the initialisation condition (1.41) presented in the Chapter 1. Moreover, if the constraint (2.21) is satisfied at a moment ν_i, it will be satisfied by all the following states belonging to the autonomously propagated trajectory:

$$M_p(\nu_i)\tilde{X}(\nu_i) = 0 \implies M_p(\nu_j)\tilde{X}(\nu_j) = 0,\ \forall \nu_j \geq \nu_i \tag{2.22}$$

This property reflects the fact that the parameter d_0 always has a constant dynamic and it can be very easily verified on the trajectory propagated using the transition matrix.

The constant dynamics of the d_0 parameter have yet another important consequence: trajectories that start arbitrarily close to a periodic trajectory will not naturally converge towards it. If d_0 becomes different from zero as a result of disturbances acting on the system, then a control law will need to be set in place to drive it back to zero and to ensure the periodicity of the relative motion. This unstable behaviour of the periodic relative trajectories is also confirmed by the properties of the monodromy matrix corresponding to the spacecraft relative motion (see the discussion in Appendix A).

2.3 Numerical analysis of the periodic relative motion

The form of expressions (2.2) suggests that the values of the parameters D are connected to the dimensions of the spacecraft relative trajectory. However, even in the case of periodic relative motion where the relative trajectory is defined by the simplified expressions in (2.18), it is not possible to precisely define the nature of this dependency just by analysing the propagation equations. Numerical examples are used here in order to support some of the observations made in the previous sections.

To simplify the analysis, we consider only planar periodic relative trajectories that have no offset on the x axis. This type of trajectory is defined by a vector of parameters of the form:

$$D = \begin{bmatrix} 0 & d_1 & d_2 & 0 & 0 & 0 \end{bmatrix}^T \tag{2.23}$$

2.3.1 The effects of the eccentricity of the leader orbit

The transformation matrix $F(\nu)$ between the Cartesian spacecraft relative state and the vector of parameters D depends on the eccentricity of the orbit of the leader satellite. This suggests that for reference orbits of different eccentricities, the same constant vector of parameters may produce periodic trajectories that display different geometrical characteristics. The influence of the eccentricity is analysed using a vector of parameters of the form (2.23) for which:

$$d_1 = -1 \quad d_2 = -1$$

For this particular choice for the vector D, Figure 2.2 illustrates the change in the shape of the obtained periodic trajectory caused by the change in the eccentricity of the reference orbit. For small eccentricities the periodic trajectory appears to be symmetrical and resembles an ellipsoid. However, for higher eccentricities the obtained trajectory becomes increasingly "irregular". This supports the observation made in [48] that the projections of a spacecraft periodic relative trajectory onto the xz, xy or yz plans are not ellipses in the general case.

2.3.2 The effects of the values of the parameters

In order to study the effect of the sign of the d_1 and d_2 parameters on the resulting periodic trajectory, we consider a vector of parameters in the form (2.23) for which:

$$|d_1| = |d_2| = 1$$

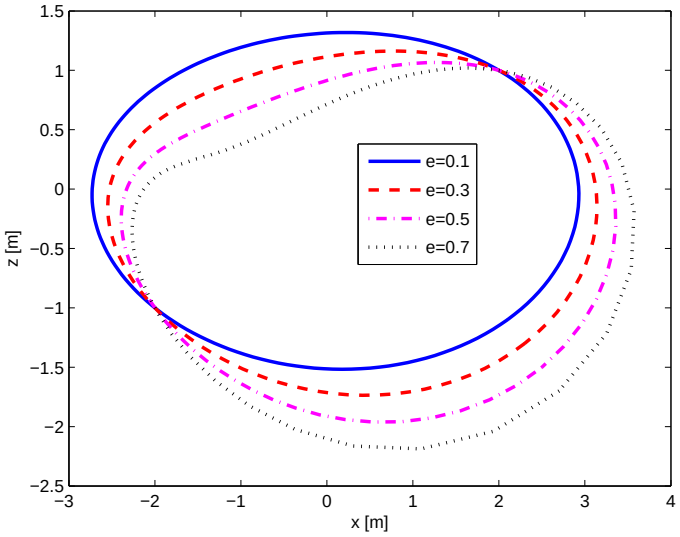

Figure 2.2: The effect of the eccentricity on the obtained periodic trajectory

Figure 2.3 depicts the periodic relative trajectories obtained for a reference trajectory of eccentricity $e = 0.5$. It can be noticed that a change in the sign of d_1 causes a rotation of 180° around the x axis of the original trajectory. A change in the sign of d_2 causes instead a rotation of 180° around the z axis of the original trajectory.

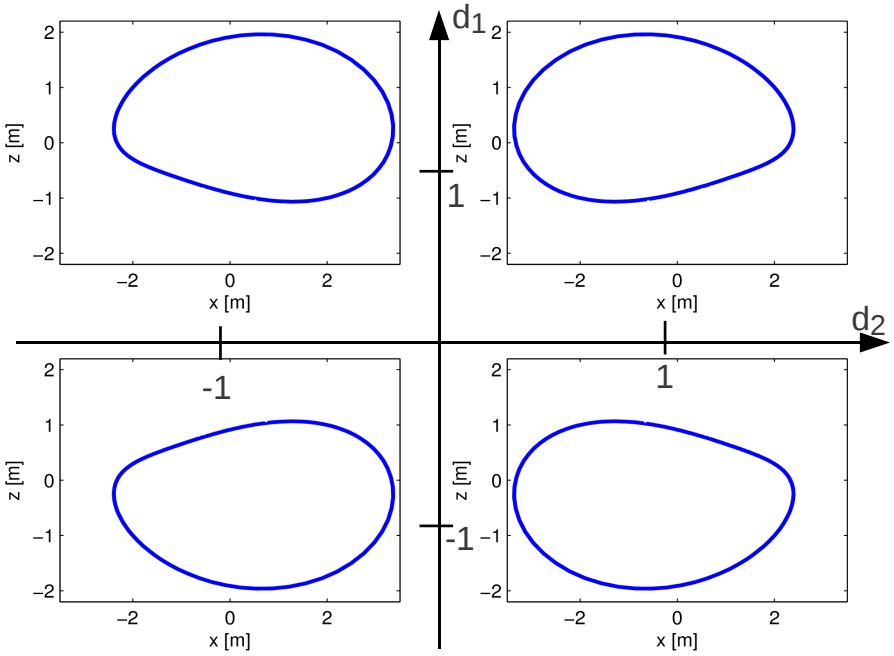

Figure 2.3: The effect of the sign of the parameters on the periodic trajectory for $e = 0.5$

For reference trajectories that have different eccentricities, Figures 2.4 and 2.5 illustrate the effects of the values of the parameters d_1 and d_2 on the spacecraft periodic relative motion. For smaller eccentricities, the obtained periodic trajectory is nearly symmetrical so the effect of increasing d_1 is similar to that of increasing d_2 (Figure 2.4). However, for higher eccentricities, the effects of the two parameters become quite different (Figure 2.5).

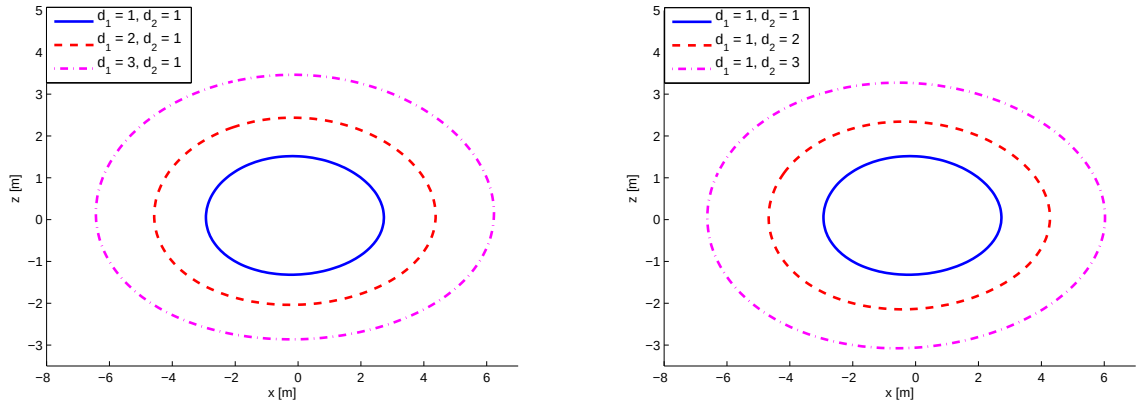

Figure 2.4: The effect of a change in the parameters for a reference trajectory of $e = 0.1$

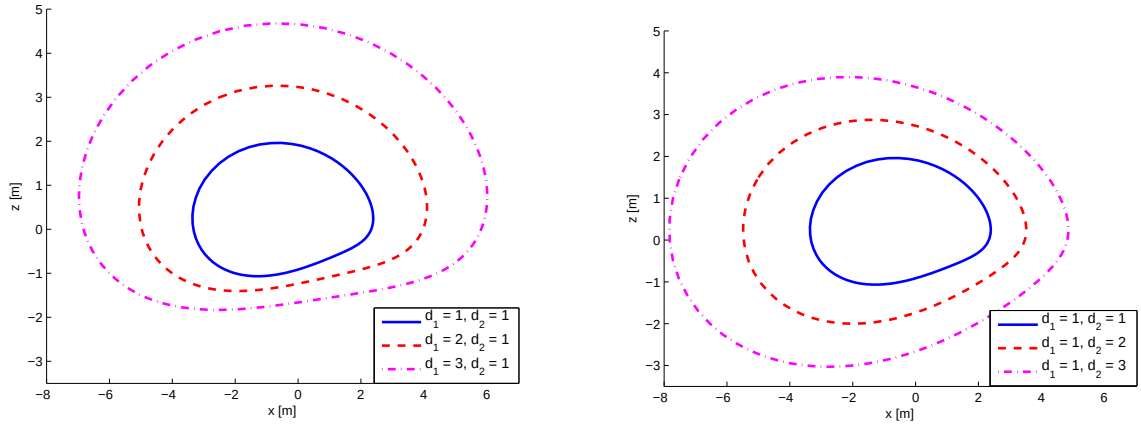

Figure 2.5: The effect of a change in the parameters for a reference trajectory of $e = 0.5$

Other than the influence on the shape of the obtained trajectory, it can be seen that the eccentricity of the orbit of the leader satellite also determines how much a change in the values of the parameters reflects into a change in the dimensions of the resulting periodic trajectory. Given the complex nature of this interaction, general conclusions cannot be drawn from just a few numerical examples. The aim of these examples was to emphasize the need for a precise mathematical characterisation of the connection between the dimensions of a periodic trajectory, the vector of parameters that describes it and the eccentricity of the reference orbit.

2.4 Conclusion

New parametric expressions for the spacecraft relative trajectory are derived from the linearized Cartesian model of relative motion. The obtained parametrization provides a new state vector whose dynamics can be used to study the properties of the spacecraft relative motion. The analysis of the equations defining the dynamics of the vector of parameters shows that every spacecraft periodic relative trajectory corresponds to an equilibrium point of this new state space representation.

The intuitive form of the parametric expressions allows us to directly identify some of the effects that the choice of some particular values for the parameters have on the resulting relative trajectory, especially in the case of periodic spacecraft relative motion. However, the presented numerical examples suggest that the shape and the dimensions of the spacecraft periodic trajectories depend in fact on the complex interaction between the eccentricity of the leader's orbit and the value of the parameters. These examples emphasise the need for a precise mathematical characterisation of the vector of parameters corresponding to relative trajectories that respect some dimensions constraints.

Chapter 3

Constrained spacecraft relative trajectories

Contents

Résumé: Le présent chapitre fournit une description formelle de l'ensemble des paramètres correspondant à des trajectoires relatives inscrites dans un sous ensemble particulier de l'espace d'état relatif. Pour caractériser le lien entre les valeurs des paramètres et la dimension des trajectoires obtenues, il faut tenir compte d'une part de l'influence de l'excentricité et d'autre part de la présence du terme intégral $J(\nu)$ dans le cas général. De plus, comme les contraintes sur la dimension doivent généralement être respectées de manière continue sur un intervalle de temps fixé, il n'est pas facile d'obtenir une description des paramètres admissibles qui soit facilement exploitable dans un algorithme de guidage des satellites. En se basant sur les propriété des polynômes non-négatifs, ce chapitre donne une description mathématique précise de l'ensemble des paramètres admissibles. Cette description est finie et compatible avec les algorithmes de programmation semi-définie positive.

The previous chapter emphasized the need for a rigorous mathematical characterization of the set of vectors of parameters that correspond to spacecraft relative trajectories which respect some dimensions constraints. Even in the simpler case of periodic relative motion, a precise description of the admissible trajectories has not yet been reached. The main difficulty lies in the characterisation, for a given set of parameters, of the influence of the eccentricity of the reference orbit on the resulting

relative trajectory. In the general case, the presence of the integral term $J(\nu)$ in the expression of the relative trajectory renders the analysis even more complex.

Another challenge comes from the fact that the dimensions constraints on the trajectory usually need to be imposed *continuously* in time over a specified interval. This translates into an *infinite* number of conditions that need to be verified in order to certify that a given trajectory respects the desired dimensions requirements.

This chapter provides a solution to these problems in the form of a finite convex description of the admissible spacecraft relative trajectories for a given set of dimensions constraints.

3.1 Definition of admissible trajectories

From a mathematical point of view, the constraints on the dimensions of the spacecraft relative trajectories can be written as linear constraints on the spacecraft relative positions:

$$\begin{array}{l} x_{\min} \leq x(t) \leq x_{\max} \\ y_{\min} \leq y(t) \leq y_{\max} \quad , \ \forall t \in [t_0 \ t_f] \\ z_{\min} \leq z(t) \leq z_{\max} \end{array} \iff \begin{array}{l} \tilde{x}_{\min}(\nu) \leq \tilde{x}(\nu) \leq \tilde{x}_{\max}(\nu) \\ \tilde{y}_{\min}(\nu) \leq \tilde{y}(\nu) \leq \tilde{y}_{\max}(\nu) \quad , \ \forall \nu \in [\nu_0 \ \nu_f] \\ \tilde{z}_{\min}(\nu) \leq \tilde{z}(\nu) \leq \tilde{z}_{\max}(\nu) \end{array} \tag{3.1}$$

Equation (3.1) illustrates the effects of the variable change (1.17) on the dimension constraints: the constant minimum and maximum bounds for the time domain transform into bounds that depend on the true anomaly of the leader spacecraft ν. The constraints must be respected continuously on the intervals $[t_0 \ t_f]$ and $[\nu_0 \ \nu_f]$ respectively.

The constraints in (3.1) can be written in a more compact way as:

$$H \, \tilde{X}(\nu) \leq \tilde{V}(\nu), \ \forall \nu \in [\nu_0 \ \nu_f] \tag{3.2}$$

where the matrices H and V define a generic polytopic set. Using the definition in (3.2), the set of spacecraft relative states starting from which the autonomously propagated trajectories remain inside the polytopic set (H, V) during the specified interval can be defined as:

$$S(H, V, \nu_0, \nu_f) = \left\{ \tilde{X}(\nu_0) \in \mathbb{R}^6 \mid \tilde{X}(\nu) = \Phi(\nu, \nu_0) \tilde{X}(\nu_0), \ H \, \tilde{X}(\nu) \leq \tilde{V}(\nu), \ \forall \nu \in [\nu_0 \ \nu_f] \right\} \tag{3.3}$$

An equivalent form can be given to the set of parameters defining relative trajectories that respect

the given trajectory constraints during the specified interval:

$$S_D(H,V,\nu_0,\nu_f)=\left\{D(\nu_0)\in\mathbb{R}^6 \mid D(\nu)=\Phi_D(\nu,\nu_0)D(\nu_0),\ H\,F(\nu)D(\nu)\leq\tilde{V}(\nu),\ \forall\nu\in[\nu_0\ \nu_f]\right\} \tag{3.4}$$

with the matrix $F(\nu)$ defined in (2.9).

The admissible spacecraft relative trajectories are described in (3.3) and (3.4) using only *linear* constraints. However, it should be noted that the trajectory constraints need to be verified *continuously* on the specified interval. As a consequence, an *infinite* number of conditions need to be checked in order to certify that a state or a vector of parameters correspond to a trajectory which respects the specified requirements.

As seen in Chapter 2, the periodic spacecraft relative trajectories can be described by a constant set of parameters. However, the set of parameters defining admissible periodic spacecraft relative trajectories is still defined by infinitely many conditions. This happens because the constraints themselves depend on the true anomaly of the leader spacecraft:

$$S_D^p(H,V)=\left\{D\in\mathbb{R}^6 \mid d_0=0,\ H\,F(\nu)D\leq\tilde{V}(\nu),\ \forall\nu\in[0\ 2\pi]\right\} \tag{3.5}$$

The interval on which the constraints need to be checked is limited to one orbital period in this case because the trajectory is periodic, but checking that a vector D defines an admissible trajectory is still a hard problem.

Inside a given polytopic set there can be found many trajectories that respect the dimensions constraints (see Figure 3.1). We are interested in obtaining a finite description of *all* these admissible trajectories.

3.2 Finite description of admissible trajectories

Imposing continuous constraints on the spacecraft relative trajectories leads to a description of the admissible trajectories using an infinite number of constraints. The provided description is accurate but not very well suited for trajectory design purposes. This is due to the difficulty in certifying that a given trajectory respects all the required conditions. Two methods for reaching a finite description of the admissible trajectories are presented in what follows.

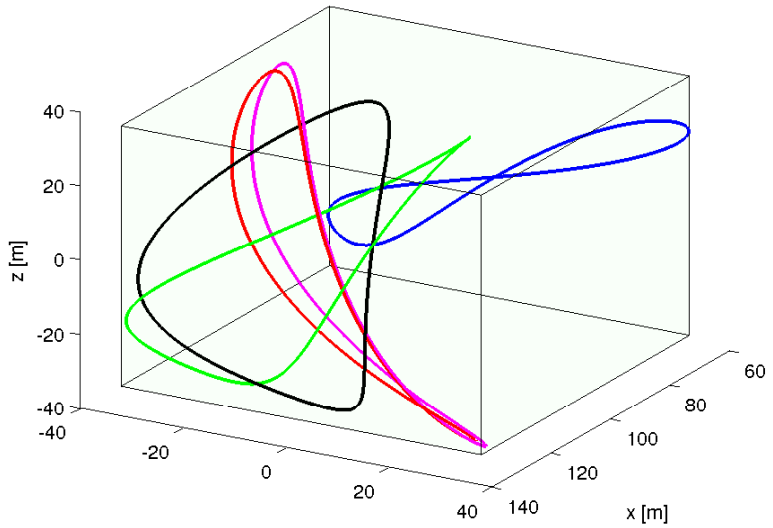

Figure 3.1: Examples of periodic spacecraft relative trajectories that evolve inside a polytopic set

3.2.1 Finite description using constraints discretization

A straightforward method for rendering the number of constraints finite consists in the so-called *constraints discretization*. The original continuous constraints are replaced by constraints that are checked only at some specified locations [17, 19, 99]. The definition in (3.4) for instance is replaced by:

$$S_D(H,V,\nu_0,m) = \Big\{ D(\nu_0) \in \mathbb{R}^6 \mid D(\nu_k) = \Phi_D(\nu_k,\nu_0)D(\nu_0),\ H\,F(\nu_k)D(\nu_k) \leq \tilde{V}(\nu_k),\ k = 1..m \Big\} \tag{3.6}$$

where m refers to the number of points where the constraints are explicitly verified.

The problem with this type of approach is that the accuracy of the obtained solution depends on the specific choice made for the different parameters, like the number of discretization points and their particular distribution over the original interval. Moreover, this type of methods do not provide a rigorous characterisation of the obtained results. There are no theoretical guarantees that no constraints violations will occur in between the discretization points and *a posteriori* checks are needed in order to validate the solution.

3.2.2 Finite description using non-negative polynomials

The idea of using the properties of non-negative polynomials to obtain a finite description of the admissible spacecraft relative trajectory came from the desire to exploit the structure of the solution

for the relative motion provided by the transition matrix. The expressions (2.18) show that for the periodic relative motion the trajectory is defined by trigonometric polynomials. In this case, the dimension constraints (3.1) can be easily written as polynomial non-negativity constraints.

In the general case, the presence of the integral term $J(\nu)$ in the expressions of the spacecraft relative trajectory renders the approach more complex. In order to reach a polynomial description of the admissible trajectories, the term $J(\nu)$ can be replaced with a suitable approximation. The complete procedure is presented in detail in the following section.

Once the dimensions constraints on the spacecraft relative trajectory are transformed into polynomial non negativity constraints of the type:

$$P(w) \geq 0, \ \forall w \in \mathcal{W} \tag{3.7}$$

the results presented by Nesterov in [73] can be used in order to obtain a finite description of the admissible trajectories without relying on discretization. It is showed that polynomial non negativity constraints can be transformed into conditions of existence of one or two constrained positive semi-definite matrices (see Appendix B). The infinite number of points where the polynomial non-negativity constraint needed to be checked can be replaced with only one Linear Matrix Inequality (LMI) constraint.

3.3 Description of constrained trajectories using non negative polynomials

3.3.1 Rational expressions for the spacecraft relative motion

The following variable change can be used in order to transform the trigonometrical terms in the expressions for the propagation of the spacecraft relative trajectory into rational terms:

$$w = \tan\left(\frac{\nu}{2}\right), \quad \cos\nu = \frac{1-w^2}{1+w^2}, \quad \sin\nu = \frac{2w}{1+w^2}, \tag{3.8}$$

Introducing (3.8) into (2.2) leads to the following expressions for the spacecraft relative positions:

$$\begin{aligned} \tilde{x}(w) &= \frac{1}{(1+w^2)^2}\left[P_x(w) + 3\,d_0\,P_{Jx}(w)\,J(w)\right] \\ \tilde{y}(w) &= \frac{1}{1+w^2}P_y(w) \qquad\qquad\qquad\qquad , w \geq w_0 \\ \tilde{z}(w) &= \frac{1}{(1+w^2)^2}\left[P_z(w) + 2\,d_0\,P_{Jz}(w)\,J(w)\right] \end{aligned} \tag{3.9}$$

where the polynomials $P_{Jx}(w)$ and $P_{Jz}(w)$ depend only on the eccentricity of the orbit of the leader satellite and are given by:

$$P_{Jx}(w) = ((1+e) + (1-e)w^2)^2 \quad P_{Jz}(w) = -3e((1-e)w + (1-e)w^3) \tag{3.10}$$

and the term $J(w)$ is obtained by introducing the variable change (3.8) into (1.33):

$$J(w) = \int_{w_0}^{w} \frac{2\,\tau^2 + 2}{((1-e)\tau^2 + e + 1)^2} d\tau \tag{3.11}$$

The polynomials $P_x(w)$, $P_y(w)$ and $P_z(w)$ are defined by:

$$P_x(w) = \sum_{i=0}^{4} p_{xi}\, w^i \quad P_y(w) = \sum_{i=0}^{2} p_{yi}\, w^i \quad P_z(w) = \sum_{i=0}^{4} p_{zi}\, w^i \tag{3.12}$$

and their vectors of coefficients, $p_x = \begin{bmatrix} p_{x0} & p_{x1} & p_{x2} & p_{x3} & p_{x4} \end{bmatrix}^T$, $p_y = \begin{bmatrix} p_{y0} & p_{y1} & p_{y2} \end{bmatrix}^T$ and $p_z = \begin{bmatrix} p_{z0} & p_{z1} & p_{z2} & p_{z3} & p_{z4} \end{bmatrix}^T$ respectively, depend linearly on the vector of parameters $D(\nu_0)$:

$$p_x = C_x\, D(\nu_0) \quad p_y = C_y\, D(\nu_0) \quad p_z = C_z\, D(\nu_0) \tag{3.13}$$

The matrices C_x, C_y and C_z depend only on the eccentricity of the reference orbit and are given by:

$$C_x = \begin{bmatrix} 0 & 0 & -2-e & 1 & 0 & 0 \\ 0 & 4+2e & 0 & 0 & 0 & 0 \\ 0 & 0 & 2e & 2 & 0 & 0 \\ 0 & 4-2e & 0 & 0 & 0 & 0 \\ 0 & 0 & 2-e & 1 & 0 & 0 \end{bmatrix} \quad C_y = \begin{bmatrix} 0 & 0 & 0 & 0 & 1 & 0 \\ 0 & 0 & 0 & 0 & 0 & 2 \\ 0 & 0 & 0 & 0 & -1 & 0 \end{bmatrix} \quad C_z = \begin{bmatrix} 0 & e+1 & 0 & 0 & 0 & 0 \\ 0 & 0 & 2e+2 & 0 & 0 & 0 \\ 0 & -2e & 0 & 0 & 0 & 0 \\ 0 & 0 & 2-2e & 0 & 0 & 0 \\ 0 & e-1 & 0 & 0 & 0 & 0 \end{bmatrix} \tag{3.14}$$

The idea behind the usage of the transformation (3.8) is to obtain a description of the spacecraft relative trajectories that contains only terms of the same nature. The final purpose is to reach some polynomial expressions for the constrained spacecraft relative motion that can lead to a finite description of the admissible trajectories. The expressions (2.2) contain a combination of integral and trigonometric terms and even expressions (3.9) are not entirely rational because of the presence of the term $J(w)$. Without further manipulations, the spacecraft relative trajectory is defined by rational expressions only in the case of periodic motion. When $d_0 = 0$, the relative trajectory is

given by:

$$\tilde{x}(w) = \frac{1}{(1+w^2)^2} P_x(w) \quad \tilde{y}(w) = \frac{1}{1+w^2} P_y(w) \quad \tilde{z}(w) = \frac{1}{(1+w^2)^2} P_z(w) \tag{3.15}$$

The advantage of introducing the variable change (3.8) is that, if the integral term $J(w)$ is replaced by a *polynomial approximation*, then the obtained expressions for the spacecraft relative motion contain only rational terms. These expressions will allow us to characterize all the spacecraft relative trajectories that respect some dimensions constraints.

Polynomial approximation of the integral term $J(w)$

Even if the integral term (3.11) has a closed form solution given by:

$$J(w) = \left[\frac{2\,e\,w}{(e^2-1)(e+1+(1-e)w^2)} - \frac{2\text{arctanh}\left(\frac{\sqrt{e-1}}{\sqrt{e+1}}w\right)}{\sqrt{(e^2-1)^3}} \right]_{w_0}^{w} \tag{3.16}$$

the nature of the terms involved in its definition does not bring us closer to our objective. Results in [21] show that a fixed-degree polynomial approximation with a *certified maximum approximation error* can be computed for the integral expression (3.11). However, the interval on which $J(w)$ can be approximated by a polynomial must be a finite subset of $\mathbb{R}$. This comes from the fact that the term $J(w)$ is discontinuous on the bounds of its definition set (i.e. from (3.16): $\lim_{w\to-\infty} J(w) \neq \lim_{w\to\infty} J(w)$) and consequently no polynomial or rational function can approximate $J(w)$ on $\mathbb{R}$.

Let $\Theta_q(w)$ be a polynomial of degree q such that:

$$\Theta_q(w) - \varepsilon \leq J(w) \leq \Theta_q(w) + \varepsilon, \ \forall w \in W \tag{3.17}$$

where W represents the interval on which the polynomial approximation is valid and ε represents the maximum approximation error on that interval. Following from (3.17), upper and lower polynomial bounds for the term $J(w)$ can be defined on the interval W:

$$\Theta_u(w) = \Theta_q(w) + \varepsilon, \quad \Theta_l(w) = \Theta_q(w) - \varepsilon \tag{3.18}$$

These polynomial bounds can be combined with expressions (3.9) in order to obtain rational

bounds for the xz spacecraft relative trajectory in the general case:

$$\begin{aligned} \tilde{x}_{l,u}(w) &= \frac{1}{(1+w^2)^2}\left[P_x(w) + 3\,d_0\,P_{Jx}(w)\,\Theta_{l,u}(w)\right] \\ \tilde{z}_{l,u}(w) &= \frac{1}{(1+w^2)^2}\left[P_z(w) + 2\,d_0\,P_{Jz}(w)\,\Theta_{l,u}(w)\right] \end{aligned}, \ \forall w \in W \tag{3.19}$$

with:

$$\begin{aligned} \tilde{x}_l(w) \le \tilde{x}(w) \le \tilde{x}_u(w) \\ \tilde{z}_l(w) \le \tilde{z}(w) \le \tilde{z}_u(w) \end{aligned}, \ \forall w \in W \tag{3.20}$$

3.3.2 Constrained non periodic trajectories

Let us consider some dimension constraints on the relative trajectories specified through a polytopic set given by some H and V matrices as in (3.2). We assume for simplicity that the constraints are imposed only on the relative positions. By expanding each constraint and integrating the variable change (3.8), we can write:

$$h_{i,1}\,\tilde{x}(w) + h_{i,2}\,\tilde{y}(w) + h_{i,3}\,\tilde{z}(w) \le \frac{1+e+(1-e)w^2}{1+w^2}\,v_i,\ \forall w \in [w_0\ w_f],\ i = 1..s \tag{3.21}$$

where $h_{i,j}$ and v_i are elements in the matrices H and V that define the polytopic set and s is the number of constraints in the definition.

Let us define expressions $\Xi_i(w)$ as:

$$\Xi_i(w) = -h_{i,1}\,\tilde{x}(w) - h_{i,2}\,\tilde{y}(w) - h_{i,3}\,\tilde{z}(w) + \frac{1+e+(1-e)w^2}{1+w^2}\,v_i,\ i = 1..s \tag{3.22}$$

Using expressions (3.22), the set of parameters corresponding to autonomous spacecraft relative trajectories that respect the polytopic constraints over a specified interval $[w_0\ w_f]$ can be defined as:

$$S_D(H, V, w_0, w_f) = \left\{D(w_0) \in \mathbb{R}^6 \mid \Xi_i(w) \ge 0,\ \forall w \in [w_0\ w_f],\ i = 1..s\right\} \tag{3.23}$$

By bringing the terms to the lowest common denominator, a more compact form can be obtained for $\Xi_i(w)$:

$$\Xi_i(w) = \frac{1}{(1+w^2)^2}\,\Gamma_i(w),\ i = 1..s \tag{3.24}$$

where the polynomials $\Gamma_i(w)$ are defined by:

$$\Gamma_i(w) = -h_{i,1}\left[P_x(w) + 3\,d_0\,P_{Jx}(w)\,J(w)\right] - h_{i,2}\,\bar{P}_y(w) - h_{i,3}\left[P_z(w) + 2\,d_0\,P_{Jz}(w)\,J(w)\right] + v_i\,T(w) \tag{3.25}$$

In the previous definition the polynomial $\bar{P}_y(w)$ is obtained as $\bar{P}_y(w) = (1+w^2)P_y(w)$ and the polynomial $T(w)$ is given by $T(w) = \sum_{i=0}^{4} t_i\, w^i$ with the vector of coefficients $t = \begin{bmatrix} 1+e & 0 & 2 & 0 & 1-e \end{bmatrix}^T$. The coefficients of the other polynomials in (3.25) depend on the vector of parameters D, as defined in (3.12).

The term $(1+w^2)^2$ in (3.24) is non negative for all $w \in \mathbb{R}$. This means that the set $S_D(H, V, w_0, w_f)$ can also be defined as:

$$S_D(H, V, w_0, w_f) = \left\{ D(w_0) \in \mathbb{R}^6 \mid \Gamma_i(w) \geq 0,\ \forall w \in [w_0\ w_f],\ i = 1..s \right\} \tag{3.26}$$

Let $\Gamma_i^l(w)$ and $\Gamma_i^u(w)$ be the polynomials obtained from expressions $\Gamma_i(w)$ after replacing the integral term $J(w)$ with its lower and upper polynomial bounds, $\Theta_l(w)$ and $\Theta_u(w)$ respectively. In this case we have:

$$\Gamma_i^l(w) \leq \Gamma_i(w) \leq \Gamma_i^u(w) \tag{3.27}$$

where:

$$\begin{aligned} \Gamma_i^l(w) &= -h_{i,1}\left[P_x(w) + 3\,d_0\,P_{Jx}(w)\,\Theta_l(w)\right] - h_{i,2}\,\bar{P}_y(w) - h_{i,3}\left[P_z(w) + 2\,d_0\,P_{Jz}(w)\,\Theta_l(w)\right] + v_i\,T(w) \\ \Gamma_i^u(w) &= -h_{i,1}\left[P_x(w) + 3\,d_0\,P_{Jx}(w)\,\Theta_u(w)\right] - h_{i,2}\,\bar{P}_y(w) - h_{i,3}\left[P_z(w) + 2\,d_0\,P_{Jz}(w)\,\Theta_u(w)\right] + v_i\,T(w) \end{aligned} \tag{3.28}$$

The degree of the polynomials $\Gamma_i^l(w)$ and $\Gamma_i^u(w)$ depends on the degree of the polynomial approximation of $J(w)$. Considering the definitions given in (3.13), it can be noted that the coefficients of the polynomials in (3.28), denoted γ_i^l and γ_i^u respectively, are constant and depend *linearly* on the value of the vector of parameters D at the beginning of the interval $[w_0\ w_f]$.

The polynomials $\Gamma_i^l(w)$ and $\Gamma_i^u(w)$ allow for the set $S_D(H, V, w_0, w_f)$ to be defined using only polynomial non negativity constraints:

$$S_D(H, V, w_0, w_f) = \left\{ D(w_0) \in \mathbb{R}^6 \mid \Gamma_i^l(w) \geq 0,\ \Gamma_i^u(w) \geq 0,\ \forall w \in [w_0\ w_f],\ i = 1..s \right\} \tag{3.29}$$

The constraints on the expressions $\Gamma_i(w)$ have been replaced by constraints on its upper and lower polynomial bounds. The resulting increased number of constraints is the price to pay for robustness with respect to approximation errors for the term $J(w)$.

Using the connection between the coefficients of non negative polynomials and the symmetric positive semi-definite matrices given in [73], the set $S_D(H, V, w_0, w_f)$ can be defined using a finite

number of constraints:

$$S_D(H,V,w_0,w_f)=\left\{ D(w_0)\in\mathbb{R}^6 \;\middle|\; \begin{array}{l} \exists\, Y_{i1}^l, Y_{i2}^l \succeq 0 \text{ s.t. } \gamma_i^l=\Lambda^*(Y_{i1}^l,Y_{i2}^l) \\ \exists\, Y_{i1}^u, Y_{i2}^u \succeq 0 \text{ s.t. } \gamma_i^u=\Lambda^*(Y_{i1}^u,Y_{i2}^u) \end{array} ,\ \forall i=1..s \right\} \tag{3.30}$$

The linear operator Λ^* is defined as in (B.4) or as in (B.5), depending on the case. The dimensions of the positive semi-definite matrices involved depend on the degree of the polynomial approximations for the $J(w)$ term, $\Theta_l(w)$ and $\Theta_u(w)$. Please note that to every non negativity constraint in (3.29) corresponds a pair of matrices Y_1, Y_2. Each polynomial non negativity constraint that needed to be checked for infinitely many points has now been replaced by an equality constraint on the coefficients of that polynomial. This means that $S_D(H,V,w_0,w_f)$ is defined using only linear restrictions on the vector of parameters D at the beginning of the chosen interval.

3.3.3 Constrained periodic trajectories

The description of the admissible trajectories is simplified in the case of periodic spacecraft relative motion. The periodic trajectories that respect some polytopic constraints can be defined directly in terms of non negativity conditions of some polynomials, without any need for approximations. In the periodic case, the expressions in (3.25) become:

$$\Gamma_i^p(w)=-h_{i,1}\,P_x(w)-h_{i,2}\,\bar{P}_y(w)-h_{i,2}\,P_z(w)+v_i\,T(w) \tag{3.31}$$

This leads to the definition of the set of constant parameters that correspond to admissible trajectories using a finite number of polynomial non negativity constraints:

$$S_D^p(H,V)=\left\{D\in\mathbb{R}^6 \mid d_0=0,\ \Gamma_i^p(w)\geq 0,\ \forall w\in\mathbb{R},\ i=1..s\right\} \tag{3.32}$$

The non negativity of the polynomials $\Gamma_i^p(w)$ needs to be checked on an infinite interval since the variable change (3.8) maps one orbital period to $\mathbb{R}$.

Using the property of non negative polynomials on infinite intervals given in [73], the set of parameters corresponding to spacecraft periodic relative trajectories that evolve inside a specified polytopic set can be defined as:

$$S_D^p(H,V)=\left\{ D\in\mathbb{R}^6 \;\middle|\; \begin{array}{l} d_0=0 \\ \exists\, Y_i\succeq 0 \text{ s.t } \gamma_i^p=\Lambda^*(Y_i),\ \forall i=1..s \end{array} \right\} \tag{3.33}$$

where γ_i^p are the vectors of coefficients corresponding to the polynomials $\Gamma_i^p(w)$. As for the non

periodic case, γ_i^p depend linearly on the value of the vector of parameters D. Since we are dealing with periodic trajectories, the vector of parameters is constant over the infinite interval. The degree of the polynomials $\Gamma_i^p(w)$ is easy to compute in this case and is less or equal to 4 (see (3.31) and (3.12)). This means that the variables Y_i are at most 3 by 3 matrices.

3.4 Conclusion

When continuous constraints need to be imposed on the spacecraft relative trajectory, the set of admissible trajectories is described using an infinite number of constraints that need to be checked in order to validate an obtained solution.

A new method for rendering the description of admissible trajectories finite is presented in this chapter. The method exploits the structure of the solution for the spacecraft relative motion provided by the transition matrix and it is based on the properties of non negative polynomials. The presence of the integral term $J(w)$ determines the usage of rational expressions for the description of the spacecraft relative motion. In this framework, the term $J(w)$ can be approximated by a polynomial, leading to a description of the admissible trajectories using only polynomial constraints.

Unlike the classical constraints discretization approach, the presented method provides a finite characterisation of the admissible trajectories that guarantees continuous satisfaction of the constraints. Checking that a solution belongs to the set of admissible trajectories is translated into checking the existence of some constrained semi-definite positive matrices. This description of the admissible trajectories is used in the following chapter as part of a spacecraft relative trajectory design procedure.

Chapter 4

Trajectory design for spacecraft rendezvous

Contents

Résumé: Le guidage en rendez-vous orbital consiste à déterminer une série des manœuvres impulsionnelles qui amènent le satellite chasseur en proximité de la cible. Le calcul des manœuvres doit tenir compte simultanément des différentes contraintes de la mission donnée, comme des contraintes de sécurité, des contraintes de visibilité ou des contraintes de passage par une série des positions prédéfinies. Les ressources en ergols étant limitées, le plan de manœuvres obtenu doit aussi minimiser la consommation de combustible. Dans un premier temps, ce chapitre formule le problème de guidage comme un problème de commande optimale sous contraintes. Le cadre choisi est celui des méthodes directes de tirs qui exploitent la transition du mouvement relatif pour convertir le problème de commande optimale en problème d'optimisation paramétrique. La description des trajectoires admissible développée dans le chapitre précédent est utilisée pour garantir que les trajectoires obtenues respectent les contraintes données.

The orbital rendezvous guidance problem consists in computing a series of orbital maneuvers

that successively bring the chaser vehicle in the vicinity of and eventually in contact with the target spacecraft. These maneuvers must account for the different conditions and constraints that must be fulfilled in order to guarantee the success of the mission. The operations in the vicinity of the target spacecraft may impose safety constraints, approach-trajectory corridors and waiting points along the trajectory for verifying the vehicle functions and other conditions. Since the propellant is such an important resource in spacecraft applications, the approach maneuvers must be optimal from a fuel consumption point of view. Moreover, the amplitude of the computed maneuvers must also respect the physical limitations of the spacecraft thrusters.

The general mathematical formulation for the fixed-time spacecraft rendezvous guidance problem is presented at the beginning of this chapter. It is showed that, in the context of direct shooting methods, the optimal control problem can be written as a linear program. In addition, the case where different types of trajectory constraints need to be introduced in the guidance problem is also considered. For each of the considered spacecraft trajectory constraints, the control problem is constructed by integrating the mathematical description of the admissible relative trajectories given in Chapter 3. The resulting solution is guaranteed to lead to a rendezvous trajectory which satisfies *continuously* the specified constraints.

4.1 Fixed-time linearized impulsive spacecraft rendezvous

In the context of the fixed-time rendezvous guidance problem, the duration of the rendezvous mission is considered to be fixed and known *a priori*. The spacecraft thrust maneuvers are approximated with impulsive maneuvers, meaning that their effect is modelled as an instantaneous change in the spacecraft relative velocity. Moreover, the number of thrusts N and the thrusting instants are also fixed *a priori*. The decision variables are represented by the amplitudes of the velocity changes expressed in the LVLH frame attached to the leader spacecraft.

4.1.1 General formulation of the guidance problem

The trajectory design for spacecraft rendezvous relies on the computation of an impulsive maneuvers plan that brings the spacecraft from some known initial conditions $\tilde{X}_0$ to some desired final conditions $\tilde{X}_f$. This needs to be done while minimising the total fuel cost of the maneuvres and while respecting the actuators saturations constraints. Since the thrusting instants $\nu_1, ..., \nu_N$ are considered known, the decision variables are the magnitudes of the thrusts $\Delta\tilde{V}_i$.

Assuming that the spacecraft relative dynamics are represented using the linearized model

defined in (1.18), the corresponding optimal control problem can be written as:

$$\begin{aligned} \min_{\Delta\tilde{V}_i} \quad & J(\boldsymbol{\Delta\tilde{\mathbf{V}}}) \\ \text{s.t.} \quad & \begin{cases} \tilde{X}'(\nu) = \tilde{A}(\nu)\tilde{X}(\nu) + B\sum_i \Delta\tilde{V}_i\delta(\nu-\nu_i) \\ \tilde{X}(\nu_1) = \tilde{X}_1 \\ \tilde{X}(\nu_N) = \tilde{X}_f \\ \Delta\tilde{V}_i \in \tilde{\mathcal{U}}_{\max}(\nu_i),\ \forall i = 1...N \end{cases} \end{aligned} \tag{4.1}$$

where the Dirac function $\delta(\nu)$ is used to model the impulsive nature of the control. This writing of the problem supposes that the first impulsive control is applied at the initial true anomaly and that the last impulsive control is applied at the final true anomaly. The variable $\tilde{X}(\nu_N)$ represents the spacecraft relative state *right after* the last thrust is fired.

The control vectors $\Delta\tilde{V}_i \in \mathbb{R}^3$ are defined in the leader's LVLH frame:

$$\Delta\tilde{V}_i = \begin{bmatrix} \Delta\tilde{V}_{i_x} \\ \Delta\tilde{V}_{i_y} \\ \Delta\tilde{V}_{i_z} \end{bmatrix},\ \forall i = 1...N \tag{4.2}$$

and $\boldsymbol{\Delta\tilde{\mathbf{V}}}$ denotes the stacked control vectors: $\boldsymbol{\Delta\tilde{\mathbf{V}}}^{\mathbf{T}} = \begin{bmatrix} \Delta\tilde{V}_1^T & \dots & \Delta\tilde{V}_N^T \end{bmatrix} \in \mathbb{R}^{3N}$.

4.1.2 Consumption criteria

The minimization criterion $J(\Delta\tilde{V})$ needs to be related to the total fuel cost of the mission in order to accurately represent the guidance requirements. According to [83], a criterion that accurately reflects the fuel consumption must take into consideration the number of thrusters of the spacecraft and their configuration.

In the case where a single thruster steers the spacecraft by gimbaling (see case (a) in Figure 4.1), the optimal fuel consumption criterion is obtained from the rocket equation as:

$$J(\Delta\tilde{V}) = \sum_{i=1}^{N} \|\Delta\tilde{V}_i\|_2 = \sum_{i=1}^{N} \sqrt{\Delta\tilde{V}_{i_x}^2 + \Delta\tilde{V}_{i_y}^2 + \Delta\tilde{V}_{i_z}^2} \tag{4.3}$$

The fuel cost in (4.3) is different from the classical quadratic cost since:

$$J(\Delta\tilde{V})^2 = \left(\sum_{i=1}^{N} \sqrt{\Delta\tilde{V}_{i_x}^2 + \Delta\tilde{V}_{i_y}^2 + \Delta\tilde{V}_{i_z}^2}\right)^2 \neq \sum_{i=1}^{N} \left(\Delta\tilde{V}_{i_x}^2 + \Delta\tilde{V}_{i_y}^2 + \Delta\tilde{V}_{i_z}^2\right) \tag{4.4}$$

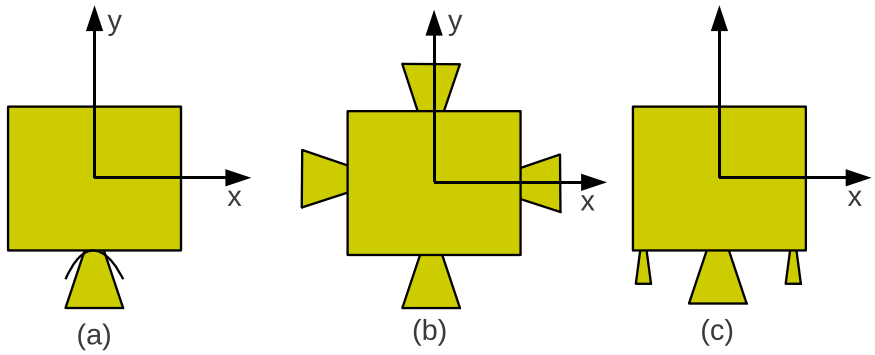

Figure 4.1: Spacecraft thrusters configurations

Reference [83] also shows that in the case where the spacecraft is equipped with six identical thrusters rigidly mounted on its axes (see case (b) in Figure 4.1), the criterion that best reflects the fuel consumption is given by:

$$J(\Delta\tilde{V}) = \sum_{i=1}^{N} \|\Delta\tilde{V}_i\|_1 = \sum_{i=1}^{N} \left(|\Delta\tilde{V}_{i_x}| + |\Delta\tilde{V}_{i_y}| + |\Delta\tilde{V}_{i_z}| \right) = \|\boldsymbol{\Delta\tilde{\mathbf{V}}}\|_1 \tag{4.5}$$

If there exists just one main engine that performs the guidance while vernier engines steer the thrust vector (see case (c) in Figure 4.1), the fuel consumption is best represented by:

$$J(\Delta\tilde{V}) = \sum_{i=1}^{N} \|\Delta\tilde{V}_i\|_\infty \tag{4.6}$$

An incorrect choice for the optimisation criterion can result in solutions with poor guidance performances. Reference [82] shows that fuel penalties as high as 50% can occur if the cost function is not properly chosen. Throughout this dissertation it is assumed that the spacecraft are equipped with two identical engines on each axis which imposes the usage of (4.5) as optimization criterion.

4.1.3 Saturation constraints

The thrusters saturation constraints have been represented in (4.1) by the generic expression:

$$\Delta\tilde{V}_i \in \tilde{\mathcal{U}}_{\max}(\nu_i), \ \forall i = 1...N \tag{4.7}$$

Given the assumption previously made on the configuration of the thrusters, the saturation constraints can be written as an upper limit on the modulus of the thrust on each axis $\Delta V_{\max}$:

$$|\Delta \tilde{V}_i| \leq \Delta \tilde{V}_{\max}(\nu_i), \ \forall i = 1...N \tag{4.8}$$

The thrust upper bound in (4.8) depends on ν since the variable transformation (1.17) must be taken into account when writing the optimisation problem and when returning the solution:

$$\Delta \tilde{V}(\nu) = \sqrt{\frac{a^3(1-e^2)^3}{\mu}} \frac{1}{1+e\cos\nu} \Delta V \tag{4.9}$$

Thus the term $\Delta \tilde{V}_{\max}(\nu_i)$ in (4.8) is obtained as:

$$\Delta \tilde{V}_{\max}(\nu_i) = \sqrt{\frac{a^3(1-e^2)^3}{\mu}} \frac{\Delta V_{\max}}{1+e\cos\nu} \mathbf{1}_3, \ i = 1...N \tag{4.10}$$

where $\mathbf{1}_l$ is a vector of dimension l containing only ones.

4.1.4 Using direct shooting methods for the guidance problem

The direct shooting methods for spacecraft trajectory design consist in transforming the optimal control problem (4.1) into a parameter optimization problem which can be efficiently solved by the existing algorithms. This is usually achieved through discretization and control parametrization [45]. The knowledge of the firing positions ν_i and the modelling of the thrusts as impulsive controls enables the usage of direct shooting methods for solving the rendezvous guidance problem. The differential equation in (4.1) can be directly replaced by the solution provided by the state transition matrix:

$$\tilde{X}(\nu) = \Phi(\nu, \nu_1)\tilde{X}_1 + \sum_i \Phi(\nu, \nu_i) B \Delta \tilde{V}_i \tag{4.11}$$

where $\Phi(\nu, \nu_i)$ is the Yamanaka-Ankersen transition matrix presented in Chapter 1. Using the following notations:

$$\mathbf{A}_i = \begin{bmatrix} \Phi(\nu_i,\nu_1)B & \Phi(\nu_i,\nu_2)B & ...\Phi(\nu_i,\nu_i)B \end{bmatrix}, \quad \mathbf{B}_i = \Phi(\nu_i,\nu_1)\tilde{X}_1, \quad \mathbf{\Delta\tilde{V}}^i = \begin{bmatrix} \Delta\tilde{V}_1 & ... & \Delta\tilde{V}_i \end{bmatrix}^T \tag{4.12}$$

and integrating the fuel consumption criterion given in (4.5), the optimal control problem (4.1) can be written as:

$$\begin{aligned} \min_{\Delta\tilde{V}_i} \quad & \|\boldsymbol{\Delta}\tilde{\mathbf{V}}\|_1 \\ \text{s.t.} \quad & \begin{cases} \tilde{X}(\nu_N) = \mathbf{A}_N \Delta\tilde{V}^N + \mathbf{B}_N \\ \tilde{X}(\nu_N) = \tilde{X}_f \\ -\Delta\tilde{V}_{\max}(\nu_i) \leq \Delta\tilde{V}_i \leq \Delta\tilde{V}_{\max}(\nu_i), \ \forall i = 1...N \end{cases} \end{aligned} \tag{4.13}$$

It can be seen that (4.13) contains only linear constraints while the norm-1 optimization criterion is piecewise linear. By replacing the criterion with a linear equivalent, the rendezvous guidance problem could be transformed into a Linear Program (LP) [19, 64, 99]. The main advantage of performing this transformation is the fact that the solution to a linear program can be efficiently computed using existing numerical tools such as interior point methods or the simplex algorithm [10].

When a distinction is made between the equality and inequality constraints, the general form of a Linear Program is given by:

$$\begin{aligned} \min_{\Upsilon} \quad & C^T \Upsilon \\ \text{s.t.} \quad & \begin{cases} A_{in}\Upsilon < b_{in} \\ A_{eq}\Upsilon = b_{eq} \end{cases} \end{aligned} \tag{4.14}$$

where Υ denotes the vector of decision variables and C, A_{in}, b_{in}, A_{eq} and b_{eq} represent the data of the problem.

The norm-1 criterion in (4.13) can be replaced with a linear equivalent by introducing some slack variables $Z_i \in \mathbb{R}^3$ such that:

$$\begin{matrix} \Delta\tilde{V}_i \leq Z_i \\ -\Delta\tilde{V}_i \leq Z_i \end{matrix}, \ \forall i = 1..N \tag{4.15}$$

In this case, minimizing the norm-1 of the thrust vector becomes equivalent to minimizing the sum of the elements of the variables Z_i:

$$\min \|\boldsymbol{\Delta}\tilde{\mathbf{V}}\|_1 \quad \Longleftrightarrow \quad \min \sum Z_i \tag{4.16}$$

Moreover, the saturation constraints can be written as constraints on the slack variables:

$$Z_i \leq \Delta\tilde{V}_{\max}(\nu_i),\ \forall i = 1..N \tag{4.17}$$

Let the new vector of decision variables Υ be defined as:

$$\Upsilon^T = \begin{bmatrix} Z_1^T & ... & Z_N^T & \Delta\tilde{V}_1^T & ... & \Delta\tilde{V}_N^T \end{bmatrix} = \begin{bmatrix} Z^T & \Delta\tilde{V}^T \end{bmatrix} \tag{4.18}$$

The optimization criterion in (4.13) can be replaced by a linear criterion defined by the matrix C:

$$C^T = \begin{bmatrix} \mathbf{1}_{3N} & \mathbf{0}_{3N} \end{bmatrix} \tag{4.19}$$

where $\mathbf{1}_{3N}$ is a line vector of the indicated dimension containing only ones and $\mathbf{0}_{3N}$ is a line vector containing only zeros. The rest of the matrices defining the data of the problem can be obtained through direct identification:

$$A_{in} = \begin{bmatrix} -I_{3N} & I_{3N} \\ -I_{3N} & -I_{3N} \\ I_{3N} & 0_{3N} \end{bmatrix} \quad b_{in} = \begin{bmatrix} \mathbf{0}_{3N} \\ \mathbf{0}_{3N} \\ \Delta\tilde{V}_{\max}(\nu_1) \\ ... \\ \Delta\tilde{V}_{\max}(\nu_N) \end{bmatrix} \quad A_{eq} = \mathbf{A}_N \begin{bmatrix} 0_{3N} & I_{3N} \end{bmatrix} \quad b_{eq} = \tilde{X}_f - \mathbf{B}_N \tag{4.20}$$

4.2 Fixed-time rendezvous with trajectory constraints

Trajectory constraints for spacecraft rendezvous and proximity operations arise from requirements that are specific to each mission. The mathematical description of spacecraft relative trajectories that evolve inside a specified polytopic area over a specified time interval has been presented in the previous chapter. It has been shown that even if the restrictions on the relative trajectory need to be respected *continuously* in time, it is still possible to describe the set of admissible trajectories using a *finite* number of constraints. This description of the admissible trajectories will be used next in order to solve different types of fixed-time rendezvous missions with trajectory constraints.

4.2.1 Guidance towards a constrained periodic relative motion

Periodic relative trajectories represent natural solutions of the autonomous spacecraft relative dynamics. In the unperturbed case, no fuel consumption is required in order to maintain such trajectories, making them a good choice for spacecraft on-orbit inspection missions or for formation

flying applications [37, 46].

Periodic relative trajectories could also be used as parking orbits between different phases of a rendezvous mission. In the Automated Transfer Vehicle (ATV) mission to the International Space Station (ISS) for instance, the approach trajectory is defined in terms of several way-points that the vehicle must validate [41]. When a way-point is reached, the spacecraft must maintain that position and wait until the ground mission control gives the authorisation to proceed to the next point. The waiting point condition could be relaxed to a requirement of natural periodic motion around the designated waiting position. This might have the benefit of reducing the fuel cost of the mission, since waiting on a naturally periodic trajectory does not imply any fuel consumption. Dimensions restrictions need to be imposed on the parking orbits, in the form of a *tolerance box* for instance (see the illustration in Figure 4.2).

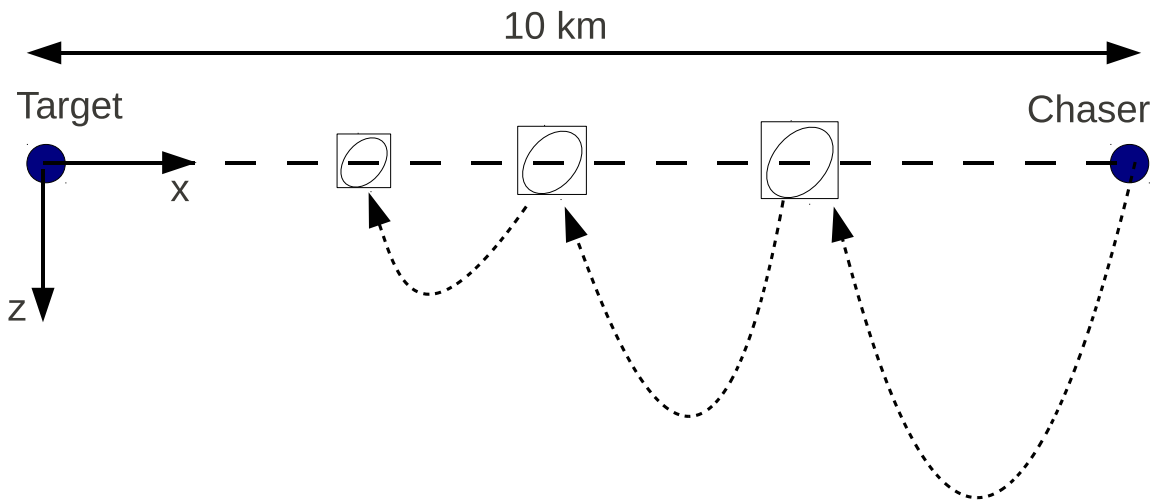

Figure 4.2: Way-points illustration for the ATV mission

Mathematical formulation of the guidance problem

The main difference with respect to the classical rendezvous guidance problem (4.13) resides in the final objective of the mission. Instead of reaching a designated final relative state X_f, the aim is now to reach an unknown final state from which the autonomously propagated trajectory is periodic and evolves inside a designated tolerance region.

The general expression for the set $S_D^p(H, V)$ containing the parameters that correspond to constrained periodic trajectories has been given in (3.33). Integrating this expression into the

general guidance problem leads to:

$$\begin{aligned} \min_{\Delta\tilde{V}_i} \quad & \|\Delta\tilde{V}\|_1 \\ \text{s.t.} \quad & \begin{cases} \tilde{X}(\nu_N) = \mathbf{A}_N\Delta\tilde{V} + \mathbf{B}_N \\ D = C(\nu_N)\tilde{X}(\nu_N) \\ D \in S_D^p(H,V) \\ -\Delta\tilde{V}_{\max}(\nu_i) \leq \Delta\tilde{V}_i \leq \Delta\tilde{V}_{\max}(\nu_i),\ \forall i = 1...N \end{cases} \end{aligned} \tag{4.21}$$

where D is the constant vector of parameters corresponding to the final autonomous periodic trajectory and $C(\nu)$ is the transformation matrix defined in (2.5). The vector D is constrained to belong to the set of parameters that generate periodic trajectories which evolve inside the tolerance box defined by the matrices H and V.

After replacing the optimization criterion with a linear equivalent as previously shown and integrating the definition of the set $S_D^p(H,V)$ from (3.33), the optimal control problem can be written as a Semi-Definite Program (SDP):

$$\begin{aligned} \min_{\Delta\tilde{V}_i, Z_i, Y_i} \quad & \mathbf{1}_{3N}\, Z \\ \text{s.t.} \quad & \begin{cases} \left.\begin{array}{l} -Z_i \leq \Delta\tilde{V}_i \leq Z_i \\ Z_i \leq \Delta\tilde{V}_{\max}(\nu_i) \end{array}\right\}, i = 1...N \\ D = C(\nu_N)(\mathbf{A_N}\mathbf{\Delta\tilde{V}} + \mathbf{B}_N) \\ d_0 = 0,\ Y_i \succeq 0,\ i = 1...s \\ \left.\begin{array}{l} \gamma_i = tv_i - (h_{i,1}C_x + h_{i,2}\bar{C}_y + h_{i,3}C_z)D \\ \gamma_i^T = \begin{bmatrix} \text{tr}\,(Y_iH_{2,1}) & ... & \text{tr}\,(Y_iH_{2,5}) \end{bmatrix} \end{array}\right., \ i = 1...s \end{cases} \end{aligned} \tag{4.22}$$

where γ_i are the vectors of coefficients corresponding to the non negative polynomials defining the set $S_D^p(H,V)$ and the matrices $H_{m,i}$ are defined as in (B.3). d_0 denotes the parameter in the vector D associated with the periodic motion condition and $h_{i,j}$ and v_i denote elements from the H and V matrices defining the tolerance region.

The semi-definite programs (SDP) are convex optimization problems that can still be efficiently solved using interior point methods [15]. Thanks to the properties of non negative polynomials, the solution to the rendezvous guidance problem with continuous trajectory constraints can be obtained in an amount of time that is polynomial in the number of the decision variables.

Always feasible formulation

The optimization problem (4.22) might not always have a feasible solution, depending on the data of the chosen rendezvous mission. Infeasibility could arise from the fact that the saturation constraints do not allow for the objective to be reached within the N steps of the plan or from the fact that no periodic trajectory can be found in the given tolerance region. The availability of a feasible solution might be critical for certain applications. In those cases, the infeasibility issues can be avoided by transforming some of the data defining the tolerance region into decision variables.

It can be noticed from (4.22) that only the elements of the V matrix can be considered as optimization variables, while still remaining in the context of convex problems. Considering the elements of the H matrix as decision variables leads to the appearance of products between the decision variables in the definition of the vectors γ_i. These vectors contain the coefficients of the polynomials which define the set of admissible periodic trajectories. Their expressions need to be linear in the decision variables in order to obtain a convex program.

To guarantee that the dimensions of the tolerance region are modified only when needed to ensure the feasibility of the problem, the minimization criterion must include the new parameters:

$$\min_{\Delta\tilde{V}_i, Z_i, Y_i, V} \quad \mathbf{1}_{3N}\, Z + \rho \sum_{i=1}^{s} v_i \tag{4.23}$$

where the parameter ρ is a positive number. The transformation of some of the parameters of the tolerance region into decision variables allows for the dimensions constraints on the periodic trajectory to be softened until a feasible solution is found.

Depending on the value of ρ, the solution might consist in a small tolerance region for which the fuel cost of the rendezvous trajectory is high. To ensure that, regardless of the value chosen for the parameter ρ, the dimensions of the tolerance region remain higher than an admissible value, a lower bound for the parameters in the matrix V can be specified:

$$V \geq V_m \tag{4.24}$$

The addition of this constraint corresponds to the fact that the purpose is not to find the smallest possible tolerance region but rather to increase the existing one in case the problem is infeasible.

4.2.2 Passively safe trajectories for spacecraft rendezvous

The ability to design a collision free spacecraft relative trajectory is of great importance, especially in the context of spacecraft proximity operations. The purpose is to provide guarantees for the

security of the mission even in the event of a system failure.

The methods for dealing with security constraints can be divided into *active methods* and *passive methods* [29]. The active security methods refer to the usage of control systems that integrate failure detection capabilities, enabling the spacecraft to compute and execute collision avoidance maneuvers in the event of a problem. These methods require the existence of an effective failure diagnosis module, capable of quickly delivering reliable information to the control system.

The passive security is based on trajectory design procedures that can guarantee *a priori* that no collision will occur for a large range of faults [17]. It does not require the computation of any collision avoidance maneuver and it ensures the safety of the system even when the spacecraft cannot use the thrusters, the on-board computer or the communication equipment. Passive security strategies are preferred for spacecraft rendezvous missions in order to avoid problems arising from the usage of the thrusters in proximity of the leader spacecraft [29].

Let us consider the failure moments as the moments when a system error prevents the computed control from being executed. In the case of passive security strategies, a system failure causes the thrusters to be stopped and the application of the rendezvous plan to be suspended. The system then enters a phase of autonomous motion following a *fail trajectory*. In order to guarantee the security of the mission, the nominal trajectory must be designed in such a way that the possible resulting fail trajectories do not run the risk of collision. This can be done by requiring for the fail trajectories to remain inside a designated safe area during a specified time interval [17,74]. Security over an infinite interval can be achieved by using constrained periodic relative trajectories as fail trajectories. In this case, the optimal control problem can be written as:

$$\begin{aligned} \min_{\Delta\tilde{V}_i} \quad & \|\Delta\tilde{V}\|_1 \\ \text{s.t.} \quad & \begin{cases} -\Delta\tilde{V}_{\max}(\nu_i) \leq \Delta\tilde{V}_i \leq \Delta\tilde{V}_{\max}(\nu_i), \ \forall i = 1...N \\ \tilde{X}(\nu_i) = \mathbf{A}_i \boldsymbol{\Delta}\tilde{\mathbf{V}}^i + \mathbf{B}_i, i = 1...N \\ \tilde{X}_f - \tilde{X}_{tol} \leq \tilde{X}(\nu_N) \leq \tilde{X}_f + \tilde{X}_{tol} \\ \left.\begin{array}{l} D_i = C(\nu_i)\tilde{X}(\nu_i) \\ D_i \in S_D^p(H,V) \end{array}\right\}, \forall i = N-S...N-1 \end{cases} \end{aligned} \tag{4.25}$$

where $\tilde{X}(\nu_i)$ is the spacecraft relative state right after that the i-th control is applied. D_i is the vector of parameters corresponding to the fail trajectory that would result in case an incident prevented the rendezvous plan from being executed starting from the step $i+1$. The definition of D_i in (4.25) corresponds to the fact that between two impulsive controls the trajectory follows

an autonomous evolution. If the $(i+1)$-th control cannot be executed then the spacecraft will continue on the relative trajectory that started from $\tilde{X}(\nu_i)$ and is on this trajectory that the security constraints must be imposed.

The fail trajectories are constrained to evolve inside a safe area, which in this case is defined as the polytopic region specified by the H and V matrices (see the definition in (3.2)). The set $S_D^p(H,V)$ represents the set of parameters that correspond to admissible periodic trajectories, defined as in (3.33). A small tolerance $\tilde{X}_{tol}$ is allowed around the final objective $\tilde{X}_f$.

Passive security constraints can be imposed on any of the N steps of the rendezvous plan. However, care must be taken to the fact that adding too many constraints will increase the total fuel cost of the mission without necessarily improving the overall probability of collision [17]. For this reason we consider in (4.25) that the security constraints are required only for the last S steps of the plan, with $S < N$. Solving (4.25) will provide a rendezvous approach trajectory which for the last S steps is composed of segments that are parts of admissible periodic trajectories.

After linearizing the fuel consumption criterion and integrating the definition of the set of admissible parameters $S_D^p(H,V)$ from (3.33), the optimal control problem can be written as an SDP:

$$
\begin{aligned}
\min_{\Delta\tilde{V}_i, Z_i, Y_i^j} \quad & \mathbf{1}_{3N}\, Z \\
\text{s.t.} \quad & \begin{cases}
-Z_i \le \Delta\tilde{V}_i \le Z_i \\
Z_i \le \Delta\tilde{V}_{\max}(\nu_i)
\end{cases}, i = 1...N \\
& \tilde{X}_f - \tilde{X}_{tol} \le \mathbf{A}_N \boldsymbol{\Delta}\tilde{\mathbf{V}} + \mathbf{B}_N \le \tilde{X}_f + \tilde{X}_{tol} \\
& D_i = C(\nu_i)(\mathbf{A}_i \Delta\tilde{V}^i + \mathbf{B}_i) \\
& d_{i0} = 0,\ Y_i^j \succeq 0,\ i = N-S...N,\ j = 1...s \\
& \gamma_i^j = tv_j - (h_{j,1}C_x + h_{j,2}\bar{C}_y + h_{j,3}C_z)D_i \\
& \gamma_i^j = \begin{bmatrix} \text{tr}\,(Y_i^j H_{2,1}) & ... & \text{tr}\,(Y_i^j H_{2,5}) \end{bmatrix}^T \quad , i = N-S...N,\ j = 1...s
\end{aligned}
\tag{4.26}
$$

where d_{i0} is the parameter related to the condition for periodic motion and s is the number of constraints that define the safe region.

4.2.3 Spacecraft rendezvous with visibility constraints

The examples of constraints presented so far were only referring to periodic spacecraft relative trajectories. However, for the last part of a rendezvous mission, the approaching spacecraft is

usually required to remain permanently in the field of vision of the target spacecraft during the execution of the final maneuvers [17, 74]. This means that the visibility constraints need to be enforced *continuously* on the non periodic nominal approach trajectory. In this case, the general optimal control problem can be formulated as:

$$\begin{aligned} \min_{\Delta\tilde{V}_i} \quad & \|\Delta\tilde{V}\|_1 \\ \text{s.t.} \quad & \begin{cases} -\Delta\tilde{V}_{\max}(\nu_i) \leq \Delta\tilde{V}_i \leq \Delta\tilde{V}_{\max}(\nu_i), \ \forall i = 1...N \\ \tilde{X}(\nu_i) = \mathbf{A}_i\Delta\tilde{V}^i + \mathbf{B}_i, \ i = 1...N \\ D_i = C(\nu_i)\tilde{X}(\nu_i) \\ D_i \in S_D(H, V, \nu_i, \nu_{i+1}) \end{cases}, \ i = 1...N-1 \\ & \tilde{X}_f - \tilde{X}_{tol} \leq \tilde{X}(\nu_N) \leq \tilde{X}_f + \tilde{X}_{tol} \end{aligned} \tag{4.27}$$

where $S_D(H, V, \nu_i, \nu_{i+1})$ has been defined in (3.30) as the set of parameters corresponding to spacecraft autonomous relative trajectories that remain inside a polytopic set over the specified interval $[\nu_i \ \nu_{i+1}]$. The polytopic set defined through the matrices H and V represents in this case the visibility cone of the target spacecraft.

The set $S_D(H, V, \nu_i, \nu_{i+1})$ is defined by infinitely many constraints but it has been shown in the previous chapter that a representation using a finite number of variables can be achieved if some approximations are made. By using upper and lower polynomial bounds for the integral term $J(w)$, worst case rational bounds can be obtained for the spacecraft relative trajectory. This leads to a description of the admissible paths through polynomial non negativity constraints that can be replaced with conditions of existence of a finite number of constrained positive semi-definite matrices. The original optimal control problem (4.27) can once again be written as an SDP:

$$\begin{aligned} \min_{\Delta\tilde{V}_i, Z_i, Y^i_{j1l}, Y^i_{j2l}, Y_{j1u}, Y^i_{j2u}} \quad & \mathbf{1}_{3N} Z \\ \text{s.t.} \quad & \begin{cases} -Z_i \leq \Delta\tilde{V}_i \leq Z_i \\ Z_i \leq \Delta\tilde{V}_{\max}(\nu_i) \end{cases}, \ \forall i = 1...N \\ & \tilde{X}_f - \tilde{X}_{tol} \leq \mathbf{A}_N\Delta\tilde{V} + \mathbf{B}_N \leq \tilde{X}_f + \tilde{X}_{tol} \\ & \begin{cases} D_i = C(\nu_i)(\mathbf{A}_i\Delta\tilde{V}^i + \mathbf{B}_i), \ i = 1...N-1 \\ Y^i_{j1l} \succeq 0, \ Y^i_{j2l} \succeq 0, \ \gamma^i_{jl} = \Lambda^*(Y_{j1l}, Y^i_{j2l}) \\ Y^i_{j1u} \succeq 0, \ Y^i_{j2u} \succeq 0, \ \gamma^i_{ju} = \Lambda^*(Y_{j1u}, Y^i_{j2u}) \end{cases}, \forall i = 1...N-1, \forall j = 1...s \end{aligned} \tag{4.28}$$

with the linear operator Λ^* defined as in (B.4) and (B.5). γ_{jl}^i and γ_{ju}^i represent the vector of coefficients corresponding to the non negative polynomials that define the set $S_D(H, V, w_i, w_{i+1})$ and they depend linearly on the corresponding vector of parameters D_i.

4.3 Numerical examples

The efficiency of the previously presented methods for computing fuel optimal impulsive maneuvers plans under control and trajectory constraints will be illustrated here through some numerical examples. The control plan is computed at the beginning of the mission and then applied by the chaser spacecraft until the end without any modifications. Perfect state knowledge is assumed for these examples and the tests are made using the linear model for the propagation of the spacecraft relative motion.

4.3.1 Reaching a constrained periodic relative trajectory

Let us consider a spacecraft rendezvous mission where the final objective is to *reach a periodic relative trajectory* in proximity of the target. The periodic trajectory is not fixed *a priori*, it is just required to evolve inside a tolerance region, specified as a box of dimensions $X_{tol} = \begin{bmatrix} x_{tol} & y_{tol} & z_{tol} \end{bmatrix}^T$ around a desired final position $X_f = \begin{bmatrix} x_f & y_f & z_f \end{bmatrix}^T$. In this case, the matrices H and V defining the polytopic set which bounds the admissible trajectories are given by:

$$H = \begin{bmatrix} 1 & 0 & 0 \\ -1 & 0 & 0 \\ 0 & 1 & 0 \\ 0 & -1 & 0 \\ 0 & 0 & 1 \\ 0 & 0 & -1 \end{bmatrix}, \quad V = \begin{bmatrix} x_f + x_{tol} \\ -x_f + x_{tol} \\ y_f + y_{tol} \\ -y_f + y_{tol} \\ z_f + z_{tol} \\ -z_f + z_{tol} \end{bmatrix} \tag{4.29}$$

The mission data for the first scenario i.e. the semi-major axis of the target orbit a, the eccentricity e, the maximum allowed thrust $\Delta V_{\max}$, the initial state X_1, the initial time t_1, the number of the impulsive thrusts N, the final time t_N and the specifications of the tolerance region are given in Table 4.1. No constraints are specified for the final velocity but its value will be determined by the periodicity condition.

After integrating the data in Table 4.1, the semi-definite program (4.22) is solved in Matlab using Yalmip [63] along with the solver SDPT3 [100]. The guidance problem is also solved using a

a [km]	e	$\Delta V_{\max}$	N	X_1 [m,m/s]	t_1 [s]	X_f [m]	X_{tol} [m]	t_N [s]
7 011	0.0237	0.26	10	[1000,50,50,0,0,0]	1 282	[100,0,0]	[20,10,10]	18 808

Table 4.1: Mission data

method based on constraints discretization [99], in order to compare the performances of the two different approaches. This constraints discretization method amounts to a Linear Program whose solution is obtained using the *linprog* function from Matlab.

The rendezvous trajectory obtained for the discretization based method and 10 verification points is presented in Figure 4.3. Taking more verification points or using the SDP method does not essentially change the computed rendezvous trajectory and the objective of achieving a periodic motion is always met. However, the differences appear when analysing the periodic relative trajectories that start at the end of the rendezvous plan.

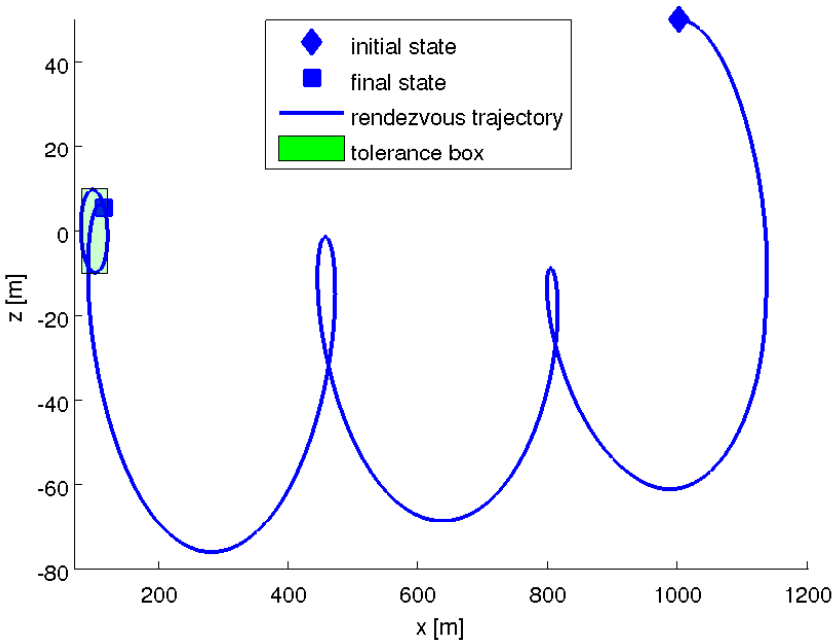

Figure 4.3: Spacecraft guidance towards proximity periodic motion

Figure 4.4 presents the resulting periodic trajectories for the constraints discretization method when considering 10, 20 and 30 verification points respectively, uniformly distributed over one orbital period (the verification points are represented by the * symbol). The trajectory obtained with the SDP method is also shown for comparison. It can be seen that the solution provided by the constraints discretization method sometimes violates the tolerance region constraints in between the chosen verification points. The precision of the solution is influenced by the number of points

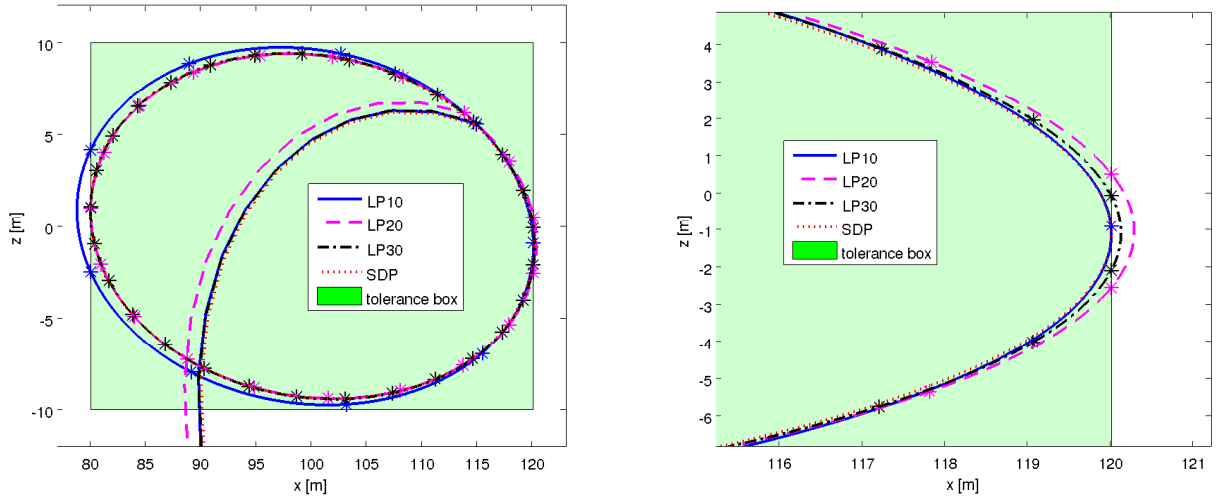

Figure 4.4: Comparison between the obtained periodic trajectories

where the constraints are explicitly checked and better accuracy might be achieved by increasing their number. No constraints violations occur when using our method which guarantees *a priori* that the constraints are respected continuously in time.

The comparison between the fuel cost, the solver time and the time spent outside the tolerance region for each of the considered methods is shown in Table 4.2. Increasing the number of verification points reduces the amount of constraints violations but it also increases the solver time and the fuel cost. It can be noticed that, as the number of discretization points increases, the obtained fuel cost approaches the solution given by the SDP method. The LP approach provides the optimal solution only for the discretized problem, while the SDP approach provides the optimal solution for the original problem.

Method	LP10	LP20	LP30	SDP
Fuel cost [m/s]	0.48907	0.48922	0.48927	0.48927
Solver time [s]	0.1972	0.6499	1.6241	0.9325
Time out of bounds [s]	1 269	737	339	0

Table 4.2: Comparison between the SDP and LP methods

The data for the second example are summarized in Table 4.3. This scenario considers a highly eccentric reference orbit which enables us to illustrate that not only the number of discretization points is important but also their distribution along the considered time horizon.

The resulting periodic trajectories are depicted in Figure 4.5, where the solution provided by the discretization based method is obtained for 15 verification points uniformly distributed over one orbital period. It can be seen that despite this uniform time distribution, the distance between the

a [km]	e	$\Delta V_{\max}$ [m/s]	N	X_1 [m,m/s]	t_1 [s]	X_f [m]	X_{tol} [m]	t_N [s]
7 011	0.8	0.26	10	[10000,100,0,0,0,0]	1 282	[100,0,0]	[50,25,25]	65 902

Table 4.3: Mission data

verification points is uneven (the points are represented in the figure by the * symbol). This comes from the fact that for eccentric orbits the spacecraft instantaneous velocity is not constant. As a consequence, larger parts of the obtained trajectory evolve outside the desired tolerance box. The solution provided by our method is not affected by this issue and the obtained trajectory evolves very close to the given bounds without ever crossing them.

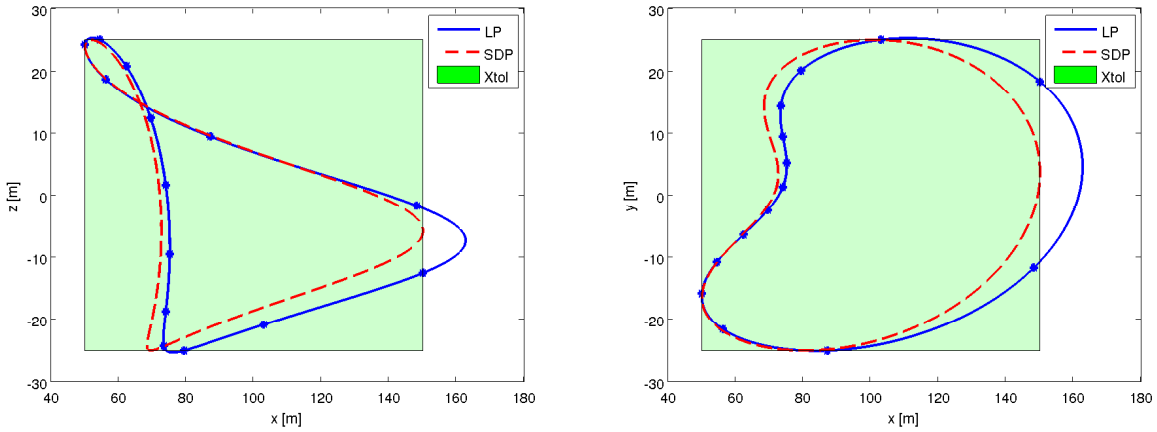

Figure 4.5: Comparison between the obtained periodic trajectories when $e = 0.8$

Always feasible formulation

Let us consider the spacecraft rendezvous mission in Table 4.3 for which the specification for the tolerance box is modified to $X_{tol} = [10\ 5\ 5]$ m. In this case, no feasible solution can be found using our method. Even removing the saturation constraints and changing the duration of the rendezvous mission does not lead to a feasible solution. In this case, it can be interesting to use the always feasible formulation of the control problem in order to compute the smallest feasible tolerance box.

The periodic trajectory obtained when considering the components of X_{tol} as decision variables is depicted in Figure 4.6 where X_m refers to the initially specified value for the tolerance box. The smallest feasible tolerance box is specified by $X_{tol} = [44.4474\ 5\ 22.2193]$ m. No expansion of the box is necessary on the y axis while a much bigger box is needed to contain the trajectory in the xz plane.

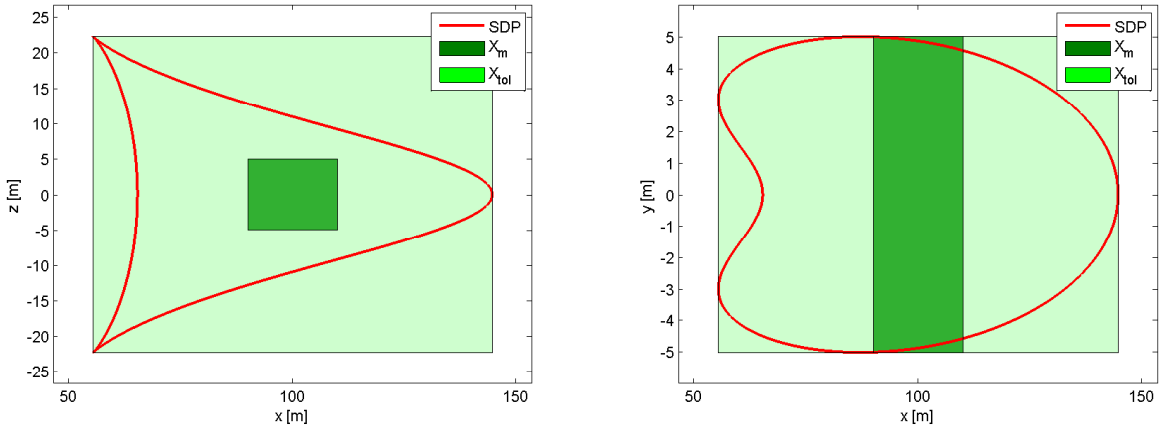

Figure 4.6: Modification of the tolerance box in order to ensure the feasibility of the problem

4.3.2 Passively safe rendezvous trajectories

Consider the rendezvous mission whose data are presented in Table 4.4. The objective is to *reach the final state on a passively safe rendezvous trajectory*. Some tolerance is permitted on the final velocity, specified by v_{tol} while the requirement for the final position is strictly maintained. In this example we consider for simplicity that the safe area is represented by an open polytope behind the chaser defined by $\tilde{x}(\nu) \leq \tilde{x}_{\text{safe}}$, where $x_{\text{safe}} = -5$ m.

a [km]	e	$\Delta V_{\max}$ [m/s]	N	X_1 [m,m/s]	t_1 [s]	X_f [m]	v_{tol} [m/s]	t_N [s]
7 011	0.0237	0.26	15	[-30,0,-3,0,0,0]	0	[-5,0,0,0,0,0]	0.01	5 843

Table 4.4: Mission data for the passively safe rendezvous

In order to identify a suitable value for the security horizon S, the rendezvous problem (4.26) is first solved without enforcing the security constraints ($S = 0$). The obtained maneuvers plan is applied and starting from every controlled state on the second half of the rendezvous horizon the autonomous trajectories are propagated. This is done in order to identify the fail trajectories which present a risk of collision. The states starting from which collision between the two spacecraft might occur need to be included in the safety horizon S.

The obtained trajectories are presented in Figure 4.7 where the * symbol corresponds to control instants from which the fail trajectories are propagated. The result suggests that a security horizon of $S = 4$ should greatly reduce the probability of collision in the event of system failure. It is interesting to note that in Figure 4.7 some of the fail trajectories overlap, in the cases where the optimal control equals zero.

Figure 4.8 depicts the fail trajectories that are obtained when solving (4.26) for a security

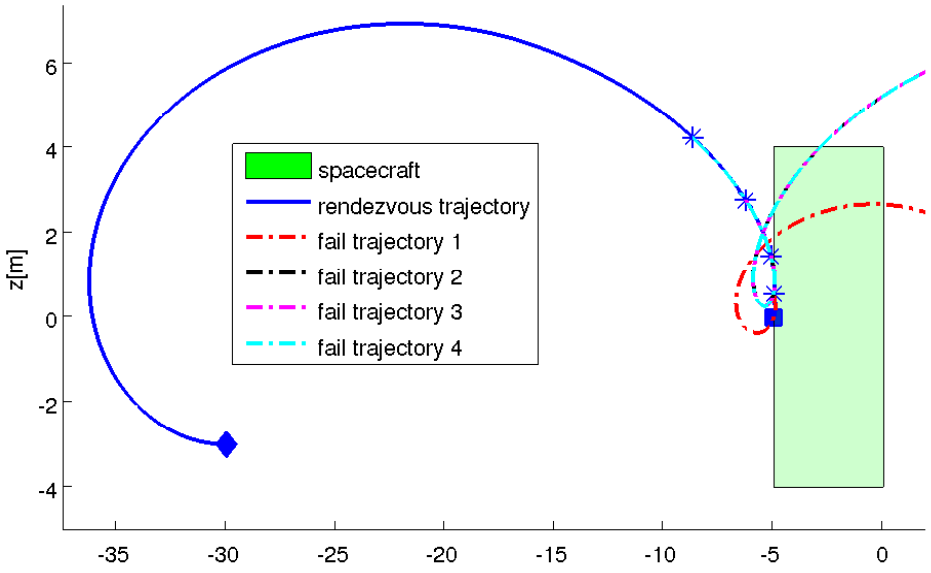

Figure 4.7: Fail trajectories when the security constraints are not enforced

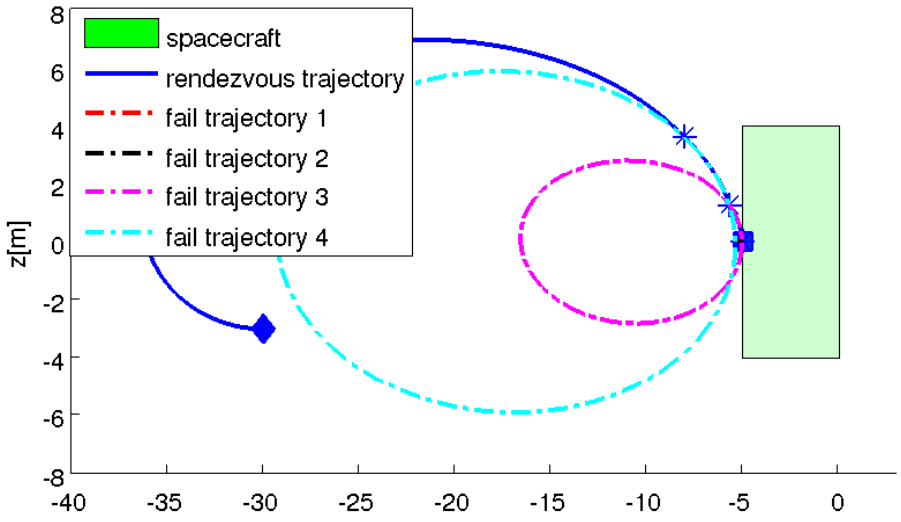

Figure 4.8: Fail trajectories obtained when the security constraints are enforced

horizon $S = 4$. The fail trajectories are now periodic and evolve inside the security area defined by x_{safe}, thus reducing the risk of collision in case of system error (some of the fail trajectories still overlap meaning that the new solution still contains thrusting instants where the optimal control is zero).

The influence of the choice of the security horizon on the fuel cost of the mission is illustrated in Table 4.5. It can be easily seen that the fuel cost increases as the security horizon increases since more and more constraints are added to the problem and this limits the choices for the possible

rendezvous trajectories.

S	0	1	2	3	4	5	6	7
Fuel cost [m/s]	0.0116	0.0121	0.0135	0.0146	0.0156	0.0163	0.0168	0.0174

Table 4.5: Evolution of the mission fuel cost with the length of the security horizon

A different geometry can be specified for the security area. In some applications, the security region may coincide with the visibility cone of the target spacecraft [17]. The visibility cone is usually represented by an open polytope defined through the aperture angle α and the offset distance x_{safe} between the docking port and the center of gravity of the target satellite (see Figure 4.9). In this case the polytopic constraints on the fail trajectories are defined by the matrices:

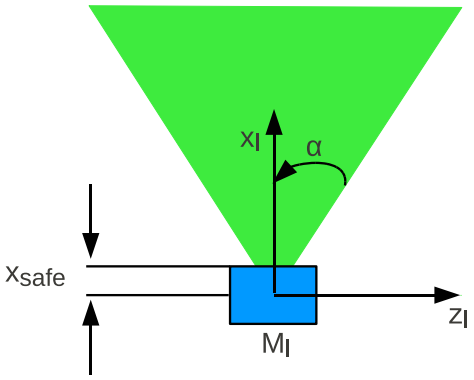

Figure 4.9: The visibility cone of the target satellite

$$H = \begin{bmatrix} 1 & 0 & \rho \\ 1 & 0 & -\rho \\ 1 & \rho & 0 \\ 1 & -\rho & 0 \\ 1 & 0 & 0 \end{bmatrix} \quad V = \begin{bmatrix} 0 \\ 0 \\ 0 \\ 0 \\ x_{\text{safe}} \end{bmatrix} \tag{4.30}$$

where $\rho = \tan(\frac{\pi}{2} - \alpha)$.

The data in Table 4.6 defining a new rendezvous scenario is used for solving the optimal control problem (4.26). The parameters for the visibility cone are given by $x_{\text{safe}} = 1.04$ m and $\alpha = 47°$.

Figure 4.10 presents the fail trajectories and the nominal rendezvous trajectory obtained with and without the security constraints. The safety horizon has been chosen $S = 3$ after inspecting the fail trajectories obtained in the case where the security constraints were not active.

a [km]	e	$\Delta V_{\max}$ [m/s]	N	X_1 [m,m/s]	t_1 [s]	X_f [m]	v_{tol} [m/s]	t_N [s]
7 360	0.0237	0.26	20	[100,0,0,0,0,0]	0	[1.04,0,0,0,0,0]	0.001	6 283

Table 4.6: Mission data for the passively safe rendezvous

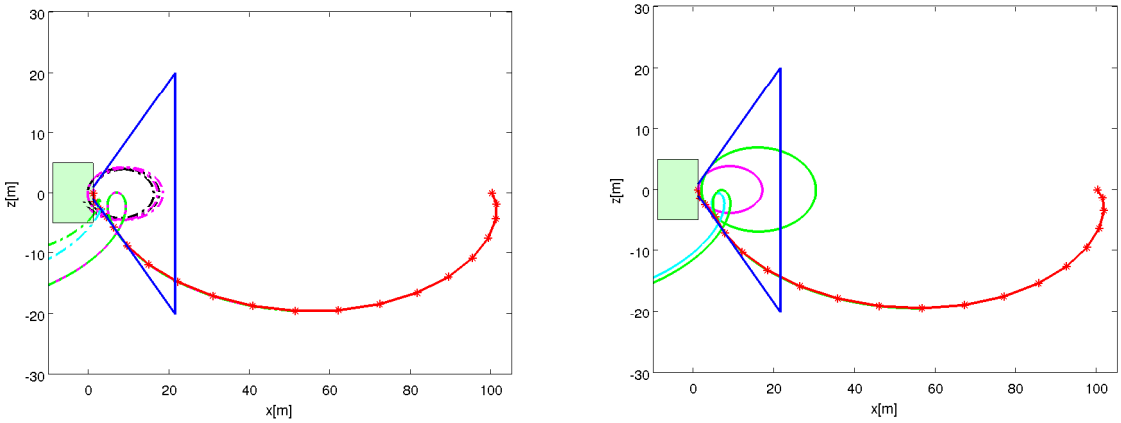

Figure 4.10: Fail trajectories obtained for $S = 0$ and $S = 3$ respectively

When the same passively safe rendezvous problem is solved using a constraints discretization method as in [17], some differences can be observed between the obtained fail trajectories. Figure 4.11 shows that, as pointed out before, violations of the constraints occur in between the chosen verification points when using the method based on constraints discretization.

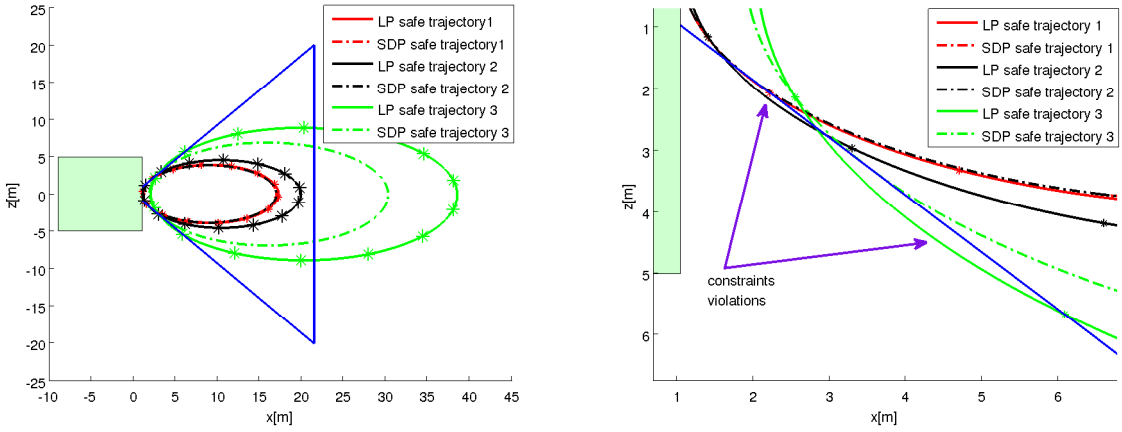

Figure 4.11: Comparison between the fail trajectories obtained when using our SDP-based method and a constraints discretization method

An iterative method for choosing the number of verification points could consist in inspecting the obtained trajectories and then increasing the number if necessary. Using this approach could eventually lead to a better choice for this important parameter. However, the SDP method delivers directly a trajectory that guarantees the continuous satisfaction of the constraints.

4.3.3 Constrained non periodic relative trajectories

For the last phase of the rendezvous maneuvers, operational requirements might impose visibility constraints on the approach trajectory. In this case, the objective is to design a spacecraft rendezvous trajectory which *remains inside the visibility cone of the target* spacecraft throughout the duration of the rendezvous maneuvers. The visibility constraints can be combined with passive security constraints for instance, but in this example we chose to focus on the case where the restrictions concern only the non periodic relative motion.

The fuel optimal maneuvers plan that generates an approach trajectory which respects the visibility requirements can be obtained by solving the semi-definite program (4.28). In order to be able to formulate the optimization problem, polynomial approximations of the term $J(w)$ on each interval between two consecutive thrusts need to be computed. The software Sollya [22] is used here for obtaining these approximations. The software requires for the values of the independent variable w to be monotonously increasing on each approximation interval. This imposes some restrictions on the rendezvous horizon since the transformation (3.8) maps each interval of one orbital period for the variable ν to $\mathbb{R}$.

The duration of the mission is chosen to be half of an orbital period, starting from $\nu_1 = -\pi/2$ and until $\nu_N = \pi/2$. This choice guarantees strictly increasing values for w on each interval between thrusts and avoids working close to the bounds of the domain on which w is defined. Accurate polynomial approximations can be obtained for the chosen rendezvous horizon (see Figure 4.12). The fact that ν_1 is negative corresponds to rendezvous maneuvers that start before the current passage of the leader spacecraft through the perigee. The data defining the rendezvous mission is summarized in Table 4.7 and the visibility cone is defined in this case by $x_{\text{safe}} = -5$ m and $\alpha = 20°$.

a [km]	e	$\Delta V_{\max}$ [m/s]	N	X_1 [m,m/s]	ν_1 [s]	X_f [m]	v_{tol} [m/s]	ν_N [s]
7 011	0.0237	0.26	5	[-50,-10,15,0,0,0]	$-\pi/2$	[-6,0,0,0,0,0]	0.001	$\pi/2$

Table 4.7: Mission data for the rendezvous with visibility constraints

The degree of the polynomial approximations is fixed to $q = 2$. For this value, the maximal certified approximation error ε provided by Sollya is 0.25%. The upper and lower polynomial bounds for the term $J(w)$ on each interval between two consecutive controls are given in Figure 4.12 (Θ_u and Θ_l respectively).

A method based on constraints discretization is used for comparison. The trajectories obtained for the two methods are given in Figure 4.13, where 10 collocation points are taken for constraints

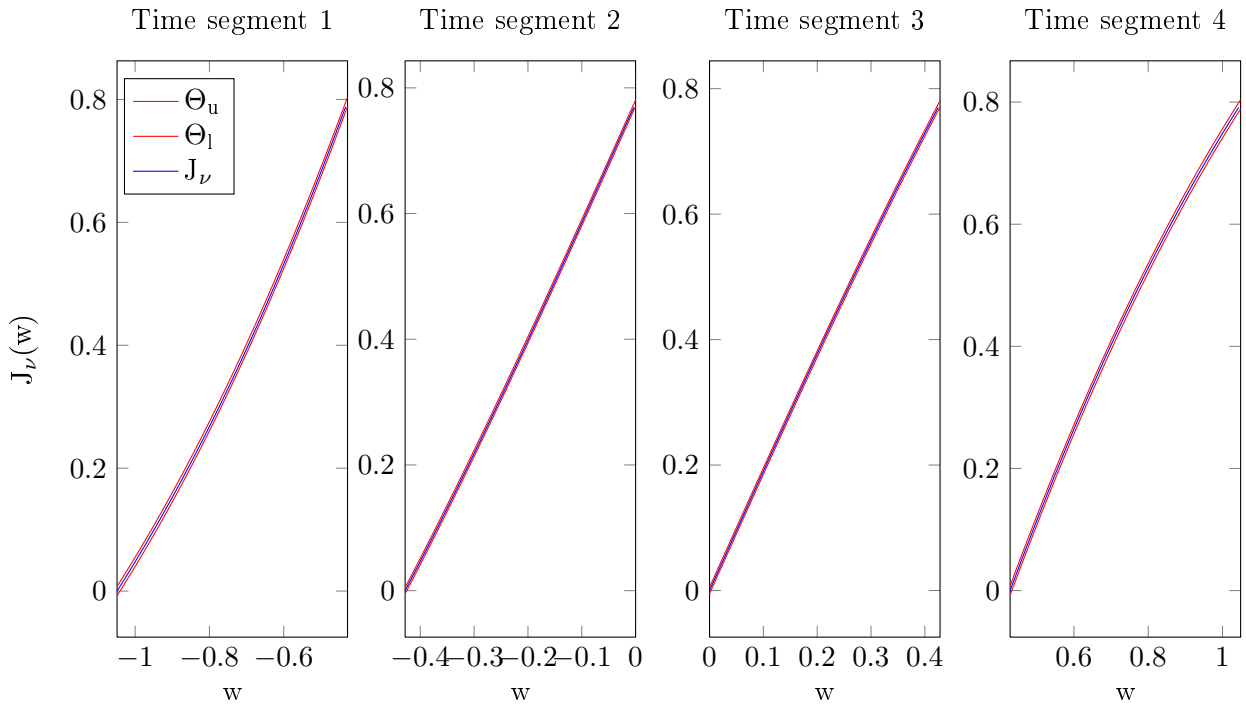

Figure 4.12: The drifting term $J(w)$ and its polynomial bounds on each time segment

discretization. As before, constraints violations occur in between the points where the constraints are explicitly checked of the LP method, while our method guarantees continuous constraints satisfaction even in the case of non-periodic spacecraft relative trajectories.

4.4 Conclusion

This chapter describes the construction of the optimal control problem that needs to be solved in order to obtain a fuel optimal maneuvers plan for the fixed-time spacecraft rendezvous. In the framework of direct shooting methods, the problem can be formulated as a Linear Program which can be easily solved using the existing numerical solvers. We show that even when constraints on the spacecraft relative trajectory are imposed *continuously in time*, the optimal control problem can still be written as a convex optimization problem. In this case, the formulation relies on the description of the admissible trajectories using polynomial non-negativity constraints which has been introduced in the previous chapter. It amounts to a Semi-Definite Program which can be solved in polynomial time by the existing interior point algorithms.

Several examples of rendezvous missions are used to illustrate the types of trajectory constraints that can be handled by the proposed method. The constraints arise from mission-specific requirements, such as passive security or visibility constraints. The examples emphasize the advantage of

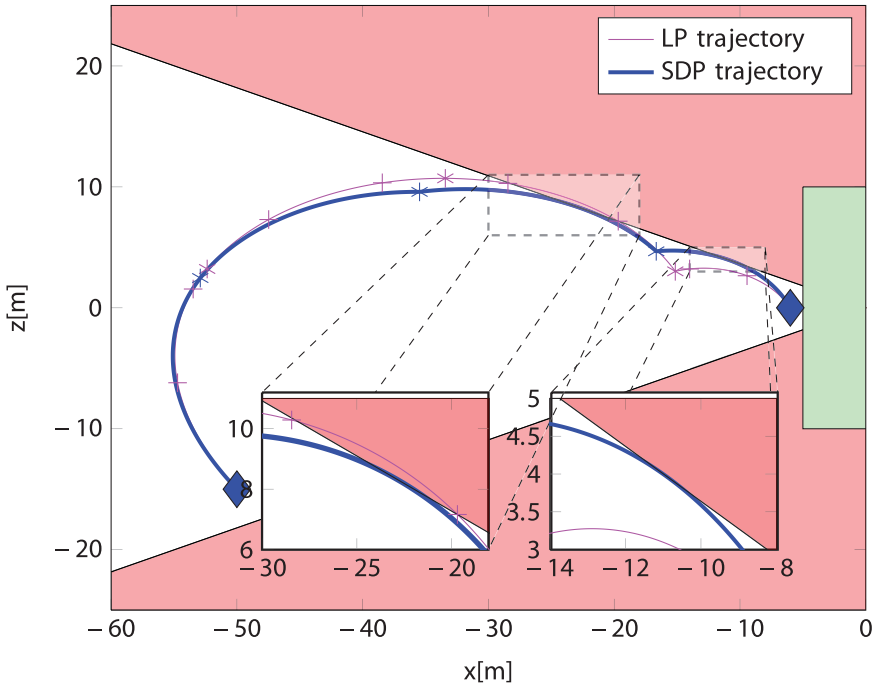

Figure 4.13: Comparison between the rendezvous trajectories obtained with the two methods

our method over the classical constraints dicretization technique for which constraints violations can occur in between the verification points. The solution provided by the constrained discretization method depends on the number of verification points that are considered and on their particular distribution over the considered horizon. Moreover, the numerical examples show that it approaches the solution given by our method as the number of verification points increases.

Chapter 5

Spacecraft rendezvous robust to navigation uncertainties

Contents

Résumé: Les techniques de design de trajectoire pour les opérations de proximité des satellites présentées dans le chapitre précédent reposent sur la parfaite connaissance de l'état relatif des satellites. En présence des incertitudes de mesure, il peut y avoir des grandes différences entre la trajectoire prédite et la trajectoire réelle des satellites. Cet écart détériore la précision finale des manœuvres et peut conduire à la violations de certaines contraintes de la mission. Ce chapitre propose deux algorithmes de guidage améliorant la robustesse vis-à-vis des erreurs de navigation. Ces algorithmes garantissent de façon déterministe la satisfaction des contraintes pour toute valeur admissible des incertitudes. Les deux techniques proposées sont basées sur le calcule d'un série des lois de commande au lieu d'un plan de manœuvres, ce qui permet de compenser les effets des incertitudes et atteindre une meilleure précision finale. Le critère de performance est ici défini par un compromis entre la précision finale des manœuvres et la consommation de combustible.

The trajectory design techniques presented in the previous chapter rely heavily on the knowledge of the spacecraft relative state. When the measurement of the spacecraft relative state is not affected by uncertainties, the computed impulsive maneuvers plan may be applied in open-loop to steer the spacecraft towards the desired objective. In presence of sensing noise, applying the plan without taking into consideration new measurement information will cause any initial navigation uncertainties to propagate until the end of the prediction horizon. This open-loop propagation might have severe effects on the final performance of the spacecraft rendezvous.

How and Tillerson showed in [44] that small errors in the estimation of the spacecraft relative velocity can result in very large prediction errors for the relative trajectory over just one orbital period. Navigation errors may be caused by alignment errors between the sensors and the spacecraft axes, by measurement performance limitations of the used sensor and/or by the information processing in the navigation filter [29]. Not accounting for the presence of these errors when designing the rendezvous trajectory can result in poor guidance performances and/or constraints violations.

Our purpose is to obtain a robust control algorithm for the spacecraft rendezvous that can guarantee the robust constraints satisfaction for all the possible realizations of the uncertainties. The performance criterion is defined as the best trade-off between the fuel cost of the computed maneuvers and the final rendezvous precision. The rendezvous precision can be understood in the sense of obtaining the smallest possible set that bounds the error with respect to the final objective for all the admissible values of the navigation uncertainties.

The fuel-optimal trajectory planning procedure presented in Chapter 4 is based on the resolution of an open-loop optimal control problem. This procedure can be used for closed-loop control with guaranteed performances by integrating it in a Model Predictive Control setting. Several Model Predictive Control approaches have been developed for dealing with uncertainties and achieving the robust control objectives in the context of spacecraft rendezvous guidance and some of them are summarized in the next section.

5.1 Model Predictive Control and spacecraft trajectory design

The classical Model Predictive Control consists in solving at each control step a constrained finite-horizon open-loop optimal control problem based on the estimation of the current state of the system. The computed optimal solution consists in a series of *control actions* $\{u_1, u_2, ..., u_N\}$, out of which only the first one is executed. The rest of the plan is discarded and a new solution based on new measurement information is computed at the next control instant. Even if the control plan is obtained using open-loop predictions for the evolution of the system, the periodic recomputation

of the optimal solution creates an *implicit closed-loop* [68].

The previous chapter emphasized the need for spacecraft trajectory planning algorithms that can handle different state and control constraints specific to each mission. In presence of navigation errors, the control algorithm must guarantee *a priori* that no transgressions of the constraints will occur for all possible realizations of the uncertainties. Simply relying on the periodic control recomputation cannot provide this type of guarantees. The optimal control problem solved at each step needs to be modified to explicitly account for the effects of the uncertainties.

The approach known as *open-loop min-max* MPC [68] is based on the resolution at each time step of an open-loop optimal control problem for which the uncertainties on the initial state are also propagated over the prediction horizon. The constraints satisfaction is explicitly checked for the worst-case disturbance sequence, providing the necessary guarantees for the obtained solution. The open-loop min-max MPC approach has been successfully used for spacecraft relative trajectory design in presence of navigation errors [19, 31, 64, 71]. The problem with this kind of approach is that it cannot include in the solved problem the performance objective related to the obtention of the best rendezvous precision. Due to the open-loop nature of the prediction, the effects of the uncertainties are taken into consideration but are not explicitly minimized. In the writing of the optimization problem, the spread of all the possible trajectories is not actually limited by the control which imposes the usage of short prediction horizons in order to ensure the feasibility of the optimization problem.

The *constraint tightening* approaches are based on the idea of maintaining the control scheme in a feasible region under the action of disturbances by *a priori* tightening the constraints on the predicted states [53]. The control problem solved at each time step is still based on open-loop predictions for the system trajectory but the constraints are modified off-line to ensure some room for future corrections. Constraints tightening procedures have been developed mainly for Linear Time Invariant (LTI) systems and are either based on the existence of a stabilizing state-feedback controller [18, 79, 96] or on the off-line resolution of an optimization problem [53, 94]. The main advantage is that the MPC with tightened constraints can guarantee the recursive feasibility of the problem in presence of uncertainties [78]. However, the precision requirements and the control saturations are not explicitly considered. Moreover, for the constraint tightening procedure becomes more complex in the case of Linear Time Varying (LTV) systems [77].

A change in the control philosophy is operated for the *feedback MPC*. The decision variables are changed from a series of control actions to a sequence of *feedback policies* $\{u_1(\cdot), ..., u_N(\cdot)\}$ and the control problem relies on the prediction of the closed-loop trajectory of the system [56]. Directly

considering feedback policies in the optimization problem avoids the open-loop propagation of the uncertainties and provides the means to actually limit the spread of all the possible trajectories. The drawback is that, in the general case, the computation of such feedback laws can be extremely difficult, since the decision variables are infinite dimensional [66]. However, restricting the admissible policies to the class of affine state feedback control laws can help reduce the complexity of the problem. This particular case is often-times called *tube-based MPC* [56,61,66]. It relies on the computation of some feedback gains that contain the spread of all the possible trajectories and limit their evolution to a tube around an optimized central trajectory. It can ensure robust constraints satisfaction and the dimension of the tube fixes the performances in terms of precision.

Method / Properties	Open-loop prediction of uncertainties	Periodic recomputation	Robust constraints satisfaction	Robust recursive feasibility
classical MPC	x	x	-	-
open-loop min-max MPC	x	x	x	-
MPC with tightened constraints	x	x	x	x
feedback MPC	-	-	x	x

Table 5.1: Comparison between the different MPC techniques

A summary of the different MPC techniques is given in Table 5.1. Our purpose is to obtain a maneuvers plan for the fixed-time spacecraft rendezvous that is robust to navigation uncertainties in terms of constraints satisfaction. The obtained solution must also provide the best trade-off between the fuel cost of the trajectory and the final rendezvous precision. For this particular problem, the feedback MPC seems to offer the best compromise between the guaranteed performances and the complexity of the control algorithm. A design procedure for the rendezvous trajectory between spacecraft on eccentric orbits will be presented in what follows.

5.2 The robust trajectory planning problem

The robust spacecraft trajectory design refers to solving the fixed-time rendezvous guidance problem defined in Section 4.1 when navigation uncertainties are affecting all the measurements of the spacecraft relative state. Our purpose is to determine a series of *affine feedback control laws* $\{u_1(\cdot), u_2(\cdot), ...\}$ such that, starting from an initial state X_1 which is affected by measurement noise, the final rendezvous objective X_f is reached at the specified time and within the best precision.

This must be done while minimizing the total fuel consumption and while guaranteeing that the imposed constraints are respected for all the possible values of the uncertainties. As before, the number of thrusts N and the thrusting instants $\nu_1, \nu_2, ...$ are considered known and the control is applied in an impulsive manner.

5.2.1 The spacecraft relative dynamics

For the fixed-time impulsive rendezvous guidance problem, the spacecraft relative trajectory propagates autonomously on each interval $[\nu_k,\ \nu_{k+1}]$ between two consecutive impulsive controls. Using the Yamanaka-Ankersen transition matrix, this propagation is given by:

$$\tilde{X}(\nu) = \Phi(\nu, \nu_k)\, \tilde{X}^+(\nu_k),\ \forall \nu \in [\nu_k,\ \nu_{k+1}] \tag{5.1}$$

The state $\tilde{X}^+(\nu_k)$ corresponds to the spacecraft relative state *right after* the k-th impulsive thrust:

$$\tilde{X}^+(\nu_k) = \tilde{X}(\nu_k) + B\, u_k,\ k \in \{1, 2, ...\} \tag{5.2}$$

where $B = [0_3\ I_3]^T$. Even if the impulsive control u_k instantaneously modifies only the spacecraft relative velocity, its effects on the whole spacecraft relative trajectory are visible on the interval of autonomous propagation that follows each thrust. For instance, the spacecraft relative state at the end of each interval $[\nu_k,\ \nu_{k+1}]$ is given by:

$$\tilde{X}(\nu_{k+1}) = \Phi(\nu_{k+1}, \nu_k)\, \tilde{X}(\nu_k) + \Phi(\nu_{k+1}, \nu_k)\, B\, u_k,\ \forall k = 1...N-1 \tag{5.3}$$

Equation (5.3) clearly shows the effects of the impulsive control u_k on the spacecraft relative position. The dynamics in (5.3) can be seen as the dynamics of an LTV system:

$$X_{k+1} = A_k X_k + B_k u_k \tag{5.4}$$

where $X_k = \tilde{X}(\nu_k)$, $A_k = \Phi(\nu_{k+1}, \nu_k)$ and $B_k = \Phi(\nu_{k+1}, \nu_k)\, B$. These simplified notations will be used throughout the chapter for constructing the robust spacecraft rendezvous guidance problem.

5.2.2 The effects of navigation uncertainties

When sensing noise is present in the navigation system, X_k, the real relative state between the two spacecraft, is unknown. However, X_k is related to the measured state X_k^m through the equation:

$$X_k = X_k^m + \delta X_k,\ \delta X_k \in E(0, Q_k) \tag{5.5}$$

where δX_k is an unknown measurement noise which is bounded by an ellipsoidal set $E(0, Q_k)$ (notation defined in (C.1)). The dynamics of the measured state can then be computed as:

$$X_{k+1}^m = X_{k+1} - \delta X_{k+1} = A_k X_k + B_k u_k - \delta X_{k+1},\ \delta X_{k+1} \in E(0, Q_{k+1}) \tag{5.6}$$

Using (5.5) to replace the unknown state of the system X_k with the measured state X_k^m leads to:

$$X_{k+1}^m = A_k X_k^m + B_k u_k + A_k \delta X_k - \delta X_{k+1} \tag{5.7}$$

Let us denote by w_k the total effect of the measurement noise over the interval between two consecutive controls. From (5.7), w_k can be defined as:

$$w_k = A_k \delta X_k - \delta X_{k+1},\ \delta X_k \in E(0, Q_k),\ \delta X_{k+1} \in E(0, Q_{k+1}) \tag{5.8}$$

This means that the domain for w_k is given by:

$$w_k \in E(0, A_k^{-T} Q_k A_k^{-1}) \oplus E(0, Q_{k+1}) \subseteq E(0, Q_k^w) \tag{5.9}$$

where the symbol $\oplus$ denotes the Minkowski sum between the two ellipsoidal sets, defined as in (C.8). The set $E(0, A_k^{-T} Q_k A_k^{-1})$ represents the ellipsoidal set obtained after the propagation of the set $E(0, Q_k)$ through the linear application A_k, defined as in (C.7). The Minkowski sum of two ellipsoids is not necessarily an ellipsoid and $E(0, Q_k^w)$ is an outer ellipsoidal approximation of the real domain of w_k. This approximation can be computed analytically, using for instance the procedure described in (C.10).

The dynamics of the measured state when the system is affected by navigation uncertainties is given by:

$$X_{k+1}^m = A_k X_k^m + B_k u_k + w_k,\ w_k \in E(0, Q_k^w) \tag{5.10}$$

It can be noticed from (5.8) that the navigation uncertainties will propagate in open-loop at least over the interval between the two consecutive control instants. The control u_{k+1} will cancel

some of the effects of w_k but in the same time it will introduce some new errors. This comes from the fact that the control is computed every time based on measurement information which is corrupted by sensing noise. This means that if the spacecraft relative state is not precisely known, the final rendezvous objective cannot be exactly reached. In this case the control objective transforms into minimizing the size of a guaranteed arrival set around the nominal objective.

5.2.3 The nominal trajectory

Let ΔV_k be the nominal control which, in the absence of navigation error, steers the spacecraft towards the final rendezvous objective. Let us define the *nominal trajectory* as the trajectory obtained when applying in perfect conditions a nominal control ΔV_k:

$$\bar{X}_{k+1} = A_k \bar{X}_k + B_k \Delta V_k, \ k = 1...N-1 \tag{5.11}$$

where $\bar{X}_k$ denotes the states that belong to the nominal trajectory. The nominal controls ΔV_k are such that, at the end of the prediction horizon, the nominal trajectory reaches the desired mission objective:

$$\bar{X}_N = X_f \tag{5.12}$$

Applying the nominal control ΔV_k on a system affected by navigation uncertainties might lead to trajectories that are significantly different with respect to the nominal path. Let the error between the perturbed trajectory and the nominal one be defined as:

$$e_k = X_k^m - \bar{X}_k \tag{5.13}$$

We are interested in the computation of some feedback control policies u_k that minimize the errors with respect to the nominal rendezvous path in presence of sensing errors.

5.2.4 General formulation of the guidance problem

The objective of minimizing the errors with respect to a nominal trajectory must be understood in the sense that the closed-loop behaviour must be as close as possible to the non-perturbed case. The nominal trajectory is not fixed *a priori*, the term is used here to refer to an ideal behaviour that also needs to be determined through optimization. Several techniques for obtaining nominal trajectories while taking into consideration different types of trajectory constraints have been presented in Chapter 4. These techniques need to be modified in the case where the system is affected by navigation errors. The first modification concerns the structure of the control law. A

feedback term is added to the nominal structure:

$$u_k = f_k(X_k^m, w_k) + \Delta V_k \tag{5.14}$$

in order to cancel the errors with respect to the nominal behaviour caused by the presence of uncertainties. The control must now guarantee that the thrusters saturation constraints are respected for all the possible realization of the uncertainties.

The optimal control problem corresponding to the robust trajectory design for the spacecraft rendezvous can be written in the general form:

$$\begin{aligned} \min_{f_k, \Delta V_k} \quad & J(u_k, e_k) \\ \text{s.t.} \quad & \begin{cases} X_{k+1}^m = A_k X_k^m + B_k u_k + w_k, \ w_k \in E(0, Q_k^w) \\ u_k = f_k(X_k^m, w_k) + \Delta V_k \\ \bar{X}_{k+1} = A_k \bar{X}_k + B_k \Delta V_k \\ e_k = X_k^m - \bar{X}_k \\ \bar{X}_N = X_f \\ u_k \in \mathcal{U}_{\max}(\nu_i), \ \forall w_k \in E(0, Q_k^w) \end{cases} \end{aligned} \tag{5.15}$$

where the decision variables are the nominal controls ΔV_k and the parameters of the functions f_k. The choice of the optimization criterion $J(u_k, e_k)$ must reflect the idea of compromise between fuel consumption and final rendezvous precision.

In order to simplify the formulation, the final rendezvous objective is considered to be a fixed state X_f. However, the control techniques that will be presented next can still be used if the final objective is to reach an unknown state belonging to a set of admissible trajectories, as it was the case for the examples in Chapter 4.

As already stated, solving (5.15) in the general case can be extremely difficult [66]. In order to reduce the complexity of the problem a special structure can be imposed for the functions f_k. We will show next that (5.15) can be written as a convex optimization problem if the control is parametrized as affine state-feedback or as affine disturbance-feedback.

5.3 Affine state-feedback MPC

Let us consider that the control policies u_k are restricted to the class of affine state feedback controllers. In this case we have:

$$u_k = K_k(X_k^m - \bar{X}_k) + \Delta V_k = K_k e_k + \Delta V_k \tag{5.16}$$

Our purpose is to compute the gain matrices $K_k \in \mathbb{R}^{3\times 6}$ and the nominal terms $\Delta V_k \in \mathbb{R}^3$ which steer the spacecraft towards the final rendezvous objective within the best possible precision, all while minimizing the total fuel cost. A design procedure for each of these terms will be presented in what follows.

5.3.1 Computation of the feedback gains

For the chosen control structure, the dynamics of the errors between the perturbed trajectory and the nominal trajectory are given by:

$$e_{k+1} = (A_k + B_k K_k)e_k + w_k,\ w_k \in E(0, Q_k^w) \tag{5.17}$$

The propagation of the errors over the prediction horizon is given by:

$$\begin{aligned}
e_1 &= X_1^m - \bar{X}_1 \\
e_2 &= (A_1 + B_1 K_1)e_1 + w_1 \\
e_3 &= (A_2 + B_2 K_2)\left((A_1 + B_1 K_1)e_1 + w_1\right) + w_2 \\
e_4 &= (A_3 + B_3 K_3)\left((A_2 + B_2 K_2)\left((A_1 + B_1 K_1)e_1 + w_1\right) + w_2\right) + w_3 \\
&\vdots
\end{aligned} \tag{5.18}$$

This objective related to the rendezvous precision can be interpreted as the search for the feedback gains K_k which minimize the dimensions of an ellipsoidal set $E(0, Q_\alpha)$ bounding the final error e_N:

$$\begin{aligned}
\min_{K_k, Q_\alpha} \quad & \text{tr } Q_\alpha \\
\text{s.t} \quad & e_N \in E(0, Q_\alpha),\ \forall w_k \in E(0, Q_k^w),\ k = 1..N-1
\end{aligned} \tag{5.19}$$

The matrix Q_α defines an ellipsoidal set which bounds the final error for all admissible values of the uncertainties. Minimizing the trace of Q_α corresponds to minimizing the sum of squares of the semi-axis of this ellipsoidal set.

Using the propagation given in (5.18), the expression for the final error contains nonlinear terms

involving the decision variables K_k. In order to reach a convex formulation of the optimization problem (5.19), the following simplifying assumption is made: the objective is changed to the research of the K_k matrices such that the error at each step e_k is bounded by the same ellipsoidal set denoted $E(0, Q_\alpha)$. The control problem (5.19) is replaced by:

$$\begin{aligned} \min_{K_k, Q_\alpha} \quad & \text{tr } Q_\alpha \\ \text{s.t.} \quad & e_{k+1} \in E(0, Q_\alpha),\ \forall e_k \in E(0, Q_\alpha),\ \forall w_k \in E(0, Q_k^w),\ k = 1...N-1 \end{aligned} \tag{5.20}$$

Under this assumption, the choice of each gain K_k becomes independent from the choice of the other gains. The common point is that for each interval between two consecutive control instants, they guarantee to maintain all the possible errors with respect to the nominal trajectory inside the same ellipsoidal set which is defined by the matrix Q_α.

While the previous assumption will help us convexify the problem, it will also generate additional constraints on the rendezvous trajectory. The ellipsoidal set $E(0, Q_\alpha)$, instead of bounding just the final error e_N, now defines a *tube* around the nominal trajectory which must contain all the possible trajectories for all admissible values of the disturbances w_k. The dimensions of the tube depend on the choice of the gains K_k and on the interval between the control instants.

The constraints in (5.20) are conditions of non negativity of a quadratic function on a domain defined by two quadratic inequalities. Using (5.17) and the definition of ellipsoidal sets given in (C.1), the constraints in (5.20) can be written as:

$$\left((A_k + B_k K_k)\, e_k + w_k\right)^T Q_\alpha \left((A_k + B_k K_k)\, e_k + w_k\right) \leq 1,\ \forall \begin{cases} e_k^T Q_\alpha e_k \leq 1 \\ w_k^T Q_i^w w_k \leq 1 \end{cases} \tag{5.21}$$

By representing the ellipsoidal sets using a homogeneous quadratic inequality as in (C.4) and then applying the S-procedure (see (C.14)) and the Schur complement, the following constraints equivalent to (5.21) are obtained:

$$\begin{aligned} & \exists \tau_{k_1}, \tau_{k_2} \geq 0 \\ & \begin{bmatrix} 1 - \tau_{k_1} - \tau_{k_2} & 0 & 0 & 0 \\ 0 & \tau_{k_1} Q_\alpha & 0 & (A_k + B_k K_k)^T \\ 0 & 0 & \tau_{k_2} Q_k^w & I \\ 0 & A_k + B_k K_k & I & Q_\alpha^{-1} \end{bmatrix} \geq 0, k = 1...N-1 \end{aligned} \tag{5.22}$$

Conditions (5.22) are not yet LMIs because of the product between decision variables $\tau_{k_1} Q_\alpha$

and of the inverted term Q_α^{-1}. According to [97], a linear form can be obtained by imposing a special structure on the matrix Q_α:

$$Q_\alpha = \frac{1}{\alpha^2} Q \tag{5.23}$$

where Q is a constant matrix, chosen by the designer, which fixes the geometry of the tube. α is an optimization parameter which scales the tube towards the smallest possible size. Using this structure for the Q_α matrix transforms (5.22) into:

$$\begin{aligned} &\exists \tau_{k_1}, \tau_{k_2} \geq 0 \\ &\begin{bmatrix} 1-\alpha^2-\tau_{k_1}\alpha^2-\tau_{k_2} & 0 & 0 & 0 \\ 0 & \tau_{k_1} Q & 0 & (A_k + B_k K_k)^T \\ 0 & 0 & \tau_{k_2} Q w & I \\ 0 & A_k + B_k K_k & I & Q^{-1} \end{bmatrix} \geq 0 \end{aligned} \tag{5.24}$$

This new form still contains some nonlinear terms in α^2. These terms can be removed by pre- and post-multiplying the matrix in (5.24) with:

$$P = \begin{bmatrix} \alpha^{-1/2} I & 0 & 0 & 0 \\ 0 & \alpha^{1/2} I & 0 & 0 \\ 0 & 0 & \alpha^{-1/2} I & 0 \\ 0 & 0 & 0 & \alpha^{1/2} \end{bmatrix} \tag{5.25}$$

After this operation, the optimization problem (5.19) can be written using only linear constraints:

$$\begin{aligned} \min_{\hat{K}_k, \alpha, \hat{\tau}_{k_1}, \hat{\tau}_{k_2}} \quad & \alpha \\ \text{s.t.} \quad & \begin{cases} \exists \hat{\tau}_{k_1}, \hat{\tau}_{k_2} \geq 0 \\ R_k \geq 0 \end{cases}, \forall k = 1..N-1 \end{aligned} \tag{5.26}$$

where the matrices R_k are defined as:

$$R_k = \begin{bmatrix} \alpha - \hat{\tau}_{k_1} - \hat{\tau}_{k_2} & 0 & 0 & 0 \\ 0 & \hat{\tau}_{k_1} Q & 0 & (\alpha A_k + B_k \hat{K}_k)^T \\ 0 & 0 & \hat{\tau}_{k_2} Q_k^w & I \\ 0 & \alpha A_k + B_k \hat{K}_k & I & \alpha Q^{-1} \end{bmatrix} \tag{5.27}$$

and $\hat{K}_k = \alpha K_k$, $\hat{\tau}_{k_1} = \alpha^{-1} \tau_{k_1}$ and $\hat{\tau}_{k_2} = \alpha \tau_{k_2}$.

Solving (5.26) enables the computation of the feedback gains K_k such that the error tube is scaled to the smallest possible size for a given shape fixed by the matrix Q. Next, we will now focus on the computation of the terms ΔV_k which define the nominal trajectory.

5.3.2 Computation of the nominal control

The objective for the nominal trajectory is to reach the final rendezvous objective X_f in a fuel-optimal manner. The main difference with respect to the fixed-time rendezvous problem defined in (4.13) is that the saturation constraints need to be modified in order to ensure the necessary margin for the feedback correction terms required for the real trajectory. The procedure resembles the constraints tightening approach described in Section 5.1. but in our case the feedback terms result from an optimization procedure which minimizes the dimensions of the final arrival set.

The nominal trajectory does not necessarily have to start from the initial measured spacecraft relative state $X_1^m = \tilde{X}_1$. According to (5.19), it is sufficient that the difference between the two initial conditions be bounded by the ellipsoidal set defined by Q_α in order to guarantee the final rendezvous precision. Hence, the initial state for the nominal trajectory can be considered as a decision variable.

With K_k and consequently Q_α computed using (5.26), the optimal control problem for the nominal trajectory can be written as:

$$\begin{aligned} \min_{\Delta V_k, \bar{X}_1} \quad & \sum_{k=1}^{N-1} \|\Delta V_k\|_1 \\ \text{s.t.} \quad & \begin{cases} \bar{X}_{k+1} = A_k \bar{X}_k + B_k \Delta V_k \\ e_1 \in E(X_1^m, Q_\alpha),\ \bar{X}_N = X_f \\ u_k = \Delta V_k + K_k e_k,\ e_k \in E(0, Q_\alpha) \\ |u_k| \leq \Delta \tilde{V}_{\max}(\nu_i),\ \forall e_k \in E(0, Q_\alpha) \end{cases} \end{aligned} \tag{5.28}$$

Problem (5.28) aims at optimizing the nominal fuel-cost rather than the worst case performance by choosing a criterion in the nominal control variables.

The saturation constraints in (5.28) have been written following the same assumptions about the configuration of the spacecraft thrusters as in (4.8). They concern the control policies u_k for the perturbed spacecraft relative trajectory but can be written as constraints on the nominal decision variables ΔV_k:

$$|\Delta V_k| \leq \Delta \tilde{V}_{\max}(\nu_i) - \max_{e_k \in E(0, Q_\alpha)} K_k\, e_k,\ k = 1...N-1 \tag{5.29}$$

The usage of ellipsoidal sets enables for (5.29) to be replaced by:

$$|\Delta V_k| \leq \Delta \tilde{V}_{\max}(\nu_i) - \|K_k P_\alpha\|_2, \;\; P_\alpha = Q_\alpha^{-1/2} \tag{5.30}$$

The saturation constraint (5.30) is the main reason why the correction gains K_k and the nominal controls ΔV_k are computed separately. If K_k is considered as a decision variable then so is P_α and in this case the norm-2 constraint in (5.30) is not convex. The separate computation of K_k and ΔV_k removes this issue but it also introduces the risk of the problem becoming infeasible if the resulting saturation constraints are too restrictive.

Finally, once K_k and ΔV_k are computed using the described procedures, the obtained rendezvous control plan can be applied without any recomputation, and it will steer the spacecraft towards the final objective with a guaranteed precision given by Q_α.

5.4 Affine disturbance feedback MPC

According to [35], a convex formulation for the control problem (5.15) can be directly found if the control policies u_k are parametrized as affine disturbance feedback control laws instead of affine state feedback control laws. In this case, the structure of u_k is given by:

$$u_k = \Delta V_k + \sum_{i=1}^{k-1} L_{k,i} w_i, \;\; w_i \in E(0, Q_i^w), \;\; k = 1...N-1 \tag{5.31}$$

where the disturbance feedback terms are considered only until $k-1$ to ensure the causality of the control.

The value of the perturbation w_k is unknown at the instant k. Its value can only be estimated at the next time step based on the effects it produces on the spacecraft relative trajectory. If the only source of errors are the navigation uncertainties then, by using (5.10), the perturbation term w_k can be evaluated from the current measure X_{k+1}^m and the prediction made in nominal conditions starting from the previous measure X_k^m. The difference between the two is due to the disturbance w_k:

$$w_k = X_{k+1}^m - (A_k X_k^m + B_k u_k) \tag{5.32}$$

For the control structure defined in (5.31), the evolution of the errors between the real trajectory

and the nominal trajectory is given by:

$$\begin{aligned} e_1 &= X_1^m - \bar{X}_1 \\ e_2 &= A_1 e_1 + w_1 \\ e_3 &= A_2 A_1 e_1 + (A_2 + B_2 L_{2,1}) w_1 + w_2 \\ e_4 &= A_3 A_2 A_1 e_1 + (A_3(A_2 + B_2 L_{2,1}) + B_3 L_{3,1})\, w_1 + (A_3 + B_3 L_{3,2}) w_2 + w_3 \\ &\vdots \end{aligned} \tag{5.33}$$

It can be seen that choosing the decision variables as in (5.31) leads to expressions for the propagation of the errors which do not contain any nonlinear products between the gain matrices. This provides an advantage with respect to expressions (5.18) obtained for the affine state feedback case and greatly simplifies the control synthesis procedure by allowing the simultaneous computation of the feedback gains $L_{k,i}$ and of the nominal controls ΔV_k.

The causality consideration in (5.31) forces the first control u_k to be equal to the first thrust of the nominal trajectory ΔV_k. This causes any initial mismatch between the perturbed trajectory and the nominal trajectory to be propagated in open-loop over the prediction horizon, as it can be seen from (5.33). This problem can be removed by no longer considering the initial state for the nominal trajectory as an optimization variable and instead imposing that:

$$\bar{X}_1 = X_1^m \tag{5.34}$$

which causes e_1 to be always equal to zero.

Let $\mathbf{X} = \begin{bmatrix} X_{1|2}^m & X_{1|3}^m & \dots & X_{1|N}^m \end{bmatrix}^T$ be the prediction of the evolution of the closed-loop perturbed trajectory starting from the initial measured state X_1^m. $\mathbf{X}$ can be written in a compact form as:

$$\mathbf{X} = \mathbf{A} X_1^m + \mathbf{B}\boldsymbol{\Delta}\mathbf{V} + (\mathbf{B}\mathbf{L} + \mathbf{C})\mathbf{w} \tag{5.35}$$

where the matrices $\mathbf{A} \in \mathbb{R}^{6(N-1)\times 6}$, $\mathbf{B} \in \mathbb{R}^{6(N-1)\times 3(N-1)}$ and $\mathbf{C} \in \mathbb{R}^{6(N-1)\times 6(N-1)}$ are defined as:

$$\mathbf{A} = \begin{bmatrix} A_1 \\ A_2 A_1 \\ \vdots \\ A_{N-1} \dots A_1 \end{bmatrix} \quad \mathbf{B} = \begin{bmatrix} B_1 & 0 & 0 & 0 & \dots \\ A_2 B_1 & B_2 & 0 & 0 & \dots \\ \vdots & \vdots & & & \\ A_{N-1} \dots A_2 B_1 & & \dots & \dots & B_{N-1} \end{bmatrix} \quad \mathbf{C} = \begin{bmatrix} I & 0 & 0 & 0 & \dots \\ A_2 & I & 0 & 0 & \dots \\ \vdots & \vdots & & & \\ A_{N-1} \dots A_2 & & & A_{N-1} & I \end{bmatrix} \tag{5.36}$$

and $\boldsymbol{\Delta}\mathbf{V} = \begin{bmatrix} \Delta V_1 & \Delta V_2 & \dots & \Delta V_{N-1} \end{bmatrix}^T$, $\mathbf{w} = \begin{bmatrix} w_1 & w_2 & \dots & w_{N-1} \end{bmatrix}^T$. The gain matrix $\mathbf{L} \in \mathbb{R}^{3(N-1)\times 6(N-1)}$

is defined by:

$$\mathbf{L} = \begin{bmatrix} 0 & 0 & 0 & ... & 0 \\ L_{2,1} & 0 & 0 & ... & 0 \\ L_{3,1} & L_{3,2} & 0 & ... & 0 \\ \vdots & & & & \\ L_{N-1,1} & ... & ... & L_{N-1,N-2} & 0 \end{bmatrix} \tag{5.37}$$

Taking into consideration the constraint (5.34), the evolution of the nominal trajectory $\bar{\mathbf{X}} = \begin{bmatrix} \bar{X}_{1|2} & \bar{X}_{1|3} & ... & \bar{X}_{1|N} \end{bmatrix}^T$ is given by:

$$\bar{\mathbf{X}} = \mathbf{A}X_1^m + \mathbf{B}\boldsymbol{\Delta}\mathbf{V} \tag{5.38}$$

The error between the perturbed trajectory and the nominal trajectory can be written in this case as a linear function of the disturbance vector $\mathbf{w}$:

$$\mathbf{e} = \mathbf{X} - \bar{\mathbf{X}} = (\mathbf{BL} + \mathbf{C})\mathbf{w} \tag{5.39}$$

It becomes clear that a good choice for the matrix $\mathbf{L}$ could limit the effects of the navigation errors on the spacecraft rendezvous trajectory. We are searching for the nominal control $\boldsymbol{\Delta}\mathbf{V}$ and the correction gains matrix $\mathbf{L}$ that guarantee the smallest error at the end of the prediction horizon e_N and the lowest fuel-cost for the nominal trajectory, all while robustly satisfying the saturation constraints on the thrusters.

The objective for the final error can once again be interpreted in terms of minimizing the dimensions of an ellipsoidal set that bounds e_N for all the possible values of the uncertainties:

$$\min_{\mathbf{L}} \ \text{tr}\ Q_f \ \text{s.t.}\ e_N \in E(0, Q_f^{-1}),\ \forall w_i \in E(0, Q_i^w),\ i = 1...N-1 \tag{5.40}$$

By using the dynamics of the errors from (5.39), the constraint in (5.40) can be written as:

$$\mathbf{w}^T(\mathbf{B_N L} + \mathbf{C_N})^T Q_f^{-1}(\mathbf{B_N L} + \mathbf{C_N})\mathbf{w} \leq 1,\ \forall w_i \in E(0, Q_i^w),\ i = 1..N-1 \tag{5.41}$$

where $\mathbf{B_N}$ and $\mathbf{C_N}$ are obtained by selecting the appropriate lines in the $\mathbf{B}$ and $\mathbf{C}$ matrices. Using the S-procedure and the Schur complement, the quadratic constraint (5.41) can be transformed into a linear matrix inequality:

$$\exists \tau_1,\ \tau_2,\ ...\ \tau_{N-1} \geq 0,\ Q_f \succeq 0 \ \text{s.t.}\ R \succeq 0 \tag{5.42}$$

where the matrix R is defined as:

$$R = \begin{bmatrix} 1 - \sum_{k=1}^{N-1} \tau_k & 0 & 0 \\ 0 & Q_w & (\mathbf{B_N L} + \mathbf{C_N})^T \\ 0 & (\mathbf{B_N L} + \mathbf{C_N}) & Q_f \end{bmatrix}, \quad Q_w = \begin{bmatrix} \tau_1 Q_1^w & & \\ & \ddots & \\ & & \tau_{N-1} Q_{N-1}^w \end{bmatrix} \tag{5.43}$$

The saturation constraints on the control u_k are written based on the same assumptions as in (4.8) about the configuration of the spacecraft thrusters. The constraints must be respected for all admissible values of the uncertainties:

$$|u_k| \leq \Delta \tilde{V}_{\max}(\nu_k), \ \forall w_i \in E(0, Q_i^w), \ i = 1...k-1, \ k = 1...N-1 \tag{5.44}$$

The usage of ellipsoidal sets enables us to transform the constraints (5.44) in tightened constraints on the nominal controls:

$$|\Delta V_k| \leq \Delta \tilde{V}_{\max}(\nu_k) - \sum_{i=1}^{k-1} \|L_{k,i} P_i^w\|_2, \ k = 1...N-1 \tag{5.45}$$

where $P_i^w = (Q_i^w)^{-1/2}$. The previous constraint is a conic constraint since only ΔV_k and $L_{k,i}$ are decision variables while the domains for the disturbances w_i are considered known. The final convex optimization problem that needs to be solved in order to find the affine disturbance feedback control laws u_k can be written as:

$$\begin{aligned} \min_{Q_f, \Delta V_k, L_{k,i}} \quad & \text{tr } (T(\nu_N)^{-1} Q_f T(\nu_N)^{-T}) + \|\mathbf{\Delta V}\|_1 \\ \text{s.t.} \quad & \begin{cases} \bar{X}_{k+1} = A_k \bar{X}_k + B_k \Delta V_k \\ \bar{X}_1 = X_1^m, \ \bar{X}_N = X_f \\ |\Delta V_k| \leq \Delta \tilde{V}_{\max}(\nu_k) - \sum_{i=1}^{k-1} \|L_{k,i} P_i^w\|_2, \ k = 1...N-1 \\ \exists \tau_1, \ \tau_2, \ ... \ \tau_{N-1} \geq 0 \\ Q_f \succeq 0, \ R \succeq 0 \end{cases} \end{aligned} \tag{5.46}$$

The optimization criterion reflects the compromise between the fuel cost of the nominal trajectory and the rendezvous precision, represented by the ellipsoidal set bounding the final error. The matrix T in the criterion accounts for the variable change (1.17) that has been performed on the spacecraft relative state in order to reach the dynamical model used for control computation. Minimizing the domain for the transformed variables might not necessarily translate into a minimal domain for

the original variables. The matrix T ensures that the optimized domain corresponds to the errors expressed using the time-domain variables and is defined by:

$$T(\nu) = \begin{bmatrix} (1+e\cos\nu)I_3 & 0_3 \\ -e\sin\nu I_3 & \dfrac{(1+e\cos\nu)}{\dot{\nu}}I_3 \end{bmatrix} \tag{5.47}$$

where ν_N is the true anomaly which corresponds to the final time of the rendezvous.

The advantage of this approach over the affine state feedback control plan is that only one optimization problem needs to be solved in order to determine all the parameters of the control laws.

5.5 Numerical evaluation of the robust control techniques

The performances of the two previously presented robust control techniques are evaluated for different rendezvous scenarios. The comparison criteria are the fuel-cost of the rendezvous trajectories and the dimensions of the set bounding the final error. The obtained performances are first illustrated in closed-loop simulations using the linear model for the propagation of the spacecraft relative motion based on the Yamanaka-Ankersen state transition matrix. The guaranteed performances are then validated using a nonlinear propagation model. The nonlinear simulator is based on Gauss Variational Equations and its detailed description can be found in [49].

5.5.1 Description of the simulation procedure

The simulations start form perturbed initial conditions, obtained by adding a random noise δX to the initial spacecraft relative state used for control synthesis. Random noise is also added to all the other relative states that are measured during the simulations. The noise is bounded by an ellipsoidal set with semi-axis of 0.02 m for the relative position and 0.002 m/s for the relative velocity.

The outer ellipsoidal approximations for the domains of the disturbances w are computed using the analytical procedure given in (C.10). The obtained ellipsoidal sets $E(0, Q_i^w)$ depend on the domain for the navigation uncertainties δX and on the time interval between two consecutive control instants. Before starting the simulations, the parameters of the robust control laws also need to be computed by solving the corresponding optimal control problems. The specific procedure for each case is detailed in what follows, but the common point is that no call to an optimization procedure is made during the simulations. This means that if the presented control techniques were

used for a spacecraft rendezvous mission, all the computational effort could be carried out using the resources available at the ground control station, followed by an upload of the resulting parameters on-board the follower spacecraft.

Affine state feedback

The gains K_k for the affine state feedback laws are computed by solving the SDP (5.26) while the nominal control are obtained from (5.28). The two optimization problems are solved using Yalmip [63] and the solver SDPT3 [100]. The obtained solution depends on the choice of the Q matrix defined in (5.23). This matrix specifies the geometry of the tube which bounds all the possible rendezvous trajectories.

One way of choosing Q comes from considering the variable change (1.17). The optimization problem (5.26) is written for the transformed variables but our purpose is to obtain good performances for the actual spacecraft relative trajectory. The transformation (1.17) introduces an artificial scale factor between the values of the spacecraft relative position and velocity, factor that depends on the orbital parameters of the leader spacecraft. A good choice for the matrix Q can normalize this difference and lead to better results in terms of rendezvous precision.

The states $\bar{X}_k$ belonging to the nominal trajectory also need to be evaluated at the predefined control instants, since their values are used for control computation. They can easily be obtained from (5.11), where the initial condition is the one provided by the resolution of (5.28). The worst case fuel consumption can be evaluated before the simulations by adding to each nominal control the maximum possible correction:

$$\Delta V_{\max} = \sum_{k=1}^{N-1} \left(\Delta V_k + \| K_k P_\alpha \|_2 \right) \tag{5.48}$$

The velocity increments are evaluated during the simulations at each control instant. Their values depend on the obtained measurements and can be computed using the definition in (5.16).

Affine disturbance feedback

The parameters defining the series of disturbance feedback control laws are obtained after solving the SDP defined in (5.46) using Yalmip [63] and the solver SDPT3 [100]. The worst case fuel consumption can be evaluated before the simulation by adding to each nominal control the maximum possible correction:

$$\Delta V_{\max} = \sum_{k=1}^{N-1} \left(\Delta V_k + \sum_{i=1}^{k-1} \| L_{k,i} P_i^w \|_2 \right) \tag{5.49}$$

The velocity increments are evaluated during the simulations, at each control instant, using the definition in (5.31). The perturbation terms w are also evaluated at each control instant during the simulations, based on the obtained relative state measurements. Their values are obtained by using (5.32) and then stored in the memory until the end of each scenario. This is necessary since the history of past disturbances contribute to the computation of the control.

The closed-loop performances are evaluated for two different rendezvous scenarios: the quasi-circular PRISMA mission [75] and the highly eccentric Simbol-X mission [30].

5.5.2 The PRISMA mission

The robust control techniques are first tested on a PRISMA spacecraft rendezvous mission. The data defining the orbital parameters of the leader spacecraft are given in Table 5.2.

Mission	a [km]	e	i [°]	Ω [°]	ω [°]	$\Delta V_{\max}$ [m/s]
PRISMA	7 011	0.004	98	190	0	0.26

Table 5.2: Reference orbit data for the PRISMA rendezvous mission

In this case, we consider the matrix Q for the affine state feedback method as:

$$Q = \text{diag}\ (1, 1, 1, 0.01, 0.01, 0.01) \tag{5.50}$$

which roughly corresponds to the difference in magnitude between the spacecraft relative position and velocity after the transformation (1.17).

The data corresponding to the chosen rendezvous scenario are given in Table 5.3. We are interested in analysing the influence of the duration of the mission on the size of the guaranteed final arrival set and on the fuel cost of the mission.

Mission	X_1 [m,m/s]	ν_1 [°]	X_f [m,m/s]	duration [s]	N
PRISMA	[10000,0,0,0,0,0]	0	[330,0,30,0,0,-0.0158]	18 000	10

Table 5.3: Simulation scenario for the PRISMA rendezvous mission

The size of the guaranteed arrival set is illustrated in Table 5.4 for different values of the mission duration. The number of impulsive thrusts is maintained constant. The presented values correspond to the semi-axes in the xz plane of the ellipsoidal sets which bound the final errors for all the possible values of the navigation uncertainties. The comparison is made between the application of the nominal plan in open-loop, the usage of the state feedback plan and the usage of the disturbance feedback plan.

mission duration [s]	9 000		12 000		15 000		18 000	
open-loop MPC [m]	56.82	1.4	70.08	0.61	93.65	1.3	105.2	0.9
state feedback MPC [m]	4.056	4.056	6.49	6.49	9.89	9.89	14.1	14.1
disturbance feedback MPC [m]	3.92	2.32	6.4	2.86	9.63	3.23	13.92	3.48

Table 5.4: Semi-axes of the arrival set in the xz plane for the PRISMA mission

As expected, the two closed-loop approaches offer great benefits over the open-loop case. If the sum of the semi-axes is considered, the precision guaranteed by the disturbance feedback approach is better for all the values considered for the mission duration. The size of the final guaranteed arrival sets increases for both robust control methods with the extension of the prediction horizon. This is to be expected since increasing the prediction horizon without increasing the number of control instants causes the navigation uncertainties to be propagated in open-loop for a longer period of time (as showed in Section 5.2.2).

The difference between the fuel cost of the nominal trajectory and the maximum possible fuel cost for the perturbed closed loop trajectory is presented in Table 5.5. It can be noticed that the lowest nominal cost is obtained every time for the state feedback approach. This is a consequence of the fact that, for this approach, the initial state for the nominal trajectory is a decision variable. This allows an extra degree of freedom for the optimization algorithm leading to a smaller fuel cost for the nominal path. However, the maximum possible fuel cost can be significantly higher, depending on the dimensions of the error tube guaranteed by the correction gains.

mission duration [s]	9 000		12 000		15 000		18 000	
open-loop MPC [m/s]	1.1951		0.9997		0.6548		0.6505	
state feedback MPC [m/s]	0.7343	1.9175	0.5826	2.4873	0.4677	3.3503	0.5403	4.6760
disturbance feedback MPC [m/s]	1.1952	1.3809	1.0015	1.1878	0.6548	0.8444	0.6505	0.8593

Table 5.5: Nominal fuel cost and maximum possible closed-loop cost for the PRISMA mission

In the disturbance feedback case, the variation between the nominal fuel cost and the maximum fuel cost is smaller. It can also be seen that in this case the nominal cost tends towards the open-loop cost as the mission duration increases. This comes from the fact that, for longer mission durations, the thrusters saturations constraints are no longer active.

Linear closed-loop simulations

The closed-loop behaviour of the system is analysed first using the linear model for spacecraft relative motion. The simulations follow the procedure that has been described in the first part of

this section.

mission duration [s]	9 000	12 000	15 000	18 000
average ΔV state feedback MPC [m/s]	1.3506	1.5304	0.75	1.0631
average ΔV disturbance feedback MPC [m/s]	1.2139	1.0206	0.6741	0.6722

Table 5.6: The average linear closed-loop fuel-cost for the PRISMA mission

The average fuel consumption obtained for the linear closed-loop simulations is presented in Table 5.6. The average is computed for 100 runs of the rendezvous scenario starting from different perturbed initial conditions. It can be seen that for the state feedback case, even if the average fuel consumption is lower than the upper bound given in Table 5.5, it is always higher than the one obtained for the disturbance feedback case.

The trajectories obtained using the two robust control methods for a mission duration of 18000 s are depicted in Figure 5.1. The open-loop trajectories are also showed in order to emphasize the spread of the perturbed rendezvous trajectories that occurs in the absence of closed-loop corrections. Even if the trajectories followed by the two robust methods are different, they both reach the final objective within the guaranteed precision.

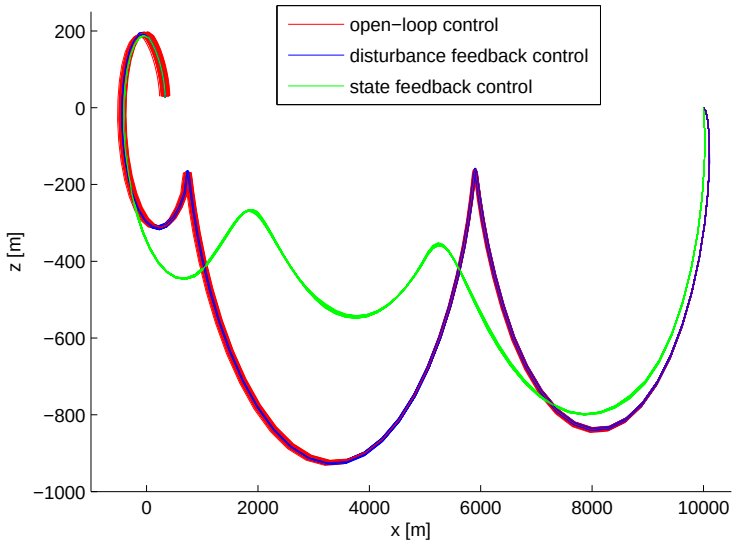

Figure 5.1: The rendezvous trajectories for the PRSIMA mission using the linear propagation model

Figure 5.2 presents the final arrival sets guaranteed by the robust algorithms, $E(0, Q_\alpha)$ for the state feedback case and $E(0, Q_f)$ for the disturbance feedback case, along with the obtained errors with respect to the mission's final objective. As expected, the final errors belong to the guaranteed arrival sets.

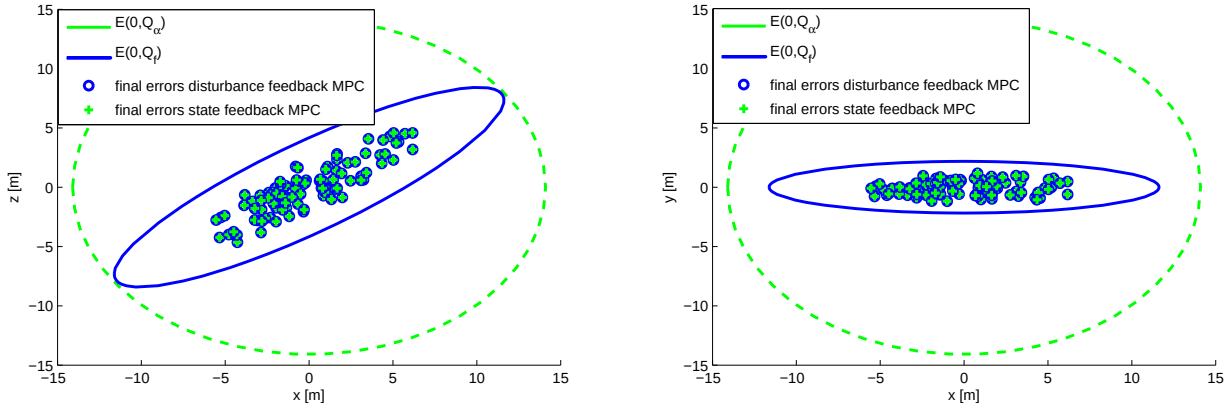

Figure 5.2: Final errors and the guaranteed arrival sets for the PRISMA mission using the linear propagation model

Nonlinear closed-loop simulations

The control performances for the nonlinear closed-loop simulations are evaluated for trajectories obtained starting from 100 different perturbed initial conditions. The average closed-loop fuel consumption is given in Table 5.7 for the same values of the mission durations considered for the linear case. It can be noticed that the average fuel consumption is higher than the one obtained for the linear case but lower than the theoretical upper bound given in Table 5.5. The difference between the linear and the nonlinear behaviour is more visible for the state feedback case where the average fuel consumption is up to 40% higher (see Table 5.6).

mission duration [s]	9 000	12 000	15 000	18 000
average ΔV state feedback MPC [m/s]	1.5012	1.6838	1.0731	1.5806
average ΔV disturbance feedback MPC [m/s]	1.3080	1.0840	0.7236	0.7083

Table 5.7: The average nonlinear closed-loop fuel-cost for the PRISMA mission

Figure 5.3 shows the comparison between the trajectories obtained for the open-loop control and for the two robust closed-loop control techniques. The mission duration is 18000 s, the same value as for the linear case. The open-loop trajectories show that, for the nonlinear model, the dispersion of the perturbed trajectories is slightly higher and accompanied by an offset with respect to the desired final position. The offset on the x axis for instance is about 800 m. This is due to the mismatch between the linear and nonlinear dynamics for the spacecraft relative motion. Even if this source of errors has not been considered during the control synthesis, the guaranteed precision with respect to the final objective is still respected for the two closed-loop approaches (see Figure 5.4).

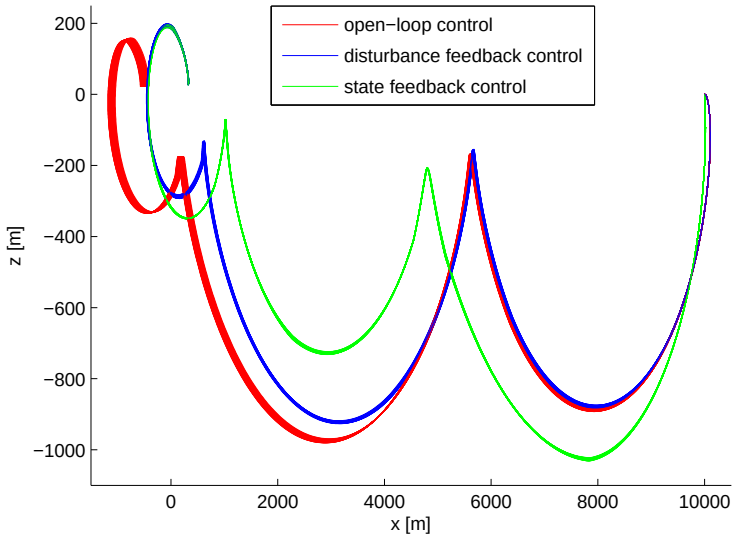

Figure 5.3: The rendezvous trajectories for the PRSIMA mission using the nonlinear propagation model

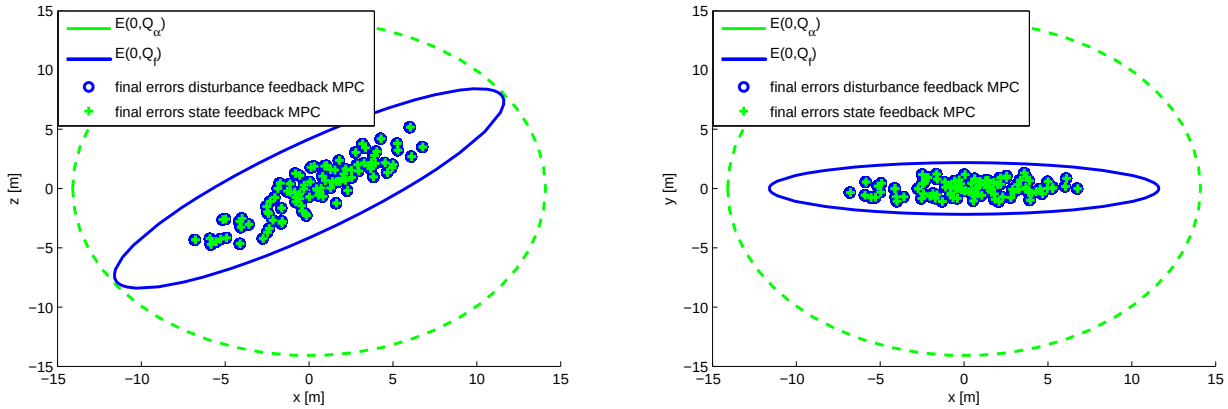

Figure 5.4: Final errors and the guaranteed arrival sets for the PRISMA mission using the nonlinear propagation model

5.5.3 The Simbol-X mission

The robust guidance techniques are also tested on a highly eccentric rendezvous mission called Simbol-X. The data for the reference orbit is summarized in Table 5.8. The simulations follow the procedure described in the first part of this section.

Mission	a [km]	e	i [°]	Ω [°]	ω [°]	$\Delta V_{\max}$ [m/s]
Simbol-X	106 247	0.7988	5.2	180	90	0.8

Table 5.8: Reference orbit data for the Simbol-X rendezvous mission

For this scenario, the Q matrix which shapes the tube for the state feedback control strategy is

taken as:

$$Q = \text{diag}\,(1, 1, 1, 0.0001, 0.0001, 0.0001) \tag{5.51}$$

in order to compensate the difference in the values of the position and velocity caused by the variable change (1.17) for this highly eccentric orbit.

The data corresponding to the particular rendezvous scenario that is considered here are given in Table 5.9. Different mission durations are considered throughout the simulations in order to analyse the influence of this parameter on the fuel-cost of the mission and on the dimensions of the guaranteed arrival set.

Mission	X_1 [m,m/s]	ν_1 [°]	X_f [m,m/s]	duration [s]	N
Simbol-X	[-305,0,396,0,0,0]	135	[-60.2,0,79.85,0,0,0]	8 000	10

Table 5.9: Simulation scenario for the Simbol-X rendezvous mission

The semi-axes in the xz plane of the guaranteed ellipsoidal arrival sets are presented in Table 5.10 for each of the control methods and for different values of the mission duration. As in the case of the PRISMA mission, the benefits of adding the feedback correction terms can be easily observed. The arrival set guaranteed by the disturbance feedback approach is always smaller than in the case of the state feedback approach, if the sum of the semi-axes is considered. For each one of the chosen rendezvous durations, the disturbance feedback control guarantees a better rendezvous precision in presence of navigation uncertainties.

mission duration [s]	8 000		12 000		16 000		20 000	
open-loop MPC [m]	16.15	15.92	24.48	23.76	33.04	31.5	41.86	39.17
state feedback MPC [m]	6.19	6.19	6.48	6.48	7.4	7.4	9.01	9.01
disturbance feedback MPC [m]	2.55	2.55	3.74	3.74	4.94	4.94	6.19	6.19

Table 5.10: Semi-axes of the arrival set in the xz plane for the Simbol-X mission

Table 5.11 presents the influence of the mission duration on the fuel cost for the nominal trajectory and on the maximum possible fuel cost for the perturbed closed loop trajectories. The nominal fuel cost for the disturbance feedback method is every time equal to the open-loop cost, meaning that the tightened saturation constraints are not active. Just like for the PRISMA mission, the nominal fuel cost for the state feedback case is always lower, accompanied by a maximum cost that is higher than for the disturbance feedback case.

mission duration [s]	8 000		12 000		16 000		20 000	
open-loop MPC [m/s]	0.1578		0.1053		0.0792		0.0637	
state feedback MPC [m/s]	0.1455	0.3777	0.0934	0.3152	0.0663	0.2974	0.0487	0.3081
disturbance feedback MPC [m/s]	0.1578	0.3161	0.1053	0.2637	0.0792	0.2379	0.0637	0.2192

Table 5.11: Nominal fuel cost and maximum possible closed-loop cost for the Simbol-X mission

Linear closed-loop simulations

The average fuel consumption obtained for the closed-loop simulations is presented in Table 5.12. The average is computed for 100 runs of the rendezvous scenario. The data show that for the state feedback case, even if the average fuel consumption is lower than the theoretical upper bound, it is always higher than the one obtained for the disturbance feedback case, regardless of the chosen mission duration.

mission duration [s]	8 000	12 000	16 000	20 000
state feedback MPC [m/s]	0.1818	0.1314	0.1055	0.0908
disturbance feedback MPC [m/s]	0.1755	0.1228	0.0957	0.0795

Table 5.12: The average linear closed-loop fuel-cost for the Simbol-X mission

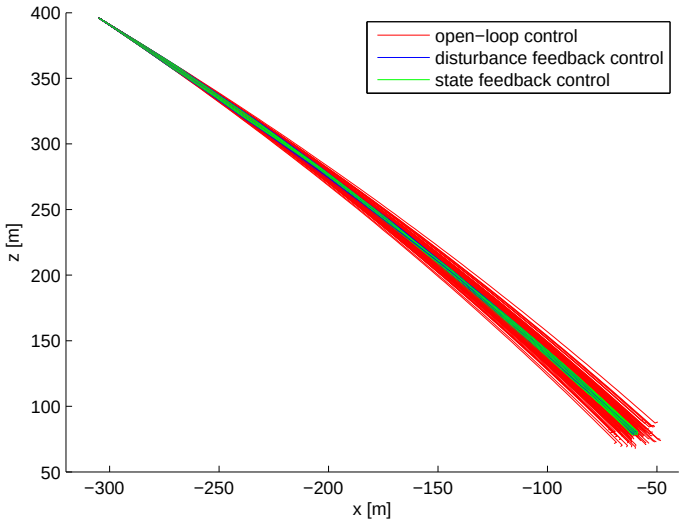

Figure 5.5: The rendezvous trajectories for the Simbol-X mission using the linear propagation model

Figure 5.5 shows the closed-loop trajectories obtained when applying the different control methods, for a mission horizon of 8000s. The open-loop trajectories corresponding to different perturbed initial conditions are also illustrated in order to evidence the spread of all the possible trajectories

under the effects of navigation uncertainties. In this case, the two methods lead to very similar closed-loop trajectories that effectively control the dispersion caused by the navigation errors.

The guaranteed arrival sets for the two robust control methods, $E(0, Q_\alpha)$ and $E(0, Q_f)$ respectively, are illustrated in Figure 5.6 along with the final errors with respect to the given rendezvous objective. As expected, the final errors are contained inside the arrival sets for all the cases considered during the simulations.

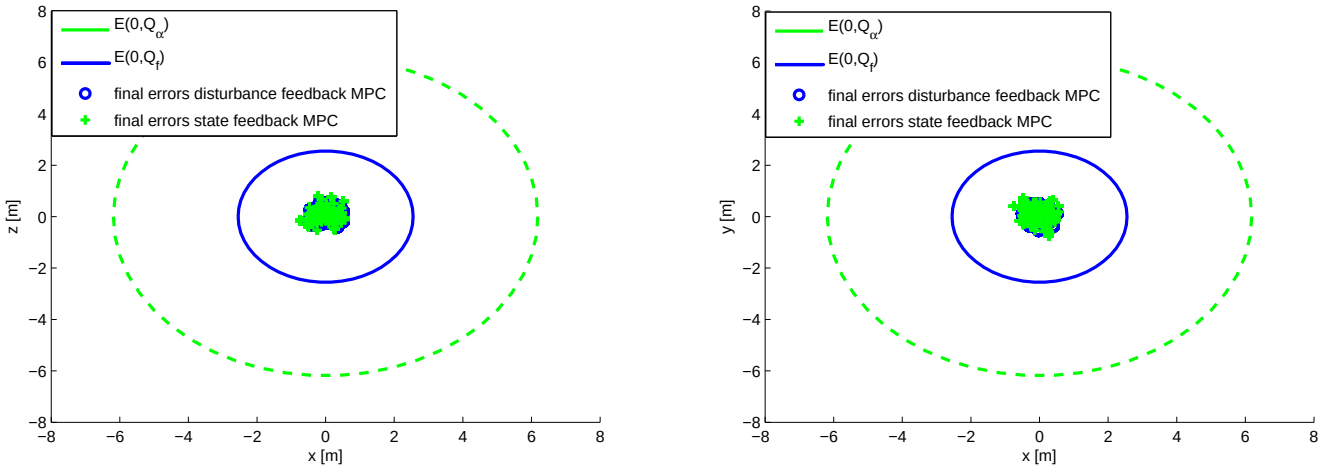

Figure 5.6: Final errors and the guaranteed arrival sets for the Simbol-X mission using the linear propagation model

Nonlinear closed-loop simulations

The average fuel consumption for the nonlinear closed-loop simulations is presented in Table 5.13 for each of the considered mission durations. The data show that, for these particular rendezvous scenarios, the average fuel consumption is very similar to the linear case. This can be explained by the small separation between the spacecraft, which limits the propagation errors, along with the short mission duration when compared to the orbital period.

mission duration [s]	8 000	12 000	16 000	20 000
state feedback MPC [m/s]	0.1821	0.1304	0.1072	0.0904
disturbance feedback MPC [m/s]	0.1755	0.1218	0.0963	0.0796

Table 5.13: The average nonlinear closed-loop fuel-cost for the Simbol-X mission

Figure 5.7 shows the nonlinear closed-loop trajectories obtained for each of the two robust control methods for the same mission horizon of 8000s. The open-loop trajectories are also illustrated in order to evidence the spread of all the possible trajectories under the effects of navigation un-

certainties. These trajectories are very similar to the linear case, suggesting that for the chosen scenario the effect of the propagation errors is very reduced.

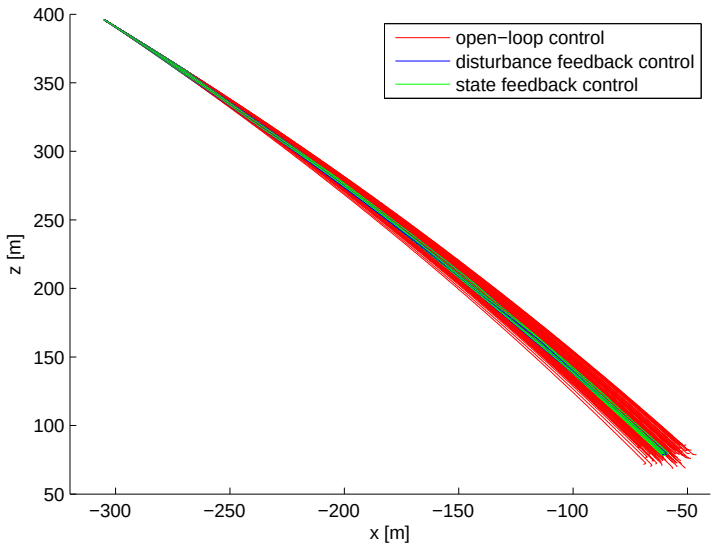

Figure 5.7: The rendezvous trajectories for the Simbol-X mission using the nonlinear propagation model

Figure 5.8 illustrates the guaranteed arrival sets, $E(0, Q_\alpha)$ for the state feedback method and $E(0, Q_f)$ for the disturbance feedback method, along with the closed-loop final errors with respect to the rendezvous objective. As expected, the final errors are contained inside the arrival sets for all the cases considered during the simulations.

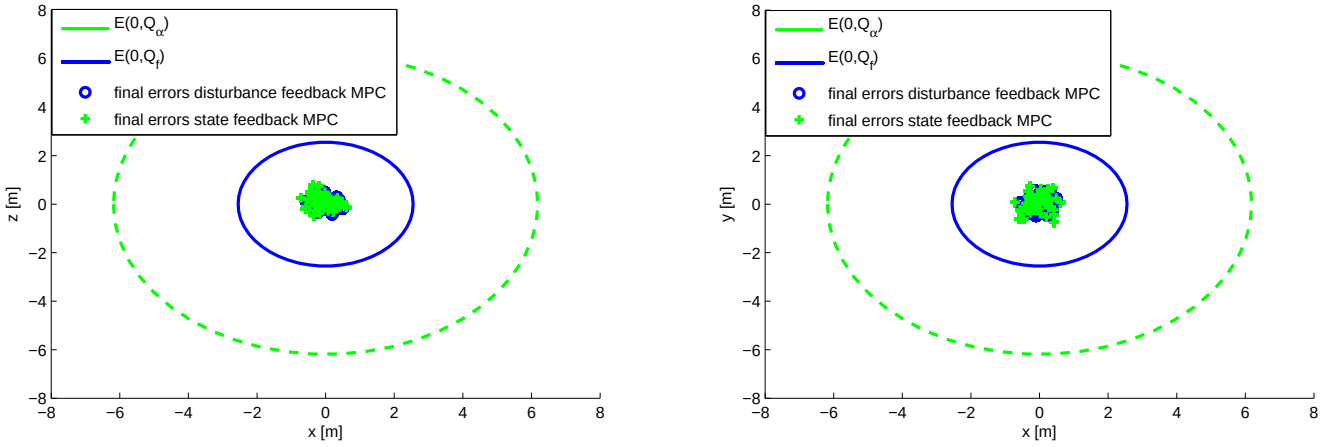

Figure 5.8: Final errors and the guaranteed arrival sets for the Simbol-X mission using the nonlinear propagation model

5.6 Conclusion

Different methods for obtaining a guidance algorithm for the spacecraft rendezvous that is robust to navigation uncertainties have been discussed in this chapter. Even if the final rendezvous objective cannot be precisely reached in presence of navigation uncertainties, this chapter proposes two control techniques which optimize the dimensions of a guaranteed final arrival set. The proposed methods rely on the computation of a series of feedback control laws that guarantee the robust constraints satisfaction and a good trade-off between the fuel cost of the resulting trajectory and the final rendezvous precision. The resulting convex optimal control problem can be solved only once before the beginning of the rendezvous maneuvers. The computed feedback laws can be then used directly at the corresponding control instant. This property might be particularly attractive in the case in which the on-board computational resources are limited. The problem can be solved using the resources available on the ground before the beginning of the maneuvers, followed by the upload of the parameters of the control laws to the spacecraft.

The difference between the developed robust control methods consists in the parametrization chosen for the computed feedback laws. Both approaches amount to solving some convex optimization problems and both method guarantee the constraints satisfaction for all the admissible values of the uncertainties. For the disturbance feedback parametrization, only one convex Semi Definite Program needs to be solved in order to obtain the solution while the state feedback parametrization imposes the decomposition of the synthesis into two separate steps. The existence of two separate steps might cause the control problem to be infeasible in cases where the disturbance feedback approach is able to provide a feasible solution. Moreover, the parametrization of the control laws as state feedback laws imposes some extra approximations in order to reach a convex formulation of the problem. It also introduces an extra tuning parameter, the matrix Q which fixes the geometry of the tube around the nominal trajectory. The quality of the obtained solution will depend on the chosen value and some guidelines for choosing this parameter have been provided.

The disturbance feedback approach enables us to specify a precision objective which concerns only the final error. In the state feedback case, limitations for the errors with respect to the nominal trajectory are enforced all along the rendezvous path. These constraints are added in order to be able to convexify the optimization problem. The disturbance feedback approach does not impose any particular constraints on the approach trajectory and this freedom is reflected by the fuel consumption. For the rendezvous missions chosen for illustration, the rendezvous performances in terms of final precision are very similar while the average fuel consumption is always higher in the state feedback case.

Chapter 6

Analytical bi-impulsive control around a desired periodic trajectory

Contents

Résumé: Ce chapitre porte sur le maintien du mouvement relatif périodique des satellites en présence des incertitudes de navigation. Le caractère instable des trajectoires périodique a été déjà mis en évidence dans le Chapitre 2. Ainsi, si l'état relatif est perturbé ou mal connu, une loi de commande doit être mise en place afin de stabiliser le mouvement périodique. Une technique de contrôle analytique à deux impulsions est développée dans ce chapitre. Cette techniques est basée sur l'observation qu'un vecteur constant de paramètres décrit entièrement une trajectoire périodique donnée. De plus, les trajectoires périodiques représentent des ensembles invariants pour le mouvement relatif des satellites. Cette loi de commande, qui est très peu gourmande en ressource numérique, est utilisée en conjonction avec les techniques de guidage robuste développées dans le chapitre précédent dans un stratégie de contrôle à deux étapes pour rejoindre et maintenir un mouvement périodique de proximité.

The spacecraft ability to maintain a proximity periodic relative motion is an important aspect of on-orbit servicing missions [85]. A precise mathematical characterisation of constrained periodic spacecraft relative trajectories has been given in Chapter 3. The resulting description of admissible

trajectories has been used in Chapter 4 to obtain a guidance algorithm towards a proximity periodic relative motion. The control technique is illustrated only in perfect conditions, with no navigation uncertainties or modelling errors. The effects of imperfect relative state information are analysed in Chapter 5. It is showed that, when measurement noise is considered, the desired final objective can no longer be exactly reached. Robust control algorithms are developed that instead can guarantee the guidance towards a minimal arrival set centered around the final desired state.

The unstable behaviour of the spacecraft periodic trajectories has been analysed in Chapter 2. The consequence of this unstable behaviour is that, even if the spacecraft arrive arbitrarily close to a desired periodic trajectory, the relative motion will not naturally converge towards it. In presence of navigation uncertainties, the robust guidance towards an arrival set centered around a desired periodic trajectory needs to be followed by a switch to a local controller which can robustly stabilize the spacecraft periodic relative motion. This chapter addresses this problem and proposes a local bi-impulsive controller. The chosen structure takes into consideration the limited computational resources available on-board the spacecraft and the preference for impulsive maneuvers.

6.1 Stability around a periodic relative trajectory

Let D be a given constant vector of parameters corresponding to a periodic spacecraft relative trajectory (see the definitions in Chapter 2). For the particular case of the periodic motion, the vector D is such that $d_0 = 0$. The set of spacecraft relative states belonging to the particular periodic trajectory defined by D is given by:

$$S_p(D) = \left\{ \tilde{X}(\nu) \in \mathbb{R}^6 \mid C(\nu)\tilde{X}(\nu) = D \; \forall \, \nu, \; \forall D \text{ such that } d_0 = 0 \right\} \tag{6.1}$$

where the matrix $C(\nu)$ is defined as in (2.5). The set $S_p(D)$ represents an *invariant set* for the autonomous spacecraft relative motion. This follows from the property of the spacecraft relative motion given in (2.20) which shows that:

$$\tilde{X}(\nu_k) \in S_p(D) \quad \Longrightarrow \quad \tilde{X}(\nu_j) \in S_p(D), \; \forall \nu_j \geq \nu_k \tag{6.2}$$

The objective of robustly stabilizing the spacecraft relative motion with respect to a chosen periodic trajectory can be translated into an objective of robust stability of the invariant set $S_p(D)$. In the general case, an invariant set S for an autonomous system $x(t_{k+1}) = f(x(t_k))$ is said to be

stable if, for each $\varepsilon \geq 0$, there exists $\delta \geq 0$ such that [51]:

$$\forall x(t_0) \text{ s.t. dist } (x(t_0), S) \leq \delta \Longrightarrow \text{dist } (x(t_k), S) \leq \varepsilon, \ \forall t_k \geq t_0 \tag{6.3}$$

where the distance from a state x to the set S is defined as:

$$\text{dist } (x, S) = \inf_{y \in S} \|x - y\| \tag{6.4}$$

An invariant set S is said to *asymptotically stable* if it is stable and δ can be chosen such that [51]:

$$\forall x(t_0) \text{ s.t. dist } (x(t_0), S) \leq \delta \Longrightarrow \lim_{k \to \infty} \text{dist } (x(t_k), S) = 0 \tag{6.5}$$

A control that stabilizes the spacecraft periodic motion in presence of navigation uncertainties must maintain bounded the distance between the spacecraft relative state and the invariant set $S_p(D)$. Following from (6.4), this distance can be defined as:

$$\text{dist } (\tilde{X}(\nu), S_p(D)) = \|C(\nu)\tilde{X}(\nu) - D\| \tag{6.6}$$

The purpose is to find a control law such that:

$$\text{dist } (\tilde{X}(\nu), S_p(D)) = 0 \tag{6.7}$$

6.2 Analytical bi-impulsive stabilizing control for the periodic motion

This section details the characteristics of an analytical bi-impulsive control law which can stabilize the spacecraft periodic relative motion. For a bi-impulsive structure of the control the condition (6.7) has an analytical solution, which can be obtained without too much computational effort. The stability of the periodic motion can be guaranteed while still relying on impulsive thrusts as in the previous chapters.

6.2.1 Computation of the control

Starting from the current spacecraft relative state measurement $\tilde{X}(\nu_k)$, two impulsive maneuvers $\Delta\tilde{V}_k$ and $\Delta\tilde{V}_{k+1}$ can be computed such that:

$$\text{dist}\ (\tilde{X}^+(\nu_{k+1}), S_p(D)) = 0 \tag{6.8}$$

where $\tilde{X}^+(\nu_{k+1})$ is the state *right after* the second impulsive control $\Delta\tilde{V}_{k+1}$. According to (5.2), $\tilde{X}^+(\nu_{k+1})$ is given by:

$$\tilde{X}^+(\nu_{k+1}) = \tilde{X}(\nu_{k+1}) + B\,\Delta\tilde{V}_{k+1}$$

Following from (5.3), $\tilde{X}^+(\nu_{k+1})$ can be written as a function of the current measured state:

$$\tilde{X}^+(\nu_{k+1}) = \Phi(\nu_{k+1}, \nu_k)\,\tilde{X}(\nu_k) + \Phi(\nu_{k+1}, \nu_k)\,B\,\Delta\tilde{V}_k + B\,\Delta\tilde{V}_{k+1} \tag{6.9}$$

Introducing this expression into (6.8) leads to the following stability condition:

$$\|C(\nu_{k+1})\left(\Phi(\nu_{k+1}, \nu_k)\,\tilde{X}(\nu_k) + \Phi(\nu_{k+1}, \nu_k)\,B\,\Delta\tilde{V}_k + B\,\Delta\tilde{V}_{k+1}\right) - D\| = 0 \tag{6.10}$$

The two impulsive controls that bring the system to the invariant set $S_p(D)$ can be obtained through direct computation:

$$\begin{bmatrix} \Delta\tilde{V}_k \\ \Delta\tilde{V}_{k+1} \end{bmatrix} = \begin{bmatrix} \Phi(\nu_{k+1}, \nu_k)\,B & B \end{bmatrix}^{-1} \tilde{e}_{k|k+1} \tag{6.11}$$

where $e_{k|k+1}$ is defined as:

$$\tilde{e}_{k|k+1} = \tilde{X}_p(\nu_{k+1}) - \Phi(\nu_{k+1}, \nu_k)\,\tilde{X}(\nu_k) \tag{6.12}$$

The term $\tilde{X}_p(\nu_{k+1})$ defines the spacecraft relative state belonging to the desired periodic trajectory specified through the vector of parameters D at the instant ν_{k+1}. Using (2.8), $\tilde{X}_p(\nu_{k+1})$ is defined as:

$$\tilde{X}_p(\nu_{k+1}) = F(\nu_{k+1})\,D \tag{6.13}$$

The term $e_{k|k+1}$ corresponds to an *anticipated error* between the spacecraft trajectory and the desired periodic trajectory, computed based on the current state measure $\tilde{X}(\nu_k)$ and assuming autonomous propagation over the interval $[\nu_k\ \nu_{k+1}]$.

It should be noted that for the matrix in (6.11) to be invertible, the interval between the two impulsive controls must be chosen such that: $\nu_{k+1} - \nu_k \neq m\pi,\ m \in \mathbb{N}$.

6.2.2 Domain of validity

The amplitude of the two impulsive controls computed using (6.11) depends on the anticipated error between the current measure and the desired periodic trajectory and on the chosen interval between the two thrusts. The obtained control is valid only in a domain where the saturation constraints of the thrusters are satisfied. We assume that the saturation constraints are defined as in (4.8) by some polytopic constraints:

$$H_\Delta \begin{bmatrix} \Delta\tilde{V}_k \\ \Delta\tilde{V}_{k+1} \end{bmatrix} \leq \tilde{V}_\Delta(\nu_{k+1}, \nu_k) \tag{6.14}$$

where the matrices H_Δ and $\tilde{V}_\Delta(\nu_k, \nu_{k+1})$ are defined by:

$$H_\Delta = \begin{bmatrix} I_6 \\ -I_6 \end{bmatrix} \quad \tilde{V}_\Delta(\nu_k, \nu_{k+1}) = \begin{bmatrix} \Delta\tilde{V}_{\max}(\nu_k) \\ \Delta\tilde{V}_{\max}(\nu_{k+1}) \\ \Delta\tilde{V}_{\max}(\nu_k) \\ \Delta\tilde{V}_{\max}(\nu_{k+1}) \end{bmatrix} \tag{6.15}$$

These constraints impose some restrictions on the initial error $\tilde{e}_k$, between the measured state and the corresponding state on the desired periodic trajectory in the moment where the analytic control (6.11) is computed:

$$\tilde{e}_k = \tilde{X}_p(\nu_k) - \tilde{X}(\nu_k) \tag{6.16}$$

Using (6.11) and the fact that the anticipated error $\tilde{e}_{k|k+1}$ can also be expressed as:

$$\tilde{e}_{k|k+1} = \Phi(\nu_{k+1}, \nu_k)\, \tilde{e}_k = \Phi(\nu_{k+1}, \nu_k) \left(F(\nu_k)\, D - \tilde{X}(\nu_k) \right) \tag{6.17}$$

the following polytopic constraints on the *initial error* $\tilde{e}_k$ are obtained:

$$\tilde{H}_e(\nu_{k+1}, \nu_k)\tilde{e}_k \leq \tilde{V}_e(\nu_{k+1}, \nu_k) \tag{6.18}$$

where:

$$\tilde{H}_e(\nu_{k+1}, \nu_k) = H_\Delta \begin{bmatrix} \Phi(\nu_{k+1}, \nu_k)\, B & B \end{bmatrix}^{-1} \Phi(\nu_{k+1}, \nu_k), \quad \tilde{V}_e(\nu_{k+1}, \nu_k) = \tilde{V}_\Delta(\nu_{k+1}, \nu_k) \tag{6.19}$$

The error in the time domain denoted by e_k is related to $\tilde{e}_k$ through:

$$\tilde{e}_k = T(\nu_k)\, e_k \tag{6.20}$$

where the matrix $T(\nu)$ is defined as in (5.47). Hence, the matrices defining the time-domain polytopic constraints on the initial error are given by:

$$H_e(t_{k+1}, t_k) = \tilde{H}_e(\nu_{k+1}, \nu_k) T(\nu_k), \qquad V_e(t_{k+1}, t_k) = \tilde{V}_e(\nu_{k+1}, \nu_k) \tag{6.21}$$

For some given saturation constraints defined in time domain by $\Delta V_{\max}$, the matrices in (6.21) defining the polytopic constraints on the initial error depend on the choice for t_k and t_{k+1}. For a fixed time interval between the two impulses Δt, a worst-case estimation for the domain of the admissible initial error, regardless of the position of the first impulse, can be obtained as:

$$e \in \mathbf{P}(H_e, V_e) = \bigcap_{k=1}^{\infty} \mathbf{P}(H_e(t_k + \Delta t, t_k), V_e(t_k + \Delta t, t_k)) \tag{6.22}$$

where $\mathbf{P}(H_e(t_k + \Delta t, t_k), V_e(t_k + \Delta t, t_k))$ denotes the polytope defined by the indicated matrices.

Figure 6.1 gives the cut through the polytope $\mathbf{P}(H_e, V_e)$ bounding the initial error following the plane corresponding to the position errors, for different values of the time interval between the two impulses. The sets are computed for $\Delta V_{max} = 0.26$ m/s and $e = 0.3$, and are obtained for the intersection of 150 different sets in (6.22) using the mpt toolbox [54] and Matlab.

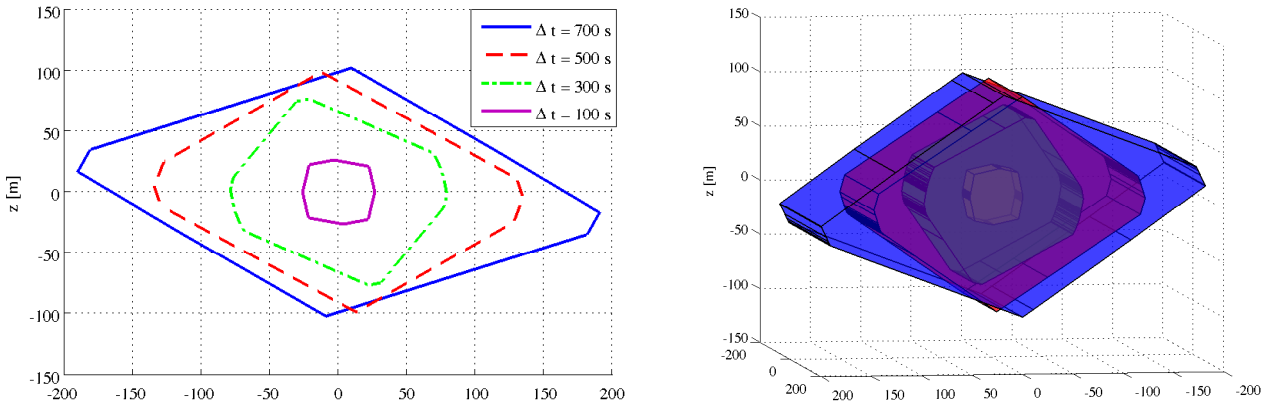

Figure 6.1: Illustration of the polytopic set bounding the initial error for $\Delta V_{max} = 0.26$ and $e = 0.3$

Even if the intersection of the polytopes gives a conservative estimation, it can be seen that the domain for admissible initial position errors with respect to the desired periodic trajectory becomes bigger as the interval between the two controls becomes larger. The longer free drift interval can be

used to naturally compensate larger initial position errors, without applying a higher thrust. The admissible initial velocity errors specifications remain unchanged, regardless of the choice for the control interval. In this case the domain for the velocity errors is defined by a cube centered in 0 and large of 0.26 m/s.

6.2.3 Performances in presence of navigation uncertainties

In the presence of navigation uncertainties, the distance with respect to the invariant set $S_p(D)$ after applying the two impulsive maneuvers computed using (6.11) will be different than zero. If the measured spacecraft relative state is affected by unknown but bounded sensing noise such that:

$$\tilde{X}(\nu_k) = \tilde{X}_m(\nu_k) + \delta X_k,\ \delta X_k \in \mathbf{E}(0, Q_k) \tag{6.23}$$

then the obtained distance with respect to the periodic trajectory when applying the control computed based on imperfect information is given by:

$$\text{dist } (\tilde{X}^+(\nu_{k+1}), S_p(D)) = \|C(\nu_{k+1})\Phi(\nu_{k+1}, \nu_k)\delta X_k\|,\ \delta X_k \in \mathbf{E}(0, Q_k) \tag{6.24}$$

The obtained value depends on the choice for the two control instants, ν_k and ν_{k+1} respectively, on the eccentricity of the orbit of the leader spacecraft and on the value of the navigation uncertainties. Because the sensing noise is assumed to be bounded by an ellipsoidal set, a worst case distance can be computed for the considered interval:

$$d_{\max}(\nu_{k+1}, \nu_k) = \max_{\delta X_k \in \mathbf{E}(0, Q_k)} \text{dist } (\tilde{X}^+(\nu_{k+1}), S_p(D)) = \|C(\nu_{k+1})\Phi(\nu_{k+1}, \nu_k)P_k\|_2 \tag{6.25}$$

where $P_k = Q_k^{-1/2}$. Worst case bounds for the performances of the analytical control law in presence of navigation uncertainties can also be computed. The performances are defined in terms of the *tracking error* for the spacecraft relative state after the second impulsive control:

$$\tilde{\varepsilon}_{k+1} = \tilde{X}_p(\nu_{k+1}) - \tilde{X}^+(\nu_{k+1}) \tag{6.26}$$

where $\tilde{X}_p(\nu_{k+1})$ is defined as in (6.13). The term $\tilde{\varepsilon}_{k+1}$ is different from the anticipated error $\tilde{e}_{k|k+1}$ defined (6.12) since it is based on the dynamics of the *controlled* spacecraft relative trajectory instead of the autonomous evolution. After integrating (6.23) and (6.11) into (6.9), the tracking

error obtained for the analytical bi-impulsive control can be written as:

$$\tilde{\varepsilon}_{k+1} = \Phi(\nu_{k+1}, \nu_k)\delta X_k,\ \delta X_k \in \mathbf{E}(0, Q_k) \tag{6.27}$$

The tracking performances are influenced by the same parameters as the distance with respect to the invariant set $S_p(D)$. Following from the expression of the propagation of an ellipsoidal set through a linear application given in (C.7), an ellipsoidal bound can be computed for the tracking error depending on the chosen values for ν_k and ν_{k+1}:

$$\tilde{\varepsilon}_{k+1} \in \mathbf{E}(0, \Phi(\nu_{k+1}, \nu_k)^{-T} Q_k \Phi(\nu_{k+1}, \nu_k)^{-1}) \tag{6.28}$$

For given navigation uncertainties specifications and a fixed time interval between the two impulses, a worst case estimation of the domain for the final error regardless of the position of the first impulse can be obtained as:

$$\tilde{\varepsilon} \in \mathbf{E}(0, Q_\varepsilon) \supseteq \bigcup_{k=1}^{\infty} \mathbf{E}(0, \Phi(\nu_{k+1}, \nu_k)^{-T} Q_k \Phi(\nu_{k+1}, \nu_k)^{-1}) \tag{6.29}$$

where $\mathbf{E}(0, Q_\varepsilon)$ denotes the minimal volume outer ellipsoidal approximation of the union of ellipsoids. The set $\mathbf{E}(0, Q_\varepsilon)$ can be computed by solving an SDP, using the procedure described in [14] page 43.

Figure 6.2 illustrates for the final position errors, the evolution of the bounding ellipsoidal set with the interval between the two impulsive controls. The illustrated values are obtained for an eccentricity of $e = 0.3$ and for navigation uncertainties bounded by an ellipsoidal set whose semi-axes are equal to 0.02 m for the spacecraft relative position and 0.002 m/s for the relative velocity.

It can be noticed from Figure 6.2 that the dimension of the set bounding the tracking errors increases as the interval between the two impulses increases. In presence of navigation uncertainties, applying only the computed bi-impulsive control does not guarantee the stability around the periodic since the distance to the invariant set $S_p(D)$ after control is different than zero and will continue to increase if no other trajectory corrections are applied. The distance to the invariant set can be maintained bounded by periodically recomputing the two impulsive controls and applying them. The choice for the frequency of recomputation needs to take into account how this parameter affects the domain of validity of the control and also its influence on the obtained tracking precision.

If the recomputation occurs after that both impulses have been applied, the initial error for

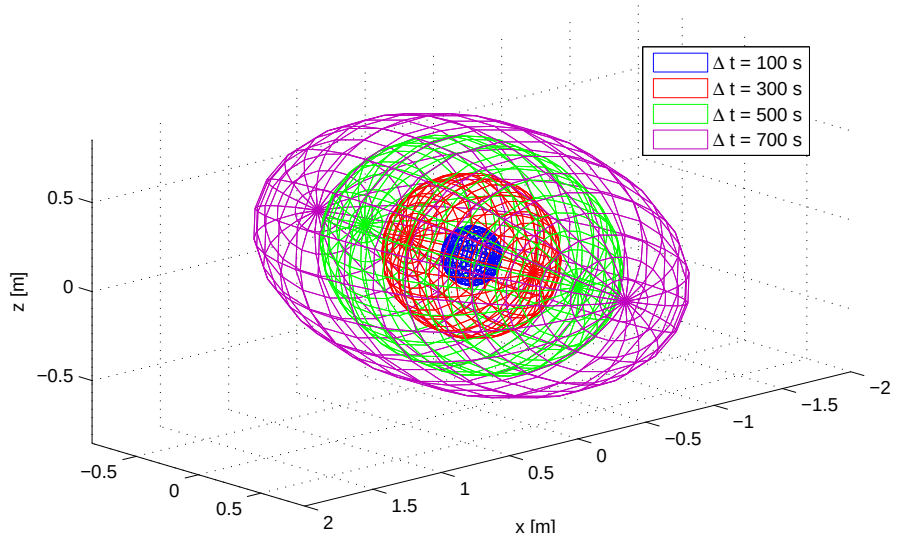

Figure 6.2: The change in the final error with the change in the interval between the impulsive controls

the new control will be bounded by the ellipsoid $\mathbf{E}(0, \Phi(\nu_{k+2}, \nu_{k+1})^{-T} Q_\varepsilon \Phi(\nu_{k+2}, \nu_{k+1})^{-1})$. This comes from the fact that the final tracking error $\tilde{\varepsilon}_{k+1}$, obtained after the application of ΔV_{k+1}, is propagated over another interval before a new control is computed. In order to guarantee that the saturation constraints are not violated, the recomputation frequency should be such that:

$$\mathbf{E}(0, \Phi(\nu_{k+2}, \nu_{k+1})^{-T} Q_\varepsilon \Phi(\nu_{k+2}, \nu_{k+1})^{-1}) \subset P(H_e, V_e) \tag{6.30}$$

The condition (6.30) can be checked during the a priori analysis using the procedure described in [14], page 70.

To improve the tracking error, the recomputation strategy could be modified following the Model Predictive Control principles: only the first of the two computed impulses is applied each time and the second one is discarded. At the next control instant a new pair of impulses is computed based on new measurement information out of which only the first one is used. This strategy can limit the propagation of the measurement errors to only one control interval instead of two leading to a smaller error with respect to the desired periodic trajectory.

In the next section it will be showed how the presented analytical bi-impulsive control law can be combined with the robust control methods developed in Chapter 5 in a two stage Model Predictive Control setting.

6.3 Robust guidance towards a spacecraft periodic relative motion

Let us consider a fixed-time rendezvous mission where the objective is to guide the spacecraft towards a periodic proximity relative motion in presence of navigation uncertainties. Starting from an initial state $\tilde{X}_1$, the purpose is to compute a robust rendezvous plan that, when applied at the fixed instants $\nu_1, ...\nu_{N-1}$, drives the spacecraft towards a final periodic relative trajectory. The periodic trajectory is not fixed *a priori*, but it must respect the following constraints: the final periodic trajectory must evolve inside a tolerance box X_{tol}, centered around a fixed position X_f. In addition to this, the periodic motion needs to be maintained during a specified period after the end of the rendezvous plan, in spite of the presence of navigation errors.

The mission's objective can be achieved by dividing the control into two phases. During the first phase the spacecraft are brought in proximity of an admissible trajectory, using the robust control techniques presented in Chapter 5 for instance. During the second phase, the stability of the spacecraft periodic relative motion is ensured by a local controller.

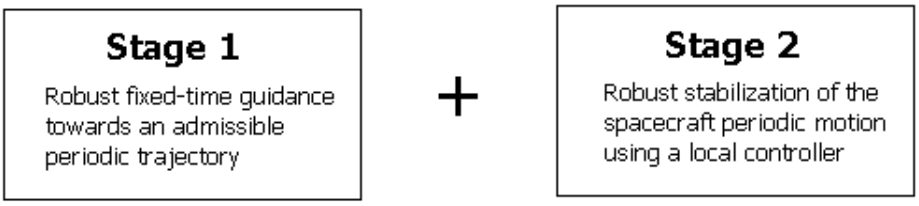

This two stages approach possesses several computational advantages. The disturbance-feedback control approach presented in Chapter 5 can be used for instance during the first stage in order to steer the spacecraft towards an admissible final state. It can guarantee to reach the smallest possible arrival set centered around a final state belonging to an admissible periodic trajectory. The corresponding optimal control problem can be obtained by modifying (5.46) to reflect the change

in the final objective:

$$\min_{Q_f,\Delta v_k,L_{k,i}} \quad \text{tr}\ (T^{-1}Q_f T^{-T}) + \|\mathbf{\Delta v}\|_1$$
$$\text{s.t.} \quad \begin{cases} \bar{x}_{k+1} = A_k \bar{x}_k + B_k \Delta v_k \\ \bar{x}_1 = x_1^m,\ x_1^m = \tilde{X}_1 \\ D = C(\nu_N)\bar{x}_N,\ d_0 = 0 \\ \exists Y_i \succeq 0 \text{ s.t. } \gamma_i^T = \left[\text{tr}\ (Y_i\, H_{2,1}) \quad ... \quad \text{tr}\ (Y_i\, H_{2,5})\right],\ i = 1...s \\ \gamma_i = t\, v_i - (h_{i,1}C_x + h_{i,2}\bar{C}_y + h_{i,3}C_z)D \\ |\Delta v_k| \leq \Delta\tilde{V}_{\max}(\nu_k) - \sum_{i=1}^{k-1} \|L_{k,i}P_i^w\|_2,\ k = 1...N-1 \\ \exists \tau_1,\ \tau_2,\ ...\ \tau_{N-1} \geq 0 \text{ s.t. } Q_f \succeq 0,\ R \succeq 0 \end{cases} \tag{6.31}$$

where the same notations as in the previous chapters are maintained. The terms $h_{i,j}$ and v_i correspond to the elements of the H and V matrices which define the tolerance box bounding the admissible periodic trajectories. For the considered case, the H and V matrices are defined in the same way as in (4.29). The terms γ_i in (6.31) correspond to the coefficients of the non-negative polynomials which define the admissible arrival set. The vector of parameters D corresponding to the final state of the nominal trajectory must belong to this arrival set.

The optimal control problem (6.31) can be solved at the ground station before the beginning of the rendezvous maneuvers and then the solution can be uploaded on-board the spacecraft. Applying the computed series of disturbance feedback laws brings the spacecraft in proximity of the periodic trajectory defined by the vector of parameters D. In presence of navigation uncertainties, the error with respect to the periodic trajectory at the end of the plan is guaranteed to belong to the ellipsoidal set $\mathbf{E}(0, Q_f)$ which is computed before starting the maneuvers.

During the second stage, the analytical bi-impulsive control defined in (6.11) can be used in order to robustly stabilize the spacecraft periodic relative motion. The periodic reference trajectory at this stage is defined by the vector D obtained at the previous stage. The following condition needs to be verified:

$$\mathbf{E}(0, Q_f) \subset \mathbf{P}(H_e, V_e) \tag{6.32}$$

in order to guarantee that, at the moment of the switch between the two control approaches, the validity conditions for the bi-impulsive control law are verified. The frequency of control recomputation for the second stage must be chosen according to the constraint imposed by (6.30).

This verification can be made before the beginning of the mission, using the computational resources available at the ground station. The bound for the error at the end of the first stage given by (6.31) makes possible the *a priori* verification of the switch condition (6.32). The choice for the recomputation frequency can be made according to the saturation restrictions and to the mission's requirement regarding the tracking precision.

6.4 Numerical examples

The fixed-time spacecraft rendezvous mission defined in Table 6.1 is used in order to illustrate the two stages control approach. The purpose is to guide the spacecraft towards a periodic proximity motion contained in the specified bounds and then to maintain the periodic motion during 10 orbital periods starting at the end of the rendezvous maneuvers, in spite of the presence of navigation uncertainties.

a [km]	e	$\Delta V_{\max}$	N	X_1 [m,m/s]	t_1 [s]	X_f [m]	X_{tol} [m]	t_N [s]
7 011	0.004	0.26	10	[1000,50,50,0,0,0]	0	[100,0,0]	[50,25,25]	3 000

Table 6.1: Spacecraft rendezvous mission data

The tests are performed using the nonlinear simulator for the spacecraft relative motion described in [49]. Random navigation errors are added to each relative state measurement that is used for control computation and the J_2 perturbation is also considered during the simulations. The disturbance feedback control is used during the first phase of the rendezvous mission, following the same procedure that has been exposed for the examples in Chapter 5. The analytical bi-impulsive control is then used in the second stage to maintain the periodic motion. In this second stage, the control is applied at a constant frequency that is fixed *a priori*.

Our purpose is to evaluate the influence of several parameters on the performances of the analytical bi-impulsive control law. The performances of the disturbance feedback strategy have already been analysed in Chapter 5 and we focus here on the switch between the two control laws, on the precision for the tracking of the periodic trajectory and on the fuel cost of the control in the second stage. We are interested in analysing the effects of the eccentricity of the reference orbit, of the interval between two consecutive control instants ν_k and ν_{k+1} and of the amplitude of navigation uncertainties.

6.4.1 Influence of the eccentricity of the reference orbit

In order to analyse the influence of the eccentricity of the orbit of the target spacecraft on the performances of the analytic control strategy, we consider that the control is applied at a constant frequency of $\Delta t = 100$ s. Random noise is added to every spacecraft relative state measurement. The navigation uncertainties are bounded by an ellipsoidal set whose semi-axes are equal to 0.02 m for the relative position and 0.002 m/s for the relative velocity.

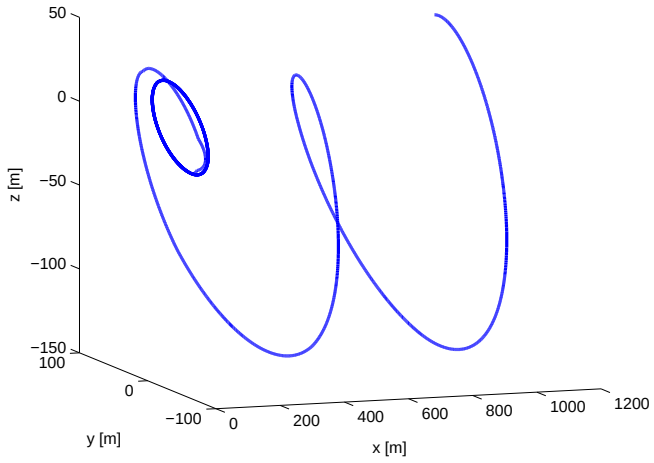

Figure 6.3: Spacecraft relative trajectory towards proximity periodic motion

Figure 6.3 shows the spacecraft relative trajectory obtained for the scenario in Table 6.1. The spacecraft arrive in proximity of an admissible periodic relative trajectory using the disturbance feedback approach. The analytic bi-impulsive control then maintains the periodic motion for the desired time in spite of the navigation uncertainties.

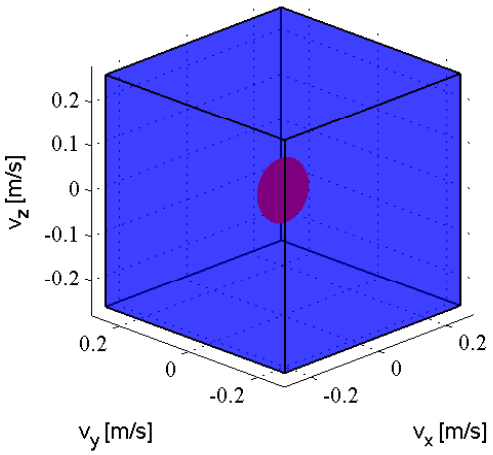

Figure 6.4: Illustration of the switch conditions for the relative velocity errors

The switch conditions for the relative velocity errors are illustrated in Figure 6.4. The blue cube indicates the restrictions imposed by the saturation constraints on the velocity errors and the red ellipsoid corresponds to the velocity errors guaranteed by the guidance algorithm at the end of phase 1. The restrictions on the relative position errors have also been verified and are largely satisfied.

The influence of the eccentricity of the leader's orbit on the tracking precision and on the average fuel consumption is analysed for the analytic bi-impulsive control. The closed-loop trajectories obtained in the second phase of the mission, for different values of the eccentricity, are presented in Figure 6.5. The projections of the periodic trajectories onto the xy and xz planes are also given in order to better show the geometry of the obtained trajectories.

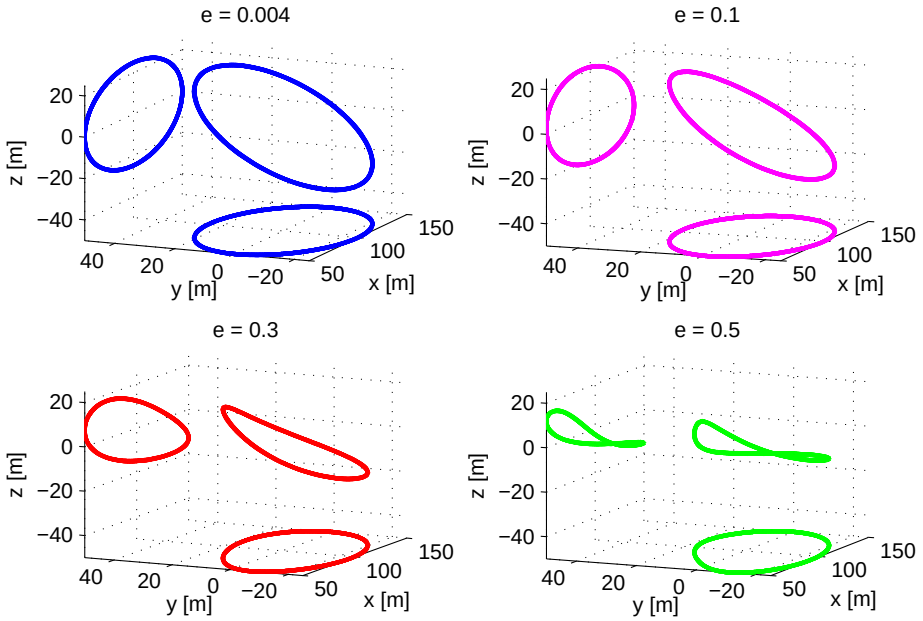

Figure 6.5: The obtained periodic trajectories for different values of the eccentricity

Table 6.2 summarizes for each of the considered eccentricities the closed-loop performances of the analytic control. It gives the maximum absolute value for the position error with respect to the periodic trajectory $dp_{\max}$, the maximum absolute value for the velocity error $dv_{\max}$ and the average fuel consumption per orbit $\Delta V/\text{orbit}$ for each case. It can be seen that for the considered interval between controls, the performances of the bi-impulsive control method are not very much influenced by the values of the eccentricity. A slight increase in the errors and in the fuel consumption can be observed for the highest considered eccentricity $e = 0.5$.

e	$dp_{\max}$ [m]	$dv_{\max}$ [m/s]	ΔV/orbit [m/s]
0.004	0.1865	0.0039	0.2494
0.1	0.1948	0.0039	0.2360
0.3	0.1800	0.0038	0.2406
0.5	0.3461	0.0061	0.2627

Table 6.2: The influence of the eccentricity on the performances of the analytic control

6.4.2 Influence of the interval between controls

The influence of the time interval between consecutive controls Δt on the tracking performances is analysed here. Like in the previous case, the navigation uncertainties belong to an ellipsoidal set whose semi-axis are equal to 0.02 m for the spacecraft relative positions and 0.002 m/s for the relative velocity.

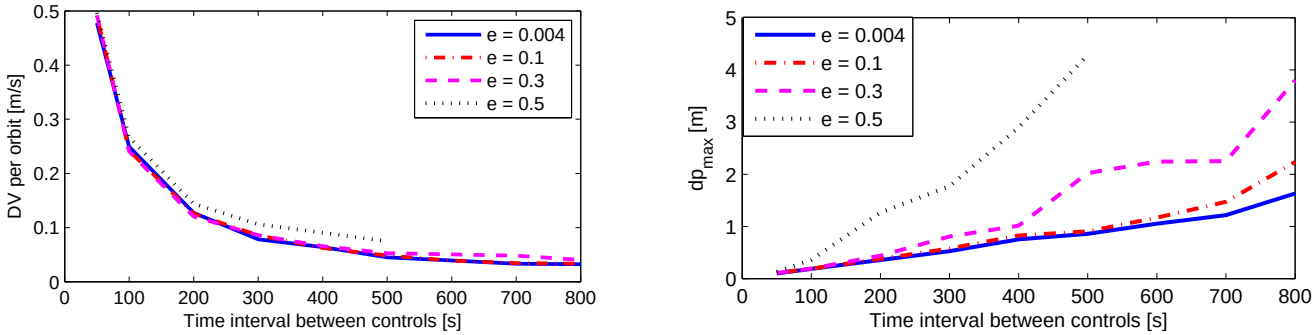

Figure 6.6: The influence of the control frequency on the tracking performances

The evolution of the tracking performances for different values of Δt is illustrated in Figure 6.6. It can be seen that for every value of the eccentricity of the reference orbit, applying the ΔV corrections less frequently results in a lower total fuel consumption per orbit. For the case where $e = 0.5$, the plot only goes until $\Delta t = 500$ s because for higher values the validity conditions are no longer verified. For lower eccentricities the average fuel consumption is very similar, regardless of the value chosen for the interval between controls. Only for the case $e = 0.5$ the average fuel cost per orbit is slightly higher.

Figure 6.6 also shows that while choosing a larger value for Δt reduces the fuel consumption, it also increases the tracking errors. For all the considered eccentricities the position tracking error increases as the interval between controls increases. It can also be noticed that the tracking errors are more sensitive to the value of the eccentricity then the average fuel cost. This can be explained by the fact that, for eccentric orbits, the spacecraft velocity is not constant throughout the orbit.

Different distances can be travelled by the spacecraft in the same time interval, depending on its position on the orbit.

The choice for the frequency of control application should reflect the best admissible compromise between the fuel cost per orbit and the desired tracking precision. Small intervals between controls guarantee the best tracking precision but in the same time are the most fuel consuming. Choosing a large interval can lead to poor tracking performances or it can violate the domain of applicability of the control.

6.4.3 Influence of the navigation uncertainties

The influence of the level of the navigation uncertainties on the control performances is analysed next. For an eccentricity of $e = 0.3$, the effects of the navigation uncertainties are presented depending on the value chosen for the control interval Δt.

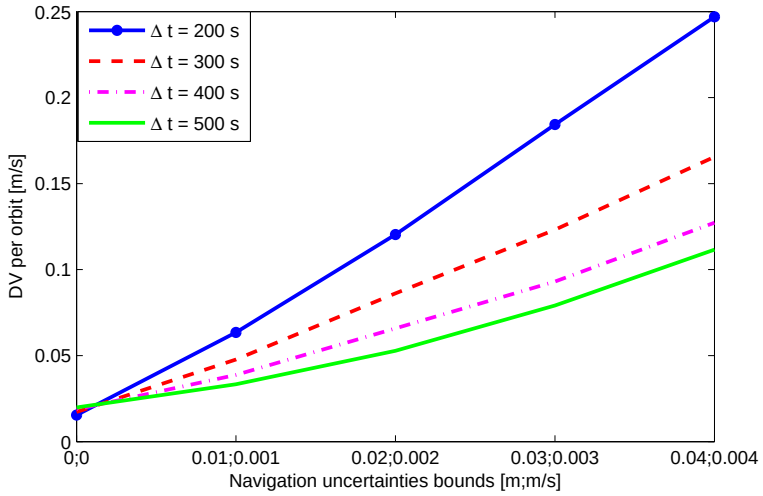

Figure 6.7: The influence of the level of measurement noise on the tracking performances

Figure 6.7 shows that even when there is no measurement noise the average fuel consumption is different than zero because the nonlinear model is used and the J_2 perturbation is active. However, it can be seen that when the spacecraft relative state is perfectly known, a smaller interval between controls actually gives a smaller fuel cost per orbit since the eventual errors do not propagate for a long time. In presence of navigation uncertainties, a larger control interval always leads to a smaller fuel consumption. This can be explained by the fact the imperfect state information might cause some unnecessary thrusting attempting to correct errors that actually come from the sensing noise. For all the values considered for the control interval, the fuel cost per orbit increases as the uncertainties levels increase.

Table 6.3 summarizes the tracking performances of the analytical control for $\Delta t = 400$ s and for every of the considered levels for the eccentricity.

δp[m];δv[m/s]	$dp_{\max}$ [m]	$dv_{\max}$ [m/s]	ΔV/orbit [m/s]
0;0	0.7790	0.0040	0.0188
0.01;0.001	0.8968	0.0042	0.0388
0.02;0.002	1.0147	0.0050	0.0658
0.03;0.003	1.3995	0.0054	0.0931
0.04;0.004	1.7207	0.0078	0.1273

Table 6.3: The influence of the level of navigation uncertainties on the performances of the analytic control for $e = 0.3$ and $\Delta t = 400$ s

6.5 Conclusion

This chapter presents an analytical bi-impulsive control method for stabilizing the spacecraft periodic relative motion. The method is based on the fact that periodic trajectories are equilibrium trajectories for the spacecraft relative motion. The states belonging to periodic relative trajectories form an invariant set for the spacecraft relative motion, whose robust stability must be ensured. The computation of the stabilizing control uses the results in Chapter 2, which show that any periodic spacecraft relative trajectory can be described by a constant vector of parameters. The bi-impulsive structure of the control is chosen because it can provide an analytical solution to the stability condition.

Spacecraft periodic relative trajectories are unstable, meaning that any autonomous trajectory starting in proximity of a periodic solution will not naturally converge towards the periodic motion. This means that in presence of navigation uncertainties the desired periodic trajectory cannot be precisely reached. Corrections need to be computed and applied periodically in order to prevent the spacecraft from drifting away from the desired trajectory. Bounds for the admissible error with respect to the periodic trajectory are given in order to guarantee that the computed controls respect the thrusters saturation constraints. Limitations on the choice for the control recomputation frequency are imposed by the fact that, for bounded navigation uncertainties, the tracking error must remain within the admissible error domain.

The analytic bi-impulsive control is integrated in a 2 stages Model Predictive Control scheme, whose purpose is to guide the spacecraft towards an admissible periodic trajectory and then to robustly maintain the periodic motion for a specified time. This control setting demonstrates that good robust guidance performances can be achieved using a control scheme which does not rely on

onboard optimization. Numerical simulations based on the nonlinear propagation model for the spacecraft relative motion are used to analyse the influence of different parameters on the control performances. The most important tuning parameter is the frequency of control recomputation and its choice can be driven by a compromise between the desired tracking precision and the fuel consumption.

Conclusions

The fixed-time spacecraft rendezvous guidance problem is investigated in this thesis. The main objectives are concentrated around obtaining guidance algorithms capable of handling different types of trajectory and control constraints that arise from spacecraft mission requirements. Another important aspect is related to the robustness properties of the control algorithms, motivated by the need for increased control authority for future spacecraft missions.

The first part of the thesis focuses on the modelling of the spacecraft relative motion and more precisely on the study of the geometric properties of the relative trajectories. A particular attention is paid to naturally periodic trajectories, motivated by their importance for ensuring the passive security of the spacecraft relative trajectory and by their potential usage as fuel-fee parking or inspection orbits. A new parametrization for the spacecraft relative trajectories is proposed, based on the Cartesian model for the spacecraft relative motion and on the expression of the transition matrix. It is showed that, in the general case, two of these parameters change over time, while in the case of periodic motion, all the parameters describing the relative trajectory are constant. This property leads to a compact, generic representation for the spacecraft periodic relative trajectories, regardless of their shape or dimensions. It provides more flexibility than the classical approach based on the usage of parametrized curves such as circles and ellipsoids for specifying a desired periodic relative trajectory.

A mathematical characterisation for the set of parameters corresponding to relative trajectories which respect some dimensions constraints, over a desired time interval, is necessary in order to simplify the spacecraft relative trajectory design process. For instance, in the case where the mission requires the usage of parking orbits, these parking orbits need to be designed such that they are periodic and contained inside a specified area around a waiting point along the rendezvous trajectory. For passively safe approach trajectories, the fail trajectories must be such that, in case of system failure, the follower spacecraft remains inside a designated safe area in proximity of the target, for the desired period of time. The important question that needed to be answered was: which is the relation between the values of the parameters and the geometric properties of the resulting spacecraft relative trajectory?

From a mathematical point of view, verifying that a trajectory respects the dimension constraints over a specified time interval, translates into numerically checking an infinite number of conditions. The classical approach for rendering finite the number of conditions is based on constraints discretization. While this solution is simple and straightforward, it does not provide a

rigorous mathematical description of the admissible trajectories. Moreover, this approach cannot guarantee that no constraints violations will occur in between the discretization points. The proposed alternative is based on the properties of non-negative polynomials. Our method exploits the structure of the solution for the spacecraft relative motion provided by the transition matrix and leads to a finite characterisation of the admissible trajectories that guarantees *continuous* satisfaction of the constraints. This result can provide the mission designer with a powerful tool for the spacecraft relative trajectory design.

The proposed characterisation of the admissible trajectories is integrated in the fuel-optimal spacecraft rendezvous guidance problem for missions that impose continuous constraints on the approach trajectory. It is showed that the constrained guidance problem can still be written as a convex optimization problem. The methods is illustrated for several examples, including the spacecraft guidance towards a parking orbit defined as a constrained periodic relative trajectory, the spacecraft rendezvous with passive security constraints on the approach trajectory or the spacecraft docking trajectory with continuous visibility constraints. The examples emphasize the advantage of our method over the classical constraints dicretization technique, for which constraints violations occur in between the verification points.

When the spacecraft relative state measure is affected by navigation uncertainties, the final rendezvous objective can no longer be precisely reached. In this case, the objective becomes to obtain a robust guidance algorithm that provides a good compromise between the fuel cost of the approach trajectory and the final rendezvous precision, while guaranteeing robust constraints satisfaction for all the admissible values of the uncertainties. Two control techniques are proposed which optimize the fuel consumption and the dimensions of a guaranteed final arrival set. The methods rely on the computation of a series of affine feedback control laws that can ensure robust constraints satisfaction and a good performance trade-off. It is emphasized that the resulting convex optimal control problem can be solved only once, before the beginning of the rendezvous maneuvers, and then the computed feedback laws can be directly used at the corresponding control instant, without any need for recomputation. This property might be particularly attractive when the on-board computational resources are limited. The problem can be solved using the resources available on the ground before the beginning of the maneuvers, followed by the upload of the parameters of the control laws to the spacecraft. The choice of the affine feedback structure for the control might impose some limitations on the achievable control performances. A further interesting development would be the estimation of lower and upper bounds on the performances, bounds that derive from this particular choice for the control parametrization.

The presence of navigation errors also affects the spacecraft periodic relative motion. The spacecraft periodic relative trajectories are showed to be unstable equilibrium trajectories, meaning that from a state arbitrarily close to a periodic trajectory, the spacecraft relative motion will not naturally converge towards the periodic solution. For this particular case, an analytical bi-impulsive control which stabilizes the spacecraft periodic relative motion is proposed. The computation of the control is based on the fact that periodic trajectories can be described using a constant set of parameters. The bi-impulsive structure is chosen because it provides an analytical solution to the stabilization problem, requiring very few computational effort to obtain the control. However, because the corrections are computed based on imperfect state information, the control needs to be applied periodically in order to guarantee the stability of the motion. For a particular choice for the control frequency, the validity domain of the analytical control can be estimated a priori.

The analytic bi-impulsive control is integrated in a 2 stage Model Predictive Control scheme which demonstrates that good robust guidance performances can be achieved using a control scheme which does not rely on onboard optimization.

Conclusions

Cette thèse est consacrée au problème de guidage en rendez-vous à temps fixé des satellites en orbite terrestre. L'objectif principal est de concevoir des algorithmes de guidage capables de prendre en compte les différents types de contraintes sur le contrôle ou sur la trajectoire relative imposées par les spécifications de chaque mission. Le caractère robuste des manœuvres obtenues, favorable à l'accroissement de l'autonomie, est également investigués.

La première partie du manuscrit est dédiée à la modélisation du mouvement relatif des satellites et plus précisément à l'étude des propriétés géométriques des trajectoires relatives. Les trajectoires relatives périodiques sont étudiées plus un détail, du fait de leur possible utilisation pour la sécurisation passive des trajectoires d'approche et de leur usage potentiel comme orbites de parking ou d'inspection qui ne nécessitent pas de dépense de combustible. Des nouvelles expressions paramétriques sont proposées pour les trajectoires relatives, basées sur le modèle cartésien local du mouvement relatif et sur l'utilisation de l'expression de la matrice de transition d'état. Pour cette nouvelle paramétrisation, deux paramètres seulement varient avec le temps et, dans le cas du mouvement périodique, les paramètres sont tous constants. Cette propriété permet l'obtention d'une description compacte des trajectoires relatives périodiques, quelle que soit leur forme ou leur dimension. La nouvelle formulation s'avère plus flexible et plus générique que l'approche classique, basée sur l'utilisation des courbes paramétrées, telles que les cercle ou les ellipses, pour spécifier une trajectoire périodique désirée.

Pour simplifier le processus de design des trajectoires relatives des satellites, il est nécessaire de traduire mathématiquement les contraintes dimensionnelles à respecter sur un intervalle de temps donné. Par exemple, si une mission donnée nécessite l'utilisation des orbites relatives de parking entre deux étapes différentes, ces orbites peuvent être choisies périodiques et de dimensions ne dépassant pas une zone spécifiée autour d'un point de passage fixé sur la trajectoire. Pour des approches qui nécessitent des garanties de sécurisation passive de la trajectoire, on peut chercher à imposer aux trajectoires de panne d'évoluer à l'intérieur d'une zone de sécurité spécifiée en proximité de la cible pour un intervalle de temps fixé. La question importante qui se pose devient alors d'identifier le lien entre les valeurs des paramètres décrivant une trajectoire relative et ses propriétés géométriques.

D'un point de vue formel, certifier qu'une trajectoire relative respecte des contraintes de dimension sur un intervalle de temps fixé revient à vérifier un nombre infini de conditions. L'approche classique pour obtenir un nombre fini des conditions à vérifier consiste à discrétiser l'intervalle

donné. Même si cette solution est simple et facile à implémenter, elle ne fournit aucune description formelle des trajectoires admissibles. De plus, cette approche ne peut pas garantir que les contraintes sont également satisfaites sur l'intervalle entre deux points de discrétisation. Une solution alternative est proposée, solution qui est basée sur les propriétés des polynômes non-négatifs. Cette nouvelle méthode exploite la structure de la solution des équations dynamiques décrivant le mouvement relatif des satellites, solution donnée par la matrice de transition. Elle amène à une caractérisation finie des trajectoires admissibles et garantit la satisfaction continue des contraintes. Ce résultat peut s'avérer très utile pour le design des trajectoires relatives de satellites pour des opérations de proximité.

La description développée pour les trajectoires relatives admissibles est intégrée dans un algorithme de guidage des satellites, adapté aux missions qui requièrent des contraintes continues sur la trajectoire d'approche. Il est montré que le problème de commande optimale sous contraintes correspondant peut être écrit comme un problème d'optimisation convexe. La méthode est illustrée par plusieurs exemples, tels que le guidage des satellites vers une orbite de parking définie comme étant une trajectoire périodique contrainte, le rendez-vous orbital avec des contraintes de sécurité passive sur la trajectoire d'approche ou le rendez-vous avec des contraintes de visibilité. Ces exemples mettent en évidence les avantages de cette nouvelle méthode par rapport à l'approche basée sur la discrétisation des contraintes, pour laquelle les contraintes ne sont pas nécessairement respectées entre les points de vérification.

Lorsque la connaissance de l'état relatif des satellites est affectée par des incertitudes de mesures, l'objectif final de la mission ne peut plus être précisément atteint. L'objectif devient alors d'obtenir des algorithmes de guidage robustes, qui fournissent des solutions permettant d'atteindre un bon compromis entre la consommation de combustible et la précision finale, tout en garantissant la satisfaction des contraintes pour toute valeur admissible des incertitudes. Deux techniques de contrôle sont proposées à cet effet. Elles optimisent à la fois la consommation de combustible et la dimension de l'ensemble d'arrivée qui contient tous les états finaux possibles. Ces méthodes sont basées sur le calcul d'une série des lois de commande au lieu d'un plan de manœuvres et peuvent assurer la satisfaction robuste des contraintes et un bon compromis au niveau des performances. Les problèmes d'optimisation convexe qui en découlent doivent être résolues une seule fois, avant le début de la mission, et puis les lois de commande obtenues peuvent être utilisées sans besoin de recalcul. Cette caractéristique peut s'avérer particulièrement intéressante pour des missions où la puissance de calcul embarqué est fortement limitée. La solution du problème d'optimisation peut donc être calculée au sol, avant le début des manœuvres, suivie par une simple transmission des paramètres

obtenus vers les satellites.

Il est à noter que le choix de travailler avec des structures affines de commande pourrait engendrer des limitations au niveau des performances du contrôle. Une direction de recherche intéressante serait d'estimer des bornes de performance supérieures et inférieures, bornes fixées par le choix de la structure affine.

La présence des incertitudes de navigation a également des effets sur le mouvement relatif périodique des satellites. Les trajectoires périodiques sont des trajectoires d'équilibre instable. Par conséquent, pour des états initiaux situés arbitrairement proche d'une trajectoire périodique, la trajectoire obtenue ne va pas converger de manière autonome vers la solution périodique. Pour remédier à ce problème, une stratégie de contrôle basée sur le calcul analytique des deux impulsions est proposée, afin de stabiliser le mouvement relatif autour d'une trajectoire périodique donnée. Cette méthode utilise le fait qu'une trajectoire périodique peut être décrite par un vecteur constant de paramètres. L'avantage de cette méthode est le fait que le calcul analytique des corrections nécessite très peu de ressources. En même temps, comme les corrections sont obtenues à partir des mesures affectées par des incertitudes, le contrôle doit être calculé et appliqué de manière périodique pour garantir la stabilité du mouvement périodique. Pour une période de recalcule fixée, le domaine de validité du contrôle à deux impulsions peut être obtenu a priori.

La méthode analytique à deux impulsions est intégrée dans une stratégie de contrôle à deux étapes, en conjonction avec les méthodes de commande robuste développées, afin de réaliser le guidage robuste en mouvement périodique de proximité. Cette stratégie fait preuve de bonnes performances de guidage, lesquelles sont obtenues en évitant la résolution embarquée de problèmes d'optimisation.

Appendix A

Stability of spacecraft periodic trajectories

The stability analysis of a system in the sense of Lyapunov studies the convergence of the system's state towards some equilibrium points. An equilibrium point is defined as a state that the system can maintain indefinitely without any change in the input. In the case of the spacecraft relative motion, the notion of equilibrium point is extended to the notion of equilibrium trajectory [51]. It has been shown in Chapter 2 that once on a periodic relative trajectory, the spacecraft will pursue the periodic motion as long as the input is maintained to zero. In this case, the stability analysis in the sense of Lyapunov consists in characterising the behaviour of the system for initial states that are arbitrarily close to a periodic trajectory.

The linearized spacecraft relative motion can be modelled by the periodic system:

$$\tilde{X}'(\nu) = \tilde{A}(\nu)\tilde{X}(\nu),\ \tilde{A}(\nu) = \tilde{A}(\nu + 2\pi) \tag{A.1}$$

where the dynamical matrix $\tilde{A}(\nu)$ is defined as in (1.19). The stability properties of the system (A.1) cannot be deduced from the stability properties of the dynamical matrix, as it is the case for LTI systems. For periodic systems, and more generally for time-varying systems, even if the dynamical matrix is stable for every value of the independent variable, this does not necessarily imply that the system is stable [28].

The solution to this system can be expressed using the state transition matrix Φ, as described in Section 1.4.1:

$$\tilde{X}(\nu) = \Phi(\nu, \nu_0)\tilde{X}(\nu_0) \tag{A.2}$$

where $\tilde{X}(\nu_0)$ denotes the initial conditions. The *monodromy matrix* is defined as the state transition matrix over one period of the coefficients of the periodic system (A.1):

$$C = \Phi(\nu_k + 2\pi, \nu_k),\ \forall \nu_k \tag{A.3}$$

Considering the Yamanaka-Ankersen state transition matrix [103] and taking $\nu_k = 0$, the mon-

odromy matrix for the spacecraft relative motion is given by:

$$C = \begin{bmatrix} 1 & 0 & -3\,J\,\dfrac{(e+1)^2(e+2)}{e-1} & 3\,J\,\dfrac{(e+1)^3}{e-1} & 0 & 0 \\ 0 & 1 & 0 & 0 & 0 & 0 \\ 0 & 0 & 1 & 0 & 0 & 0 \\ 0 & 0 & 0 & 1 & 0 & 0 \\ 0 & 0 & 0 & 0 & 1 & 0 \\ 0 & 0 & 3\,J\,e\dfrac{(e+1)(e+2)}{e-1} & -3\,J\,e\dfrac{(e+1)^2}{e-1} & 0 & 1 \end{bmatrix} \tag{A.4}$$

where the term J is defined as in (1.33) over the interval $[0\ 2\pi]$.

The eigenvalues of the matrix C are called the *characteristic multipliers* denoted here by λ_i. The values of the characteristic multipliers are independent of the particular choice of ν_k in (A.3) [28]. The stability properties of the periodically time-varying system (A.1) can be studied by looking at the properties of the characteristic multipliers.

According to the theorems in Chapter 4 of [80], the periodic system (A.1) is *stable* if and only if:

$$|\lambda_i| < 1,\ \forall i \tag{A.5}$$

In the case where there is only one characteristic multiplier with unity magnitude then there exists some initial conditions for which the solution of the system is *periodic* [46]. If the multiplicity of the unity eigenvalue is greater than one then the system is *unstable*, in the sense that the natural response of the system does not always remain bounded as time goes to infinity [80].

The eigenvalues of the monodromy matrix C corresponding to the linearized spacecraft relative dynamics are all equal to 1. According to the previous observation, there exists some particular initial conditions for which the response of the system is periodic, which confirms the results in Chapter 2. However, the periodic spacecraft relative trajectories are unstable since the multiplicity of the unity characteristic multiplier is greater than 1. As a consequence, if the spacecraft relative motion starts arbitrarily close to a periodic solution, it will not naturally converge towards the periodic motion.

Appendix B

Properties of non negative polynomials

The results presented in Chapter 3 are based on the properties of non-negative polynomials given by Nesterov in [73]. Nesterov proves that the cone of coefficients of univariate polynomials which are non-negative on some segment of the real axis can be represented as the linear image of the cone of positive semi-definite matrices. This result enables the usage of the semi-definite programming for optimization problems with polynomial non-negativity constraints.

The definitions presented here are extracted from [73] and they concern only the concepts needed in order to understand the developments in Chapter 3.

B.1 Checking polynomials non negativity on a finite interval

Let $\mathcal{K}_{a,b}$ be the convex, closed and pointed cone of the coefficients of polynomials that are non negative on a finite interval $[a\ b] \in \mathbb{R}$:

$$\mathcal{K}_{a,b} = \left\{ p \in \mathbb{R}^{n+1},\ P(w) = \sum_{i=0}^{n} p_i\, w^i,\ \forall w \in [a\ b] \right\} \tag{B.1}$$

Reference [73] shows that a polynomial $P(w)$, represented through its vector of coefficients $p = \begin{bmatrix} p_0 & \dots & p_n \end{bmatrix}^T$, belongs to $\mathcal{K}_{a,b}$ if and only if there exist two symmetric positive semi-definite matrices Y_1 and Y_2 such that:

$$p \in \mathcal{K}_{a,b} \iff \exists\, Y_1, Y_2 \succeq 0 \text{ s.t. } p = \Lambda^*(Y_1, Y_2) \tag{B.2}$$

The definition of the linear operator Λ^* and the dimensions of the matrices Y_1 and Y_2 depend on whether the polynomial $P(w)$ has an odd or even degree.

For n odd take $Y_1, Y_2 \in \mathbb{R}^{(m+1)\times(m+1)} \succeq 0$, where $m = (n-1)/2$. Let $H_{k,i} \in \mathbb{R}^{(k+1)\times(k+1)}$ be

some Hankel matrices that contain ones on the i-th anti-diagonal and zeros everywhere else:

$$H_{k,1} = \begin{bmatrix} 1 & 0 & 0 & \dots \\ 0 & 0 & 0 & \dots \\ 0 & 0 & 0 & \dots \\ \vdots & & & \ddots \end{bmatrix} \quad H_{k,2} = \begin{bmatrix} 0 & 1 & 0 & \dots \\ 1 & 0 & 0 & \dots \\ 0 & 0 & 0 & \dots \\ \vdots & & & \ddots \end{bmatrix} \quad H_{k,3} = \begin{bmatrix} 0 & 0 & 1 & \dots \\ 0 & 1 & 0 & \dots \\ 1 & 0 & 0 & \dots \\ \vdots & & & \ddots \end{bmatrix} \tag{B.3}$$

In this case, the operator Λ^* is defined as:

$$\Lambda^*(Y_1, Y_2) = \begin{bmatrix} \text{tr } (Y_1(-a\, H_{m,1})) + \text{tr } (Y_2(b\, H_{m,1})) \\ \text{tr } (Y_1(H_{m,1} - a\, H_{m,2})) + \text{tr } (Y_2(b\, H_{m,2} - H_{m,1})) \\ \vdots \\ \text{tr } (Y_1(H_{m,i-1} - a\, H_{m,i})) + \text{tr } (Y_2(b\, H_{m,i} - H_{m,i-1})) \\ \vdots \\ \text{tr } (Y_1\, H_{m,2m+1}) + \text{tr } (Y_2(-H_{m,2m+1})) \end{bmatrix} \tag{B.4}$$

For n even take $Y_1 \in \mathbb{R}^{(m+1)\times(m+1)} \succeq 0$ and $Y_2 \in \mathbb{R}^{m\times m} \succeq 0$, where $m = n/2$. In this case, the operator Λ^* is defined by:

$$\Lambda^*(Y_1, Y_2) = \begin{bmatrix} \text{tr } (Y_1\, H_{m,1}) + \text{tr } (Y_2(-a\, b\, H_{m-1,1})) \\ \text{tr } (Y_1\, H_{m,2}) + \text{tr } (Y_2((b+a)H_{m-1,1} - a\, b\, H_{m-1,2})) \\ \text{tr } (Y_1\, H_{m,3}) + \text{tr } (Y_2((b+a)H_{m-1,2,} - H_{m-1,1} - a\, b\, H_{m-1,3})) \\ \vdots \\ \text{tr } (Y_1 H_{m,i}) + \text{tr } (Y_2((b+a)H_{m-1,i-1} - H_{m-1,i-2} - a\, b\, H_{m-1,i})) \\ \vdots \\ \text{tr } (Y_1\, H_{m,2m}) + \text{tr } (Y_2((b+a)H_{m-1,2m-1} - H_{m-1,2m-2})) \\ \text{tr } (Y_1\, H_{m,2m+1}) + \text{tr } (Y_2(-H_{m-1,2m-1})) \end{bmatrix} \tag{B.5}$$

B.2 Checking polynomials non negativity on an infinite interval

The necessary and sufficient conditions for non negativity of univariate polynomials on infinite intervals have also been given in [73]. A polynomial $P(w)$ is non negative on $\mathbb{R}$ if and only if there exists a symmetric positive semi-definite matrix $Y \in \mathbb{R}^{(m+1)\times(m+1)}$ such that p, the vector of coefficients of $P(w)$, verifies:

$$p \in \mathcal{K}_\infty \iff \exists\, Y \succeq 0 \text{ s.t. } p = \Lambda^*(Y) \tag{B.6}$$

where the linear operator Λ^* is defined by:

$$\Lambda^*(Y)(j) = \text{tr } (Y\, H_{m,j}),\ j = 1..2m+1 \tag{B.7}$$

Appendix C

Ellipsoidal sets

C.1 Representations of ellipsoidal sets

There are several ways of representing an ellipsoidal set, each one with its own advantages. An ellipsoidal set E of dimension n can be described using a vector $c \in \mathbb{R}^n$ for its center and a positive semi-definite matrix Q for its shape:

$$E(c, Q) = \{x \in \mathbb{R}^n \mid (x - c)^T Q(x - c) \leq 1\} \tag{C.1}$$

Using this representation, the semi-axes of the ellipsoid a_i are given by:

$$a_i = \sqrt{\frac{1}{\lambda_i(Q)}} \tag{C.2}$$

where $\lambda_i(Q)$ denotes the i-th eigenvalue of the Q matrix.

By expanding the terms in (C.1), the ellipsoid E is defined by an non homogeneous quadratic inequality:

$$E(c, Q) = \{x \in \mathbb{R}^n \mid x^T Q x - 2c^T Q^T x + c^T Q c - 1 \leq 0\} \tag{C.3}$$

This can be written as a homogeneous quadratic inequality by augmenting the variable:

$$E(c, Q) = \left\{ x \in \mathbb{R}^n \mid \begin{bmatrix} x^T & t \end{bmatrix} \begin{bmatrix} -Q & Qc \\ c^T Q & 1 - c^T Q c \end{bmatrix} \begin{bmatrix} x \\ t \end{bmatrix} \geq 0 \right\} \tag{C.4}$$

where $t = 1$.

The positive definite matrix Q can also be written as:

$$Q = U \Lambda U^T = U \Sigma^2 U^T$$

where Λ and Σ are diagonal matrices. Using this decomposition, alternative descriptions for the ellipsoidal set $E(c, Q)$ can be obtained:

$$E(c, Q) = \{x \in \mathbb{R}^n \mid \|\Sigma U^T (x - c)\| \leq 1\} = \{x \in \mathbb{R}^n \mid \|Q^{\frac{1}{2}}(x - c)\| \leq 1\} \tag{C.5}$$

By defining $v = \Sigma U^T(x - c)$ we have:

$$E(c, Q) = \{x \in \mathbb{R}^n \mid x = c + U\Sigma^{-1}v,\ \|v\| \leq 1\} \tag{C.6}$$

C.2 Operations with ellipsoids

An ellipsoidal set $E(c, Q)$, propagated through a linear function $Ax + b$ is still an ellipsoidal set defined by:

$$y = Ax + b,\ \forall x \in E(c, Q) \Longleftrightarrow y \in E(Ac + b, A^{-T}QA^{-1}) \tag{C.7}$$

The Minkowski sum $\oplus$ of two ellipsoidal sets $E_1(c_1, Q_1)$ and $E_2(c_2, Q_2)$ is defined as:

$$E_1 \oplus E_2 = \{x \in \mathbb{R}^n \mid x = x_1 + x_2,\ x_1 \in E_1,\ x_2 \in E_2\} \tag{C.8}$$

The Minkowski sum of two ellipsoids is not usually an ellipsoid. However an analytical ellipsoidal outer approximation of the Minkowski sum of two ellipsoids can be obtained by using the procedure described in [81]:

$$E_1(c_1, Q_1) \oplus E_2(c_2, Q_2) \subseteq E_M(c_1 + c_2, Q_M) \tag{C.9}$$

where the matrix Q_M defining the ellipsoidal set E_M is defined by:

$$Q_M = (A^{\#})^T(Q_0 - Q_0N(N^TQ_0N)^{\#}N^TQ_0)A^{\#} \tag{C.10}$$

and

$$Q_0 = \begin{bmatrix} Q_1/2 & 0_n \\ 0_n & Q_2/2 \end{bmatrix} \quad A = \begin{bmatrix} I_n & I_n \end{bmatrix} \tag{C.11}$$

The matrix N defines the orthogonal complement of the matrix A (i.e. $NA = 0$) and the symbol $\#$ denotes the pseudo-inverse of the matrix.

C.3 The S-procedure

The S-procedure studies the non negativity of a quadratic form on a domain defined by quadratic inequalities, such as ellipsoidal sets (C.3). Given the quadratic functions:

$$f_i(x) = x^TM_ix + 2m_i^Tx + \mu_i,\ i = 0..l$$

the purpose is to verify if:

$$f_0(x) \geq 0,\ \forall x \text{ such that } f_i(x) \geq 0,\ i = 1..l \tag{C.12}$$

For $l = 2$, the previous inequality is verified if and only if the quadratic function f_0 is a linear consequence of the quadratic functions f_1 and f_2. Using the representations based on homogeneous quadratic forms as in (C.4), the condition (C.12) becomes:

$$\begin{bmatrix} x^T & t^T \end{bmatrix} \begin{bmatrix} M_0 & m_0 \\ m_0^T & \mu_0 \end{bmatrix} \begin{bmatrix} x \\ t \end{bmatrix} \geq 0, \forall x \text{ such that } \begin{bmatrix} x^T & t^T \end{bmatrix} \begin{bmatrix} M_i & m_i \\ m_i^T & \mu_i \end{bmatrix} \begin{bmatrix} x \\ t \end{bmatrix} \geq 0,\ i = 1..2 \tag{C.13}$$

As reminded in [72], the condition (C.13) is equivalent to the following Linear Matrix Inequality:

$$\exists \tau_1, \tau_2 \geq 0 \text{ such that } \bar{M}_0 \geq \tau_1 \bar{M}_1 + \tau_2 \bar{M}_2 \tag{C.14}$$

where the matrices $\bar{M}_i$ correspond to the homogeneous quadratic functions in (C.13).

For $l > 2$ the existence of a positive semi-definite linear combination between the matrices corresponding to the quadratic inequalities does not necessarily mean that (C.12) holds. A supplementary condition on the matrix M_i needs to be added, the condition of the matrices being simultaneously diagonalizable [76].

In the case where $l = 1$, condition (C.12) translates into the problem of checking whether an ellipsoidal set is contained inside another ellipsoidal set.

Bibliography

[1] K.T. Alfriend and H. Schaub. Dynamics and control of spacecraft formations- Challenges and some solutions. *Journal of the Astronautical Sciences*, 48(2):249–267, 2000.

[2] C. Andrade and R. Ramirez-Mendoza. Robust Control Applied Towards Rendezvous and Docking. In *Europeean Control Conference*, 2009.

[3] D. Arzelier, M. Kara-Zaitri, C. Louembet, and A. Delibasi. Using Polynomial Optimization to Solve the Fuel-Optimal Linear Impulsive Rendezvous Problem. *Journal of Guidance, Control, and Dynamics*, 34(5):1567–1576, September 2011.

[4] D. Arzelier, C. Louembet, A. Rondepierre, and M. Kara-Zaitri. A New Mixed Iterative Algorithm to Solve the Fuel-Optimal Linear Impulsive Rendezvous Problem. *Journal of Optimization Theory and Applications*, 2013.

[5] M. Bando and A. Ichikawa. Periodic Orbits of Nonlinear Relative Dynamics and Satellite Formation. *Journal of Guidance, Control, and Dynamics*, 32(4):1200–1208, July 2009.

[6] M. Bando and A. Ichikawa. Periodic Orbits of Nonlinear Relative Dynamics Along an Eccentric Orbit. *Journal of Guidance, Control, and Dynamics*, 33(2):385–395, 2010.

[7] D. Barnhart. Phoenix Operations BAA : Technical Elements and Interfaces. Technical report, DARPA Conference Center, Arlington, 2013.

[8] R.H. Battin. *An Introduction in the Mathematics and Methods of Astrodynamics*. American Institute of Aeronautics and Astronautics, 1999.

[9] A. Ben-Tal and A. Nemirovski. Robust convex optimization. *Mathematics of Operations Research*, 23(4), 1998.

[10] D. Bertsimas and J.N. Tsitsiklis. *Introduction to Linear Optimization*. Athena Scientific, 1997.

[11] J.T. Betts. Survey of numerical methods for trajectory optimization. *Journal of Guidance, Control, and Dynamics*, 21(2):193–207, 1998.

[12] J.D. Biggs and C.R. McInnes. Time-delayed feedback control in astrodynamics. *Journal of Guidance, Control and Dynamics*, 32:1804–1811, 2009.

[13] C. Bonnal, J-M. Ruault, and M-C. Desjean. Active debris removal: Recent progress and current trends. *Acta Astronautica*, 85:51–60, 2013.

[14] S.P. Boyd, L. El Ghaoui, E. Feron, and V. Balakrishnam. Some standard problems involving LMIs. In *Linear Matrix Inequalities in System and Control Theory*. SIAM, 1994.

[15] S.P. Boyd and L. Vandenberghe. *Convex Optimization*. Cambridge University Press, 2009.

[16] L.S. Breger and J.P. How. Gauss's variational equation-based dynamics and control for formation flying spacecraft. *Journal of Guidance, Control and Dynamics*, 30(2):437–448, 2007.

[17] L.S. Breger and J.P. How. Safe Trajectories for Autonomous Rendezvous of Spacecraft. *Journal of Guidance, Control, and Dynamics*, 31(5):1478–1489, September 2008.

[18] L.S. Breger, J.P. How, and A.G. Richards. Model predictive control of spacecraft formations with sensing noise. In *American Control Conference (ACC)*, pages 2385–2390, 2005.

[19] L.S. Breger, G. Inalhan, M. Tillerson, and J.P. How. Cooperative Spacecraft Formation Flying: Model Predictive Control with Open- and Closed-Loop Robustness. In P. Gurfil, editor, *Modern Astrodynamics*, chapter 8, pages 237–277. Elsevier Academic Press, 2007.

[20] T.E. Carter. State Transition Matrices for Terminal Rendezvous Studies: Brief Survey and New Example. *Journal of Guidance, Control, and Dynamics*, 21(1):148–155, 1998.

[21] S. Chevillard, J. Harrison, M. Joldes, and Ch. Lauter. Efficient and accurate computation of upper bounds of approximation errors. *Theoretical Computer Science*, 412(16):1523–1543, 2011.

[22] S. Chevillard, M. Joldes, and Ch. Lauter. Sollya: An environment for the development of numerical codes. In *Mathematical Software–ICMS 2010*, pages 3–6, 2010.

[23] W.H. Clohessy and R.S. Wiltshire. Terminal Guidance System for Satellite Rendezvous. *Journal of Astronautical Sciences*, 27(9):653–658, 1960.

[24] B. Conway. *Spacecraft trajectory optimization*. 2010.

[25] G. Deaconu, C. Louembet, and A. Théron. Constrained periodic spacecraft relative motion using non negative polynomials. In *American Control Conference (ACC)*, 2012.

[26] S. Di Cairano, H. Park, and I. Kolmanovsky. Model Predictive Control approach for guidance of spacecraft rendezvous and proximity maneuvering. *International Journal of Robust and Nonlinear Control*, 22(12):1398–1427, 2012.

[27] P. Falugi, S. Olaru, and D. Dumur. Robust multi-model predictive control using LMIs. In *17th IFAC World Congress*, number 2, pages 8809–8814, 2008.

[28] C. Farges. *Méthodes d'analyse et de synthèse robustes pour les systèmes linéaires périodiques*. PhD thesis, 2006.

[29] W. Fehse. *Automated Rendezvous and Docking of Spacecraft*. Cambridge University Press, 2003.

[30] P. Ferrando, A. Goldwurm, P. Laurent, and O. Limousin. SIMBOL–X a formation flying mission for hard X-rays astrophysics. In *SPIE conference "Optics for EUV, X-Ray, and Gamma-Ray Astronomy II"*, page Vol. 5900, 2005.

[31] F. Gavilan, R. Vazquez, and E.F. Camacho. Robust Model Predictive Control for Spacecraft Rendezvous with Online Prediction of Disturbance Bounds. In *IFAC Workshop on Aerospace Guidance, Navigation and Flight Control Systems*, 2009.

[32] F. Gavilan, R. Vazquez, and E.F. Camacho. Chance-constrained model predictive control for spacecraft rendezvous with disturbance estimation. *Control Engineering Practice*, 20(2):111–122, February 2012.

[33] D-W. Gim and K.T. Alfriend. State Transition Matrix of Relative Motion for the Perturbed Noncircular Reference Orbit. *Journal of Guidance, Control, and Dynamics*, 26(6):956–971, 2003.

[34] D-W. Gim and K.T. Alfriend. Satellite Relative Motion Using Differential Equinoctial Elements. *Celestial Mechanics and Dynamical Astronomy*, 92(4):295–336, August 2005.

[35] P.J. Goulart, E.C. Kerrigan, and J.M. Maciejowski. Optimization over state feedback policies for robust control with constraints. *Automatica*, 42(4):523–533, April 2006.

[36] G. Grimm, M.J. Messina, S.E. Tuna, and A.R. Teel. Nominally Robust Model Predictive Control With State Constraints. *IEEE Transactions on Automatic Control*, 52(10):1856–1870, 2007.

[37] P. Gurfil. Relative Motion between Elliptic Orbits: Generalized Boundedness Conditions and Optimal Formationkeeping. *Journal of Guidance, Control, and Dynamics*, 28(4):761–767, July 2005.

[38] P. Gurfil and K.V. Kholshevnikov. Manifolds and Metrics in the Relative Spacecraft Motion Problem. *Journal of Guidance, Control, and Dynamics*, 29(4):1004–1010, 2006.

[39] J-F. Hamel and J. de Lafontaine. Linearized Dynamics of Formation Flying Spacecraft on a J2 Perturbed Elliptical Orbit. *Journal of Guidance, Control, and Dynamics*, 30(6):1649–1658, 2007.

[40] J-F. Hamel and J. de Lafontaine. Autonomous guidance and control of Earth-orbiting formation flying spacecraft: Closing the loop. *Acta Astronautica*, 63(11-12):1246–1258, 2008.

[41] E.N. Hartley, P.A. Trodden, A.G. Richards, and J.M. Maciejowski. Model predictive control system design and implementation for spacecraft rendezvous. *Control Engineering Practice*, 20(7):695–713, 2012.

[42] G.W. Hill. Researches in the lunar theory. *American Journal of Mathematics*, 1(1):5–26, 1878.

[43] M. Holzinger, J. DiMatteo, J. Schwartz, and M. Milam. Passively safe Receding Horizon Control for satellite proximity operations. In *47th IEEE Conference on Decision and Control*, pages 3433–3440, 2008.

[44] J.P. How and M. Tillerson. Analysis of the impact of sensor noise on formation flying control. In *American Control Conference (ACC)*, volume 5, pages 3986–3991, 2001.

[45] D.G. Hull. Conversion of Optimal Control Problems into Parameter Optimization Problems. *Journal of Guidance, Control, and Dynamics*, 20(1):57–60, 1997.

[46] G. Inalhan, J.P. How, and M. Tillerson. Relative dynamics and control of spacecraft formations in eccentric orbits. *Journal of Guidance, Control, and Dynamics*, 25(1), 2002.

[47] D.J. Irvin, R.G. Cobb, and T.A. Lovell. Fuel-Optimal Maneuvers for Constrained Relative Satellite Orbits. *Journal of Guidance, Control, and Dynamics*, 32(3):960–973, 2009.

[48] F. Jiang, J. Li, H. Baoyin, and Y. Gao. Study on Relative Orbit Geometry of Spacecraft Formations in Elliptical Reference Orbits. *Journal of Guidance, Control, and Dynamics*, 31(1):123–134, 2008.

[49] M. Kara-Zaitri. *Modélisation et guidage robuste et autonome pour le problème du rendez-vous orbital.* PhD thesis, Université Toulouse III - Paul Sabatier, 2010.

[50] J. A. Kechichian. Motion in a general elliptic orbit with respect to a dragging and precessing coordinate frame. *Journal of Astronautical Sciences*, 1(46):25–46, 1998.

[51] H.K. Khalil. *Nonlinear Systems.* Pearson Education International, New Jersey, third edit edition, 2000.

[52] K.V. Kholshevnikov and N.N. Vassiliev. On the distance function between two Keplerian elliptic orbits. *Celestial Mechanics and Dynamical Astronomy*, pages 75–83, 1999.

[53] Y. Kuwata, A. Richards, and J.P. How. Robust Receding Horizon Control using Generalized Constraint Tightening. In *American Control Conference*, pages 4482–4487, July 2007.

[54] M. Kvasnica, P. Grieder, and M. Baotic. Multi-Parametric Toolbox (MPT), 2006.

[55] C. Lane and P. Axelrad. Formation design in eccentric orbits using linearized equations of relative motion. *Journal of Guidance, Control, and Dynamics*, 29(1):146–160, 2006.

[56] W. Langson, I. Chryssochoos, S.V. Rakovic, and D.Q. Mayne. Robust model predictive control using tubes. *Automatica*, 40(1):125–133, 2004.

[57] G. Lantoine and R. Epenoy. Quadratically Constrained Linear-Quadratic Regulator Approach for Finite-Thrust Orbital Rendezvous. *Journal of Guidance, Control, and Dynamics*, 35(6):1787–1797, 2012.

[58] D.F. Lawden. *Optimal trajectories for space navigation.* 1963.

[59] Y.I. Lee and B. Kouvaritakis. Robust receding horizon predictive control for systems with uncertain dynamics and input saturation. *Automatica*, 36:1497–1504, 2000.

[60] Junfeng Li, Xin Meng, Y. Gao, and Xiang Li. Study on relative orbital configuration in satellite formation flying. *Acta Mechanica Sinica*, 21(1):87–94, February 2005.

[61] D. Limon, I. Alvarado, T. Alamo, and E.F. Camacho. Robust tube-based MPC for tracking of constrained linear systems with additive disturbances. *Journal of Process Control*, 20(3):248–260, 2010.

[62] P.M. Lion and M. Handelsman. Primer vector on fixed-time impulsive trajectories. *AIAA Journal*, 6(1):127–132, 1968.

[63] J. Lofberg. YALMIP: A toolbox for modeling and optimization in MATLAB. In *IEEE International Symposium on Computer Aided Control Systems Design*, pages 284–289, 2004.

[64] C. Louembet, D. Arzelier, G. Deaconu, and P. Blanc-Paques. Robust rendezvous planning under navigation and maneuvering errors. In *International ESA Conference on Guidance and Navigation Control Systems*, 2011.

[65] T.A. Lovell and S G Tragesser. Near-optimal reconfiguration and maintenance of close spacecraft formations. *Annals of the New York Academy of Sciences*, 1017:158–76, 2004.

[66] D.Q. Mayne, E.C. Kerrigan, and P. Falugi. Robust model predictive control : advantages and disadvantages of tube-based methods. In *18th IFAC World Congress*, pages 191–196, Milano, 2011.

[67] D.Q. Mayne, S.V. Rakovic, R. Findeisen, and F. Allgöwer. Robust output feedback model predictive control of constrained linear systems: Time varying case. *Automatica*, 45(9):2082–2087, 2009.

[68] D.Q. Mayne, J.B. Rawlings, C.V. Rao, and P.O.M. Scokaert. Constrained model predictive control : Stability and optimality. *Automatica*, 36(6):789–814, 2000.

[69] D.Q. Mayne, M.M. Seron, and S.V. Rakovic. Robust model predictive control of constrained linear systems with bounded disturbances. *Automatica*, 41(2):219–224, February 2005.

[70] R.G. Melton. Time-Explicit Representation of Relative Motion Between Elliptical Orbits. *Journal of Guidance, Control, and Dynamics*, 23(4):604–6010, 2000.

[71] J.B. Mueller and R. Larsson. Collision avoidance maneuver planning with robust optimization. In *7th International ESA Conference on Guidance, Navigation and Control Systems*, number June, Tralee, Count Kerry, Ireland, 2008.

[72] S.A. Nazin, B.T. Polyak, and M.V. Topunov. Rejection of bounded exogenous disturbances by the method of invariant ellipsoids. *Automation and Remote Control*, 68(3):467–486, March 2007.

[73] Y. Nesterov. Squared functional systems and optimization problems. In *High performance optimization*, chapter 17. Kluwer Academic Publishers, 2000.

[74] H. Park, S. Di Cairano, and I. Kolmanovsky. Model Predictive Control of spacecraft docking with a non-rotating platform. In *18th IFAC World Congress*, number 2003, 2011.

[75] S. Persson, P. Bodin, E. Gill, J. Harr, and J. Jörgensen. PRISMA – An Autonomous Formation Flying Mission. In *ESA Small Satellite Systems and Services Symposium*, number September, pages 25–29, Sardinia, Italy, 2006.

[76] B.T. Polyak. Convexity of quadratic transformations and its use in control and optimization. *Journal of Optimization Theory and Applications*, 99(3):553–583, 1998.

[77] A.G. Richards. Robust Model Predictive Control for Time-Varying Systems. In *Proceedings of the 44th IEEE Conference on Decision and Control*, number 3, pages 3747–3752. Ieee, 2005.

[78] A.G. Richards, L.S. Breger, and J.P. How. Analytical performance prediction for robust constrained model predictive control. *International Journal of Control*, 79(8):877–894, August 2006.

[79] A.G. Richards and J.P. How. Robust variable horizon model predictive control for vehicle maneuvering. *International Journal of Robust and Nonlinear Control*, 16(7):333–351, May 2006.

[80] J.A. Richards. *Analysis of Periodically Time-Varying Systems.* Springer-Verlag Berlin, Heidelberg, 1983.

[81] L. Ros, A. Sabater, and F. Thomas. An ellipsoidal calculus based on propagation and fusion. *IEEE transactions on systems, man, and cybernetics. Part B: Cybernetics*, 32(4):430–42, 2002.

[82] I.M. Ross. How to Find Minimum-Fuel Controllers. In *AIAA Guidance, Navigation and Control Conference and Exhibit*, pages AIAA Paper No 2004–5346, 2004.

[83] I.M. Ross. Space Trajectory Optimization and L1-Optimal Control Problems. In P. Gurfil, editor, *Modern Astrodynamics*, chapter 6, pages 155–188. Elsevier Academic Press, 2007.

[84] J.A. Rossiter. *Model-Based Predictive Control - A practical approach.* Control series. CRC Press Web, Boca Raton, 2004.

[85] J.H. Saleh, D.E. Hastings, E.S. Lamassoure, and D.J. Newman. Flexibility and the Value of On-Orbit Servicing: New Customer-Centric Perspective. *Journal of Spacecraft and Rockets*, 40(2):279–291, 2003.

[86] M. Saponara, V. Barrena, A. Bemporad, E.N. Hartley, J.M. Maciejowski, and A.G. Richards. Model Predictive Control application to spacecraft rendezvous in Mars Sample Return scenario. In *4th European Conference for Aerospace Sciences (EUCASS)*, 2011.

[87] D.P. Scharf. A survey of spacecraft formation flying guidance and control. Part II: control. In *American Control Conference (ACC)*, number Part 11, pages 2976 – 2985, 2004.

[88] D.P. Scharf, F.Y. Hadaegh, and S.R. Ploen. A survey of spacecraft formation flying guidance and control (part 1): guidance. In *American Control Conference (ACC)*, volume 2, pages 1733–1739. Ieee, 2003.

[89] H. Schaub and K.T. Alfriend. Impulsive Feedback Control to Establish Specific Mean Orbit Elements of Spacecraft Formations. *Journal of Guidance, Control, and Dynamics*, 24(4):739–745, 2001.

[90] H. Schaub and J.L. Junkins. *Analytical Mechanics of Space Systems.* AIAA education series, 2003.

[91] S. A. Schweighart and R. J. Sedwick. High-Fidelity Linearized J2 Model for Satellite Formation Flight. *Journal of Guidance, Control, and Dynamics*, 25(6):1073–1080, 2002.

[92] P. Sengupta and S.R. Vadali. Relative Motion and the Geometry of Formations in Keplerian Elliptic Orbits. *Journal of Guidance, Control, and Dynamics*, 30(4):953–964, 2007.

[93] P. Sengupta and S.R. Vadali. Analytical Solution for Power-Limited Optimal Rendezvous near an Elliptic Orbit. *Journal of Optimization Theory and Applications*, 138(1):115–137, 2008.

[94] R.C. Shekhar and J.M. Maciejowski. Optimal constraint tightening policies for robust variable horizon model predictive control. In *51st IEEE Conference on Decision and Control (CDC)*, number 2, pages 5170–5175, December 2012.

[95] P. Singla, K. Subbarao, and J.L. Junkins. Adaptive output feedback control for spacecraft rendezvous and docking under measurement uncertainty. *Journal of Guidance, Control, and Dynamics*, 29(4):892–902, 2006.

[96] D. Sui, L. Feng, and M. Hovd. Robust output feedback model predictive control for linear systems via moving horizon estimation. In *American Control Conference*, number 978, pages 453–458. Ieee, June 2008.

[97] F. Tahir. Efficient Computation of Robust Positively Invariant Sets with Linear State-feedback Gain as a Variable of Optimization. In *7th International Conferenceon Electrical Engineering, Computing Science and Automatic Control (CCE)*, number Cce, pages 199–204, 2010.

[98] M. Tillerson. *Coordination and Control of Multiple Spacecraft using Convex Optimization Techniques*. PhD thesis, Massachusetts Institute of Technology, 2002.

[99] M. Tillerson, G. Inalhan, and J.P. How. Co-ordination and control of distributed spacecraft systems using convex optimization techniques. *International Journal of Robust and Nonlinear Control*, 12:207–242, February 2002.

[100] K.C. Toh, R.H. Tütüncü, and M.J. Todd. SDPT3—a Matlab software package for semidefinite-quadratic-linear programming. *Optimization Methods and Software*, 11:545—-581, 1999.

[101] J. Tschauner. Elliptic orbit rendezvous. *AIAA Journal*, 5(6):1110–1113, 1967.

[102] K. Yamada and M. Kimura. New State Transition Matrix for Formation Flying in J2 Perturbed Elliptic Orbits. *Journal of Guidance, Control, and Dynamics*, 35(2):536–547, 2012.

[103] K. Yamanaka and F. Ankersen. New state transition matrix for relative motion on an arbitrary elliptical orbit. *Journal of Guidance, Control, and Dynamics*, 25(1):60–66, 2002.

[104] Q. Yan, G. Yang, V. Kapila, and M. de Queiroz. Nonlinear Dynamics and Output Feedback Control of Multiple Spacecraft in Elliptical Orbits. In *Proceedings of the American Control Conference*, number June, pages 839–834, 2000.

[105] H-H. Yeh and A. Sparks. Geometry and Control of Satellite Formations. In *American Control Conference (ACC)*, number June, pages 384–388, 2000.